Study on confined biexciton properties in semiconductor quantum dots by two-photon excitation spectroscopy and mid-infrared transient absorption spectroscopy

Kensuke Miyajima

Osaka University

Graduate School of Engineering Science
Department of Physical Science
Division of Materials Physics

2004

Study on confined biexciton properties in semiconductor quantum dots by two-photon excitation spectroscopy and mid-infrared transient absorption spectroscopy

Kensuke Miyajima

Osaka University

Graduate School of Engineering Science
Department of Physical Science
Division of Materials Physics

2004

Contents

Chapter 1

Introduction

1.1 Background

Electronic energy structures in low-dimensional semiconductors transfer the continuous structure in bulk crystals to the quantized discrete levels that is derived from the restricted kinetic energy of the carrier. The discrete energy levels of electrons or holes result in the convergence of the oscillator strength and the energy shift of the absorption band, which are called "quantum size effect" [1, 2]. Therefore, optical properties of the low-dimensional semiconductors, such as thin films, wires and dots, have attracted great attention in a few decades from the view point of both fundamental physics and application to novel optical devices. In addition, progress in crystal-growth techniques of nanostructures have been achieved in these days, such as molecular beam epitaxy method [3] or chemical-vapor deposition [4] and so on, that make possible of the control of nanostructures within the accuracy of the atomic levels. Researches of nanostructured materials have become more and more prosperous and important at present.

In nanoparticles, the quantum confinement occurs three dimensionally, that realize the completely discrete electronic energy levels. Therefore, nanoparticles are called "quantum dots" or expressed as "artificial atoms" with the discrete energy levels. Since the quantum dots acquire the completely discrete energy levels, it is the most competent candidate for the nano-devices utilizing the quantum size effect. Accordingly, the quantum dots are prospected to be available for various novel optical devices, e.g., high efficient solid-state lasers [5 - 7], photo-detectors [8], infrared light emitting diodes [9],

and so on.

Since the success of the fabrication of the semiconductor nanoparticles or quantum dots grown in glass materials [10], alkali halide crystals [11, 12] and organic solvents [13], a lot of investigations have been carried out on the optical properties of the semiconductor quantum dots. The optical spectroscopy of the semiconductors is basically related to a photoexcited e–h pair, so-called exciton. The exciton is expressed as an electrically neutral quasi-particle composed of an electron and a hole through the Coulomb interaction. The energy shift of the exciton due to the quantum size effect is approximately classified into two limiting cases which are determined by the relation of the size of the nanocrystal and the exciton effective Bohr radius [14 - 16]. When the exciton effective Bohr radius is sufficiently larger than the dot radius, the concept of the exciton as a quasi-particle is broken, and the kinetic energies of the electron and hole are quantized individually. On the other hand, when the exciton effective Bohr radius is smaller than the dot radius, the quantum confinement affects mainly the center-of-mass motion of the excitons and less the relative motion of the electron and hole. We call the former and latter cases strong and weak confinement, respectively.

To date, a lot of studies on the application of quantum dots to nano-devices have been carried out about the materials of "strong confinement" [5 - 9]. However, it is interesting to study the materials of the "weak confinement" because the coupled mode of the exciton and an electromagnetic field is expected to enhance the optical nonlinearities, and thus useful for the new optical applications [17].

Moreover, we should notice the phenomena of confined multiexciton states in the quantum dots. In the confinement system, a compulsory correlation of the carriers is expected to generate distinctive energy levels and transition dynamics, which never appear in the bulk crystal, and induce the large optical nonlinearities. A biexciton consisting of the two excitons is the most important quasi-particle that reveals the strong correlation effect of the electrons and holes in the quantum dots. In addition to this, the biexciton is strongly related to the optical nonlinear response of semiconductors and serves the useful exciton-related state for optical-devices [18]. Therefore, the study of the quantum size effect of the biexcitons is important subject.

CuCl is one of the most appropriate semiconductors for the study of the fundamental properties of excitons because of its simple band structure [19] and large exciton binding energy [20]. Furthermore, CuCl quantum dots show a typical nature of weak

confinement, because of the small effective Bohr radius. The optical measurements of CuCl quantum dots embedded in glass [10, 21 - 23] or alkali halide matrices [11, 24 - 26] have been carried out mainly on the confined excitons extensively. Consequently, the many interesting features have been reported; e.g., large oscillator strength [22, 27], large optical nonlinear susceptibility [23, 24, 26, 28], exciton superradiance [21, 25, 29], and so on.

On the other hand, the study on confined biexcitons in CuCl quantum dots also have been reported for the basic features; e.g., the biexciton binding energy [30, 31], the relaxation process of the excitons and biexcitons [32 - 35], the excited-biexciton states (weakly correlated two excitons) [31, 36, 37]. In addition, lasing action of biexciton photoluminescence and the large optical gain have been reported [38], so that the confined biexcitons are suggested to be available realizing for the highly efficient quantum-dot laser.

However, a lot of unresolved questions still remain on the confined biexciton properties. First, there is no report on the resonant two-photon absorption of the confined biexciton state, which is observed clearly for bulk crystals [39]. Study on the two-photon absorption process for the quantum dots is very important because the two-photon absorption coefficient is one of the parameters related to the optical nonlinearlity. In addition, it will serve a new experimental method to provide us further information about the quantum size effect to the biexciton states. Second, there is no report on the excited-state properties of the confined biexcitons. However, we should look more carefully into the quantum size effects not only on the lowest state but also on the excited states of the biexciton. The excited biexciton properties are attractive since the specific properties are expected to emerge because of much larger correlation between the excitons in the confinement system.

Based on these contexts, I have performed two experiments, the resonant two-photon excitation and the mid-infrared transient absorption for the study on the confined biexciton properties in CuCl quantum dots embedded in NaCl matrices. In the following sections in Chapter 1, I will introduce the basic theory of the quantum size effect and the exciton and the biexciton properties of CuCl quantum dots which are previously reported. In Chapter 2, the experimental procedure will be explained. In Chapter 3, I will show the evidences of the resonant two-photon excitation process of the confined biexcitons. In Chapter 4, I will show photoluminescence (PL) spectra

under the two-photon excitation of the confined biexcitons and discuss the size-selective excitation of the biexcitons. In Chapter 5, I will show the experimental results of the infrared transient absorption and discuss the excited-states of the confined biexciton. Finally, I will summarize them in Chapter 6.

1.2 Exciton

When the electronic system of a semiconductor or an ionic crystal absorbs a photon with the energy larger than the band-gap energy, an electron is excited from the valence band into the conduction band leaving a hole in the valence band. The electron and the hole are bound through the Coulomb interaction and such an electron–hole (e–h) pair state is called "exciton". The exciton is an electronic excitation with the lowest energy when pure semiconductors are weakly excited, and the energy consists of three components, a band gap, a center-of-mass motion and a relative motion of the electron and the hole. In a semiconductor with a small electron or hole mass and a large dielectronic constant, a wave function of the relative motion of the e–h pair spreads over many unit cells and this weakly bound e–h pair state is called a Wannier exciton.

The hamiltonian of the e–h pair bound by the Coulomb interaction is expressed by

$$H = \frac{p_e^2}{2m_e} + \frac{p_h^2}{2m_h} - \frac{e^2}{\varepsilon|\boldsymbol{r}_e - \boldsymbol{r}_h|} + E_g \qquad (1.1)$$

where m_e, $\boldsymbol{p}_e$ and $\boldsymbol{r}_e$, and m_h, $\boldsymbol{p}_h$ and $\boldsymbol{r}_h$, are the effective mass, momentum and position vector of the electron and hole, respectively. Here the band gap energy E_g is taken into account. The coordinate conversion of Eq. (1.1) can be carried out using the relative and center-of-mass positions (r and R) of the electron and hole. Therefore, Eq.(1.1) can be converted into

$$H = \left(-\frac{\hbar^2}{2\mu_{ex}} \cdot \nabla_r^2 - \frac{e^2}{\varepsilon r} \right) - \frac{\hbar^2}{2M_{ex}} \cdot \nabla_R^2 + E_g \qquad (1.2)$$

where

$$\mu_{ex} = \frac{m_e m_h}{m_e + m_h} \qquad (1.3)$$

and

$$M_{ex} = m_e + m_h \qquad (1.4).$$

Here, μ_{ex} and M_{ex} are a reduced mass and a translational mass of the exciton, respectively. The energy dispersion of the exciton $E_{ex}(n, \boldsymbol{K})$ is expressed as follows;

$$E_{ex}(n, \boldsymbol{K}) = E_g - E_{Ry}\left(\frac{1}{n^2}\right) + \frac{\hbar^2 \boldsymbol{K}^2}{2M_{ex}} \qquad (1.5)$$

$$E_{Ry} = \frac{\mu e^4}{2\varepsilon^2 \hbar^2} = Ry \frac{\mu_{ex}}{m_0 \varepsilon^2} \qquad (1.6)$$

where n and $\boldsymbol{K}$ are a Rydberg principal number and a wave vector of the exciton, Ry and m_0 are Rydberg energy of hydrogen atom and an electron mass in vacuum. The second term on the right hand side of Eq. (1.5) exhibits the hydrogen-like energy levels, originating from the relative motion of the e–h pair, with a principal quantum number n (= 1, 2, ...) and the orbital quantum number l (= 0, 1, ..., n – 1). These energy states of the exciton are expressed as 1s, 2s, 2p, ... and so on. On the other hand, the third term of right hand side of Eq. (1.5) indicates the kinetic energy of the exciton, which is associated with the center-of-mass motion of the exciton.

In addition, the effective Bohr radius a_B of the exciton can be expressed as

$$a_B = \frac{\varepsilon \hbar^2}{\mu_{ex} e^2} = r_A \frac{m_0 \varepsilon}{\mu_{ex}} \qquad (1.7).$$

Here, r_A is Bohr radius of the hydrogen atom.

Thus, a Wannier exciton is, in many respects analogous, to a hydrogen atom.

1.3 Biexciton

With increasing the exciton concentration from low-density limit, many kinds of new optical phenomena occur, which are induced by the interaction between excitons. The bound state of two excitons, which are formed through the effective interaction potential, is called "excitonic molecule" or "biexciton". Up to now, the optical properties of the biexciton state have been studied in many semiconductors [40 - 43].

According to the consideration that an exciton is analogous to the hydrogen atom, the biexciton can be the analogy to the hydrogen molecule, the positive holes playing the role of protons. However, the translational mass of the biexicton is considered to be only twice that of the excitons, and it is much smaller in comparison with that of the hydrogen molecule. Therefore, the binding energy of the biexciton, which is defined as the dissociation energy into two isolated excitons, is much different between various semiconductors and depends on an effective mass ratio of the electron and hole $\sigma = m_e/m_h$. Figure 1-1 shows the biexciton binding energy G_m in a unit of the exciton binding energy G_{ex} as a function of σ, which is obtained theoretically by means of a variational method [44] and so on [45, 46], together with experimental results for a variety of crystals. According to the theoretical calculation, the biexciton state should exist regardless of the magnitude of σ.

The essential difference of the biexciton from the hydrogen molecule is the transient state of excitations with a short lifetime. In addition, the biexcitons constitutes an open system in close contact with the radiation field. Therefore, a variety of optical methods are used not only to create the biexcitons but also to study its properties.

There are three optical processes related to the biexciton states. The first one is a luminescence process, in which one of the two excitons composing the biexciton is radiatively annihilated and the other one remains in the crystal. The second process is an one-photon absorption process from the exciton to the biexciton, i.e., it is the process reverse to luminescence of the biexciton. The last one is a two-photon absorption process of the biexciton [47].

1.3.1 Luminescence

The luminescence due to the biexciton is originated from a radiative annihilation of one of the two excitons composing the biexciton with leaving another exciton. Therefore, the luminescence photon energy is expressed as

$$\hbar\omega = \left(2E_{ex} - E_b + \frac{\hbar^2 K^2}{2M_{mol}}\right) - \left(E_{ex} + \frac{\hbar^2 K^2}{2M_{ex}}\right)$$

$$= E_{ex} - E_b - \frac{\hbar^2 K^2}{2M_{mol}} \qquad (1.8).$$

Here, E_{ex}, E_b and M_{mol} indicate the exciton energy of 1s state, the biexciton binding

energy and a translational mass of the biexciton which is twice that of the exciton.

When the Boltzmann distribution with the effective temperature T_{eff} is assumed for the kinetic energy of the biexcitons, the luminescence spectrum of the biexcitons is expressed as follows;

$$W_{\mathrm{l}}(\omega) \propto \sqrt{E_{\mathrm{ex}} - E_{\mathrm{b}} - \hbar\omega} \cdot \exp[-(E_{\mathrm{ex}} - E_{\mathrm{b}} - \hbar\omega)/k_{\mathrm{B}}T_{\mathrm{eff}}] \qquad (1.9)$$

for $\hbar\omega \leq E_{\mathrm{ex}} - E_{\mathrm{b}}$,

As a result, luminescence spectrum rises by the biexciton binding energy below the exciton energy and the spectral shape shows an inversed Boltzmann distribution which has a tail to the lower energy side.

1.3.2 Giant oscillator strength

An effect of giant oscillator strength works in one-photon absorption in presence of single excitons due to conversion of excitons into biexcitons, which is reverse to the luminescence process of the biexcitons. The ratio of the transition probability from the ground state to the exciton state $W_{\mathrm{ex}}^{(1)}$ and that from the exciton state to the biexciton state $W_{\mathrm{c}}^{(1)}$ is expressed as follows;

$$W_{\mathrm{c}}^{(1)}/W_{\mathrm{ex}}^{(1)} = 64\pi a_{\mathrm{mol}}{}^{3}\rho_{\mathrm{ex}} \qquad (1.10)$$

where a_{mol} expresses the effective radius of the biexciton and ρ_{ex} is exciton density.

This strong enhancement of the transition from the exciton to the biexciton state is attributed to the effect of giant oscillator strength, which is coming from that the biexciton could be created by exciting any valence electron in the large biexciton orbital around the existing the first exciton.

1.3.3 Giant two-photon absorption

In general, the biexcitons is formed from two excitons by the relaxation process due to the their interaction with the lattice system, and its existence can be observed from the luminescence spectrum. However, direct creation process of the biexcitons is shown theoretically and experimentally to be capable of being fulfilled by using the giant two-photon absorption (GTA) due to the biexciton.

The two-photon absorption of the biexciton is extremely enhanced by two factors.

The first enhancement factor comes from the giant oscillator strength of the transition between the biexciton and exciton states. The second factor is resonant effect at the excitation photon energy of $E_{ex} - E_b/2$. As a result, in two-photon spectroscopy, the biexciton will be confirmed as the sharp absorption peak at $E_{ex} - E_b/2$. which are embedded in the rather weak background of the one-photon absorption tail of an exciton and the ordinary two-photon absorption due to band-to-band transition.

The selection rules for direct creation of biexcitons by two-photon absorption processes have been discussed on symmetry basis [48]. There are three types of the selection rules, i.e., dipole selection rule, geometrical selection rule and dynamical selection rule for the two-photon absorption.

1.4 Physical properties of CuCl bulk crystal

CuCl has a zinc-blende crystal structure at the normal condition and the symmetry is T_d^2 in the space group. It is a direct semiconductor, that is, the top of the valence band and the bottom of the conduction band are located at the Γ-point in the *k*-space.

In the zinc-blende structure, in general, the conduction band consists of *s*-orbit of cations, which is a non-degenerated state with Γ_6 symmetry. The valence band origins from the *p*-orbit of anions, which is a triply degenerated state with Γ_{15} symmetry. The degeneracy of Γ_{15} is separated into a doubly degenerated state Γ_8 and a non-degenerated state Γ_7 by spin-orbit splitting. In the ordinal zinc-blende structures, Γ_8 band is located above Γ_7 band. This structure of the valence band leads to two series of the exciton, that is, the $Z_{1,2}$ and Z_3 exciton states associated with the Γ_8 band and Γ_7 band, respectively.

In the case of CuCl, the conduction band origins from the 4s electrons of Cu^+, and the valence band is as admixture of the 3p electrons of Cl^- and 3d electrons of Cu^+. Differently from the other cupper halide crystal, CuCl shows the peculiar valence band structure that Γ_8 band is located beneath Γ_7 band because of the negative spin-orbit splitting due to the contribution of d electrons to the valence band. The energy band structure of CuCl is shown in Fig. 1-2.

Consequently, the lowest absorption peak of CuCl is due to Z_3 exciton state which consists of the hole at the Γ_7 valence band and the electron at the Γ_6 conduction band. Z_3

exciton has a simple band structure that has only spin degeneracy at Γ-point. Z_3 exciton has two states, Γ_5 exciton (total angular momentum of an exciton $J_{ex} = 1$) and Γ_2 exciton ($J_{ex} = 0$), originating from Γ_6 electron and Γ_7 hole. The energy levels of the Γ_5 exciton and Γ_2 exciton are split by exchange interaction, and the optical transition from ground state to Γ_5 exciton is allowed but that to Γ_2 exciton is forbidden.

CuCl is an appropriate material for the study of basic properties of the exciton since the exciton state is very stable because of the large binding energy compared to the other semiconductors. Therefore, the series of the exciton Rygberg states can be observed clearly in the absorption spectra. Saito *et al.* reported the one- and two-photon absorption spectra of CuCl single crystals and found the Rydberg s- and p-series of the Z_3 exciton [20].

In addition, for the study of the biexciton, CuCl is the appropriate material because of the large biexciton binding energy and the simple energy structure. The optical properties of the biexciton in CuCl have been clarified experimentally, the PL spectrum [40], the radiative decay time [49], giant two-photon absorption [39, 50 - 52], and so on. Figure 1-3 shows the energy diagram and the selection rules of excitons and biexcitons in CuCl. The transition from Γ_5 exciton to the lowest biexciton state (Γ_1) is optically allowed but that to the Γ_4 state is forbidden. In the case of two-photon resonant absorption of biexciton, only Γ_1 state is optically allowed. The polarization selection rules of the biexciton of CuCl have been discussed by Doni, *et al.* [48]. Accordingly, when one uses a single laser beam, the two-photon absorption of the biexciton occurs with the linearly polarized beam. However, the biexciton can not be created by the circularly polarized beam because the geometrical factor (Table A-1) becomes zero.

The important physical properties of the CuCl crystal and of the exciton and biexciton are shown in Table 1-1.

1.5 Quantum size effect on exciton

When an electron, a hole or an exciton exists in low-dimensional semiconductors, the size of which is comparable with their de Broglie wavelength, they can be treated as a spatially confined particle. Since the kinetic energy of such particle is quantized by the

confinement effect, the blue shift of the band-gap energy or the absorption band is observed, which is attributable to the increasing the kinetic energy. This phenomenon is called "quantum size effect" and one of the most characteristic features of the low-dimensional semiconductors.

In this section, the quantum size effect on the exciton confined in a spherical particle, i.e., quantum dot, is discussed. It can be classified into two limiting cases which is determined by the relation of the dot radius a and the exciton effective Bohr radius a_B, i.e., "weak confinement (or exciton confinement)" for the condition of $a/a_B >> 1$, and "strong confinement (or individual confinement)" for $a/a_B << 1$.

1.5.1 Weak confinement

Firstly, it is considered that an e–h pair is confined in a spherical well, the radius of which a is sufficiently larger than the exciton Bohr radius a_B. The hamiltonian of the e–h pair in this case is acquired by adding a term of a potential well to Eq. (1.2);

$$H = \left(-\frac{\hbar^2}{2\mu}\cdot\nabla_r^2 - \frac{e^2}{\varepsilon r} \right) - \frac{\hbar^2}{2M_{ex}}\cdot\nabla_R^2 + V(R) + E_g \qquad (1.11)$$

$$V(R) = \begin{cases} 0 & (\mathrm{R} < a) \\ \infty & (\text{otherwise}) \end{cases} .$$

Consequently, the exciton energy is expressed as

$$E_{ex}(nl, n'L) = E_g - \frac{E_{Ry}}{n^2} + \frac{\hbar^2}{2M_{ex}}\left(\frac{\pi\xi_{n'L}}{a}\right)^2 \qquad (1.12)$$

where $\xi_{n'L}$ is a n'-th root of the spherical Bessel equation of the L-th order $j_L(\pi\xi_{n'L}) = 0$. The last term of the right hand side of Eq. (1.12) shows the quantized kinetic energy of the exciton due to the confinement effect. n' (=1, 2, 3) represents a confined principle quantum number, and L (=0, 1. 2,...) represents the orbital quantum number which determines the angular momentums in this system. Consequently, the quantum confined states of the exciton are labeled as 1S, 1P, 1D,.. 2S, 2P, 2D..., 3S, 3P,... . The exciton energy of the lowest state (1s, 1S) is

$$E_{ex}(1s, 1S) = E_g - E_{Ry} + \frac{\hbar^2}{2M_{ex}}\left(\frac{\pi}{a}\right)^2 \qquad (1.13).$$

As a result, the energy shift of the lowest-energy exciton ΔE resulted from the confinement effect is expressed by

$$\Delta E = \frac{\hbar^2}{2M_{ex}}\left(\frac{\pi}{a}\right)^2 \qquad (1.14).$$

1.5.2 Strong confinement

In the case that the radius of the spherical particle is sufficiently smaller than exciton effective Bohr radius, also the internal motion of the exciton is influenced by the quantum confinement. Here, let us consider a simple confinement model that an electron and a hole are affected individually by quantum confinement and the Coulomb interaction between them is negligible.

The energy of the e–h pair in such system can be expressed by

$$E_{\text{e-h}}(n_e l_e, n_h l_h) = E_g + \frac{\hbar^2}{2m_e}\left(\frac{\pi\xi_{n_e l_e}}{a}\right)^2 + \frac{\hbar^2}{2m_h}\left(\frac{\pi\xi_{n_h l_h}}{a}\right)^2 \qquad (1.15),$$

where n_e, l_e and n_h, l_h represent a principal quantum number and an orbital quantum number of quantum confined states of the electron and hole, respectively. The energy shift of the lowest e–h pair state ($1s_e$, $1s_h$) is expressed by

$$\Delta E = \frac{\hbar^2}{2m_e}\left(\frac{\pi}{a}\right)^2 + \frac{\hbar^2}{2m_h}\left(\frac{\pi}{a}\right)^2$$

$$= \frac{\hbar^2}{2\mu_{ex}}\left(\frac{\pi}{a}\right)^2 \qquad (1.16).$$

From this result, we can see that the energy shift is larger than that in the case of weak confinement model, Eq. (1.14) by a factor of M_{ex}/μ_{ex}. Figure 1-4 shows the confinement models of the weak and strong confinement, respectively.

Next, we consider the confinement regime where the e–h pair is confined in the space of the order of the exciton Bohr radius and the Coulomb interaction can not be negligible. The hamiltonian of this system is expressed by

$$H = \frac{p_e^2}{2m_e} + \frac{p_h^2}{2m_h} - \frac{e^2}{\varepsilon|\boldsymbol{r}_e - \boldsymbol{r}_h|} + V(\boldsymbol{r}_e, \boldsymbol{r}_h) \qquad (1.17)$$

$$V(R) = \begin{cases} 0 & (|\boldsymbol{r}_e|, |\boldsymbol{r}_h| < a) \\ \infty & (\text{otherwise}) \end{cases}$$

To solve Eq. (1.17) is rather complicated. However, by treating the Coulomb term as perturbation, several kinds of calculation have been performed with using variational approach. According to the calculation reported by Kayanuma [16], the lowest energy of the e–h pair is obtained as

$$E_{e-h}(1s_e, 1s_h) = E_g + \frac{\hbar^2}{2\mu}\left(\frac{\pi}{a}\right)^2 - 1.786\frac{e^2}{\varepsilon a} - 0.248E_{Ry} \qquad (1.18).$$

The second and third term in the right hand side of Eq. (1.18) show the kinetic energies of the electron and hole and calibration of the Coulombic energy taking account of the shortening relative distance of the e–h pair, respectively. The fourth term indicates the binding energy of the e–h pair by the exciton effect. In this confinement region, the exciton as a particle is strongly deformed, and the electron and hole is affected by quantum confinement individually.

1.6 Exciton properties confined in CuCl quantum dots

CuCl quantum dot shows typical properties of "weak confinement" regime because of the very small exciton Bohr radius (a_B = 0.7 nm). To date, many studies of optical properties of CuCl quantum dots embedded in alkali halide matrices [11, 24 - 26] or glass material [10, 21 - 23] have been performed, and they provided the fundamental and interesting properties of the confined exciton in "weak confinement" regime, for example, the superradiation of the confined exciton [21, 25], large nonlinear susceptibility [23, 24] and persistent hole burning [26], etc. These results indicate that the confined exciton has large coherence overwhelming the quantum dot and it induces the large optical nonlinearity in the mesoscopic system.

In this section, I introduce the previous studies of the quantum size effect on the confined exciton in CuCl quantum dot. First, the relation between the energy shift of the 1s exciton and the size and shape of CuCl quantum dots embedded in NaCl matrix is discussed. Second, the quantum size effect on the higher Rydberg states (2p, 3p...) of the exciton is described.

1.6.1 CuCl nanocrystals in NaCl matrix

As described in the previous section, the quantum size effect on the exciton is explained by two-limiting cases, so-called "strong confinement" and "weak confinement". For CuCl nanocrystal, the quantum size effect on the excitons is considered to show the nature of "weak confinement" because of the small exciton effective Bohr radius. However, it is important to investigate the size and shape of the CuCl quantum dots in a matrix, to discuss more detailed quantum size effect.

For CuCl quantum dots embedded in a NaCl matrix, there was the report that the sizes and shapes of the dots were determined by means of small angle X-ray scattering (SAXS), and the identification of the quantum size effect on the excitons was carried out by taking account into the relation between the dot size and the PL energy of the confined exciton [11].

The SAXS was measured for various samples after the different thermal treatments. The relation between SAXS intensity $I(S)$ and the radius of gyration R_g is expressed as

$$I(S) \propto \exp\left[-\frac{(2\pi S R_g)^2}{3}\right] \qquad (1.19).$$

Here, S is expressed, by using scattering angle 2θ and the wavelength λ of the X-ray, as

$$S = \frac{2}{\lambda}\sin\theta . \qquad (1.20)$$

Figure 1-5 shows the exciton PL spectra of CuCl quantum dots in NaCl, in which R_g were obtained by the results of SAXS. The PL spectrum of sample 01, which was not performed heat treatment, has the small peak at the Z_3 exciton energy of 1s state in the CuCl bulk crystal and the main peak at the higher energy side. As R_g is decreased, the PL peak energy is shifted to the higher energy side and the PL band becomes broadened with long tail to the higher energy side. This broadening of the PL band is related to the blueshift of the PL energy and reflects the size-distribution of the quantum dots.

When it is assumed that the shape of the quantum dot is spherical, the radius of the dot a is obtained as follows:

$$a = \sqrt{\frac{5}{3}} R_g \qquad (1.21).$$

Following this assumption, the PL peak energy is plotted versus the dot radius a in Fig. 1-6, together with some calculated lines of the quantum size confinement with using exciton parameters of CuCl. Solid curves of 1 and 2 were obtained by Eq. (1.16) and (1.14) assuming of "strong confinement" and "weak confinement", respectively. The experimental values are close to the curve 2. Furthermore, line 2' was obtained by taking account of the dead layer, the thickness of which is estimated to be $0.5a_B$. The experimental values agreed well to this line. From this result, for the CuCl quantum dots in NaCl matrix, the energy shift of the 1s exciton ΔE due the quantum size effect is expressed as

$$\Delta E = \frac{\hbar^2}{2M_{ex}} \left(\frac{\pi}{a^*} \right) \qquad (1.22)$$

$$a^* = a - 0.5a_B . \qquad (1.23)$$

Here, a^* is defined as effective dot radius.

1.6.2 Excited states of the exciton confined in CuCl quantum dots

It have been revealed that quantum size effect on the exciton of lowest 1s state in CuCl quantum dots can be explained by weak confinement. However, the study on the excited exciton states (2s, 2p,...) is also important and interesting. The quantum size effect on the excited excitons is expected to be different from that of the lowest exciton because of their larger or anisotropic wave functions.

Yamanaka and co-workers reported the infrared transient absorption (IRTA) attributed to the transition between Rydberg 1s and 2p states of confined exciton for CuCl quantum dots embedded in NaCl matrix by means of pump-probe spectroscopy [53]. They used the second harmonic (SH) light of Ti:sapphire laser pumped by Q-switch YAG laser (pulse width: 15 ns, repetition rate: 10 Hz) as a tunable pump light and pulsed Xe lamp (pulse width: 8 μs) with MgF_2 window as a probe one with time resolution of several ns.

Figure 1-7 shows a typical temporal decay profile of the observed transient absorption at 77 K. The IRTA exhibits two decay components. The decay time of the

faster component (τ_1) was estimated to be less than 1 ns by taking into account the temporal pulse profile of the pump light. The fast component was concluded to be originated from the transition from Rydberg 1s to 2p state of the exciton since the decay time is consistent with that of the exciton (~380 ps [33]) and the size-dependence of the transition energy which is mentioned later.

On the other hand, the decay time of the slow component (τ_2>>100 μs at 77 K) was increased up to ~10 ms with decreasing the sample temperature to 4.2 K. This persistent IRTA does not show the simple exponential decay but the logarithmic decay behavior. This decay feature is similar to that of the hole-burning phenomena reported in CuCl or other semiconductor nanocrystals [26]. From these results, the origin of the slower component was concluded to be some trapping centers of carriers, which is induced by the intense laser excitation at or near the interface between the dots and NaCl matrix.

Figure 1-8 shows the IRTA spectra of the fast decay component. It was observed that the absorption peak energy increased monotonously with decreasing the effective radius of the dots under the size-selective excitation. As the results, the quantum size effect on the 2p-like states of the exciton is much deviated from the "weak confinement" regime toward to the "strong confinement" regime, since the energy shift of the 2p exciton due to the confinement effect is larger than that of the 1s exciton. This is owing to the fact that the effective Bohr radius of the 2p-exciton is lager twice or four times than that of the 1s exciton, so that the confinement effect on the relative motion between the electron and hole has to be take into account. In other words, the Rydberg energy of the confined exciton has dot size dependency.

On the other hand, Uozumi and Kayanuma reported theoretically the energy levels of the exciton confined in a spherical quantum dot in a weak confinement regime within the effective mass approximation (EMA) [54, 55]. In this report, the exciton states were denoted by different sets of two quantum numbers which are different among the two limiting cases that are determined by the relative ratio of the exciton Bohr radius and dot radius.

In the case that the dot radius is larger than the exciton Bohr radius, the confined exciton state are denoted by (*nl*, *n'L*). Here, *nl* shows the exciton Rydberg states (1s, 2s, 2p, 3s, ···) and *n'L* shows the quantum confined states of the tranlational motions of the exciton (1S, 1P,··, 2S, 2P,··, 3S, 3P,··,). On the other hand, for the smaller dot size where the confinement effect on the relative motion of the electron and hole is no

more negligible, the confined exciton states are expressed by (n_el_e, n_hl_h). Here, n_el_e (n_hl_h) indicates the quantum confined states of the electron (hole).

Figure 1-9 shows the calculated IRTA spectra due to the transition from the lowest exciton (1s, 1S) state to the higher excited states denoted in the figure. The vertical line indicates the transition energy and oscillator strength of each transition, and the continuous curve with finite spectral width was obtained by the convolution of a Gaussian function with $0.1E_{Ry}^*$ width (HWHM). For the larger dot ($R/a_B > 3$), the IRTA peak is dominated with the transition to the (2p, 1S) state, and the IRTA spectra has a asymmetric shape with a tail to the higher energy side, showing contributed by the higher excited states other than the (2p, 1S) states. The transition energy between 1s and 2p state increased with decreasing the dot radius. The dot-size dependency of the IRTA peak energy experimentally almost coincides fairly well with that of the theoretical calculation, as shown in Fig. 1-10.

1.7 Biexciton properties confined in CuCl quantum dots

The quantum size effect on the biexciton is expected to show the energy shift different from that of the single exciton because of the heavier translational mass and the larger effective radius. As a result, the biexciton binding energy, which is defined by the difference energy between twice the single exciton energy and the biexciton energy, depends on the sizes of the quantum dots. Added to this, in the confinement system like the quantum dot, the excited biexciton state possessing the energy larger than twice the single exciton energy becomes significant for the transition dynamics between the biexciton and exciton states although such biexciton states have been hardly discussed in the case of the bulk crystal.

In this section, I describe the previous works on the confined biexciton properties in CuCl quantum dots, with respect to the energy levels and the transition dynamics.

1.7.1 Energy levels and oscillator strength of confined biexcitons

One exciton and two-exciton pair (biexciton) states in a spherical dot in the weak confinement regime were investigated, and the energies and oscillator strengths of

several exciton and biexciton states were calculated by Nair and Takagahara [36, 37]. They investigated the transition energy and oscillator strength from the lowest exciton Γ_5 state with j = 1 to the biexciton states with J = 0, 1 and 2. Here, there are two biexciton states with J = 0; a bound exciton pair and an unbound pair, respectively. Namely, the bound exciton pair (J = 0) is the "lowest biexciton" state, and the unbound states of J = 0, 1 and 2 are called "excited biexciton" states.

Figure 1-11 shows the transition dipole moments for the transition from the ground (denoted by 0) to the j = 1 exciton state (X_{10}) and for those from the exciton states (X_{00}, X_{10}, X_{11}) to the various biexciton states (BX, XX0, XX1, XX2). Here, the exciton states are denoted by $X_{j,jz}$, assuming that the incident light has z-polarization. On the other hand, the biexciton states are denoted by BX for the bound exciton pair (the lowest biexciton state) or XX*J* for unbound biexciton states (excited biexciton states). The noticeable feature in the Fig. 1-11 is that the transition dipole moment to the J = 2 state (XX2) is the strongest among those from the exciton to the biexciton states.

Figure 1-12 shows the energies of the induced absorption from the exciton to the biexciton states of J = 0 or 2 as a function of the lowest exciton energy. The strongest excited-state absorption due to the J = 2 biexciton state has a nearly linear dependence on the exciton energy with a slope of about 2.4. By invoking the tranlational mass confinement picture, it is speculated that the weakly correlated exciton pair has an energy equal to that of two excitons independently confined in a region of half the volume of the dot. According to this assumption, the confined kinetic energy of the weakly correlated exciton pair is $2\times\sqrt[3]{4}=3.174$ times that of a single exciton. Consequently, the corresponding excited-state absorption energy will shows the linear dependence on the exciton energy with a slope about $3.174-1\approx 2.2$, in close agreement with the calculated value.

Masumoto and co-workers reported the transition energy from the lowest exciton to the biexciton states for CuCl quantum dots embedded in NaCl matrix by means of pump-probe spectroscopy [30, 31]. Figure 1-13 (b) shows the differential absorption spectra with the resonant excitation of confined exciton in the quantum dots. The induced absorption due to the transition from the exciton to the lowest and excited biexciton states were observed as the dips indicated by the open and close triangles. Figure 1-14 shows the excitation energy dependence of the absorption change. It is consistent with the theoretical results shown in Fig. 1-12 and the observed excited

biexciton state is associated with the state of J = 2. Experimentally, the exciton energy dependence of the transition energy to the excited biexciton state shows linear with a slope of 2.0.

1.7.2 PL energy of biexcitons confined in CuCl quantum dots

For CuCl quantum dots embedded in NaCl matrix, Itoh reported the PL energies of the biexciton as a function of the exciton energy [32].

The PL spectra was obtained by using the pulsed dye laser with a peak power of several hundred kW/cm^2 pumped by a N_2 laser. When the exciton absorption band, which is inhomogeneously broadened due to the dot size distribution, is selectively excited, pairs of position-changing peaks which are dependent on the excitation energy appear superimposition the PL bands of M and Ex as indicated by 1 and 1', 2 and 2' etc. in Fig. 1-15. It is suggested that the peaks denoted as *n'* in the M band are PL due to the biexcitons confined in quantum dots of the same sizes for the confined excitons indicated by peaks *n* in the Ex band. The energy relations between n and n' are shown by open squares in Fig. 1-16, together with that of the PL peaks of the Ex and M bands which were obtained for the samples with different dot size by the band-to-band excitation (open circles). When the radius of the biexciton is sufficiently smaller than the dot size, it is assumed approximately that the center-of-mass motion of the biexcitons is affected by quantum confinement. On this assumption, the energy shift of the biexciton PL in a spherical quantum dot of the radius a is expressed as the following equation.

$$\Delta\hbar\omega_m = -\frac{\hbar^2}{2}\left(\frac{1}{M_{ex}} - \frac{1}{M_m}\right)\left(\frac{\pi}{a}\right)^2 \qquad (1.24)$$

Here, M_{ex} and M_m are translational masses of the exciton and biexciton, respectively. The size dependence of the biexciton PL energy obtained by this equation, using the mass relation of $M_m = 2.3M_{ex}$ in the bulk crystal, is expressed by dashed line in Fig. 1-16. Here, the low-energy shift experimentally obtained is well reproduced for $a \geq 3$ nm. As a result, the effective radius of the biexciton was estimated to be ~3 nm which is nearly four times larger that the effective Bohr radius of the exciton. For $a < 3$ nm, on the other hand, the PL peaks experimentally obtained shows the high-energy shift and the confinement model of center-of-mass motion of the biexciton does not seem to be

applicable because the internal motion of the biexciton is deformed. In this case, the biexciton binding energy depends on the dot size, and it is given by

$$E_m^b(a) = E_{ex}(a) - \hbar\omega_m(a) \qquad (1.25)$$

The biexciton binding energy is increased as the dot size is decreased, and this tendency is qualitatively consist of the theoretical report. In addition, the reason for the difference of the open squares and circles in the case of $a < 3$ nm is that giant oscillator strength of the transition between the exciton and the biexciton is in proportion to the volume of the biexciton. That is to say, when volume of the quantum dot is smaller than that of the biexciton in the bulk crystal, giant oscillator strength decreased with the dot volume, so that PL efficiency decreases. Accordingly, in the case of the band-to-band excitation, M band, of which band width is resulted from the inhomogeneous broadening owing to the size distribution, has a peak in the lower energy side due to more important contribution from the larger dots.

In Fig. 1-16, the transient absorption energies originating from the transition from the exciton to biexciton state which were obtained by pump-probe spectroscopy which was reported by Masumoto and coworkers are also plotted by closed inverted triangles [31]. The obtained absorption energy does not agree with that obtained by the PL spectra, in particular, for $a < 3$ nm. This is unresolved question.

1.7.3 Transition dynamics of confined biexcitons and excitons

Up to now, the transition dynamics related to the biexciton and exciton in the CuCl quantum dots in NaCl matrix have been investigated by means of time-resolved luminescence obtained by using a streak camera or by using the up-conversion method with temporal resolution of the subpicosecond, and the optical gain and induced absorption obtained by subpicosecond pump-probe spectroscopy [33 - 35]. The energy diagrams related to the exciton and biexciton at the sample temperature of 77 K and 2K are shown in Fig. 1-17.

In the case of 77 K, the biexciton and exciton decay times were reported to be 65 ps and 380 ps, respectively, which were obtained by using the streak camera [33], The formation process from an excited e–h pair to an exciton have been clarified by the analysis of the temporal change of the luminescence obtained by the up-conversion

method, where the cascade relaxation model which is drawn in Fig. 1-18 have been suggested. As a result, the formation time of the exciton is estimated to be 1.6 ps.

On the other hand, the dynamics process of the excitons at 2 K is more complicated than that at 77 K because of the coexistence of "free" and "bound" excitons, and of "free" and "bound" biexcitons. The decay times of bound exciton, bound biexciton and free biexciton were reported to be 800, 70, and 125 ps, respectively, which were obtained by using the streak camera and by the absorption changes for the bound biexcitons and free biexcitons obtained by pump-probe spectroscopy. In addition, also the transition rate of the non-radiative relaxation between them were proposed by analyzing the time-resolved luminescence obtained by the up-conversion method similarly to the case of 77 K. The obtained values are shown in Fig. 1-18.

From these previous reports, it is concluded that the transition dynamics of the biexcitons and excitons confined in the quantum dots can be explained by the cascade relaxation model.

1.8 Motivations and purpose

Up to now, optical properties of biexciton states confined in CuCl quantum dots have been studied extensively. However, many unresolved properties still remains.

First, dot-size dependence of the biexciton energy is still ambiguous. The biexciton energy has been investigated by the two methods until now; one is the transient absorption from the exciton to the biexciton, and another is PL energy relation between the biexcitons and excitons. However, these results are not consistent quantitatively. The answer to this question has been asked because it is one of the most important information in order to evaluate a variety of optical properties associated with the confined biexcitons. I propose that two-photon excitation of the confined biexciton is expected to derive this answer. Since the direct creation of the biexciton by two-photon absorption gives rise to simple relaxation process of the biexciton and exciton in a dot, the analysis of the confined biexciton energy is expected to be easy and it become possible to examine the differences between the absorption energy and luminescence energy of the biexicitons. However, there is no report on the two-photon excitation of

the biexciton in CuCl quantum dots. Therefore it is necessary first thing to confirm the two-photon excitation process of the confined biexcitons. In addition, it is interesting to investigate how large the two-photon absorption coefficient is and whether the selection rule of the biexciton is kept or not even in confinement system like a quantum dot.

Next, the quantum size effect not only on the lowest state but also on the excited states of the biexciton is an interesting subject. To date, the excited biexciton states (J = 2) composed of weakly correlated two of lowest (Rydberg 1s state) excitons were already studied. The large transition probability from the exciton to the excited biexciton was observed, which never appear in the bulk crystal. Similarly, the excited biexciton states associated with the excitons with higher Rydberg states are suggested to be stable in the quantum dots although such biexciton states have not been reported yet. For confined excitons in CuCl quantum dots, Rydberg 1s – 2p transition has been reported by using the infrared transient absorption [53]. However, in this measurement, the temporal resolution, the spectral resolution and the pump power are insufficient to evaluate the fine energy structure of the confined exciton and biexcitons. Therefore, more sophisticated pump-probe spectroscopy was necessary to study the excited states of the excitons and biexcitons confined in the quantum dots.

In this research work, my goals are to solve these questions about the confined biexciton properties. The points of the purpose of this thesis are summarized as follows:

1. To investigate the resonant two-photon excitation of the confined biexcitons in CuCl quantum dots and confirm the polarization selection rule of the biexcitons for the excitation laser beam.
2. To discuss the dot size dependence and the possibility of size-selective excitation of confined biexciton state by using the two-photon excitation spectroscopy.
3. To investigate the excited excitons and biexcitons by means of the infrared transient absorption (IRTA) by ultrafast pump-probe spectroscopy.

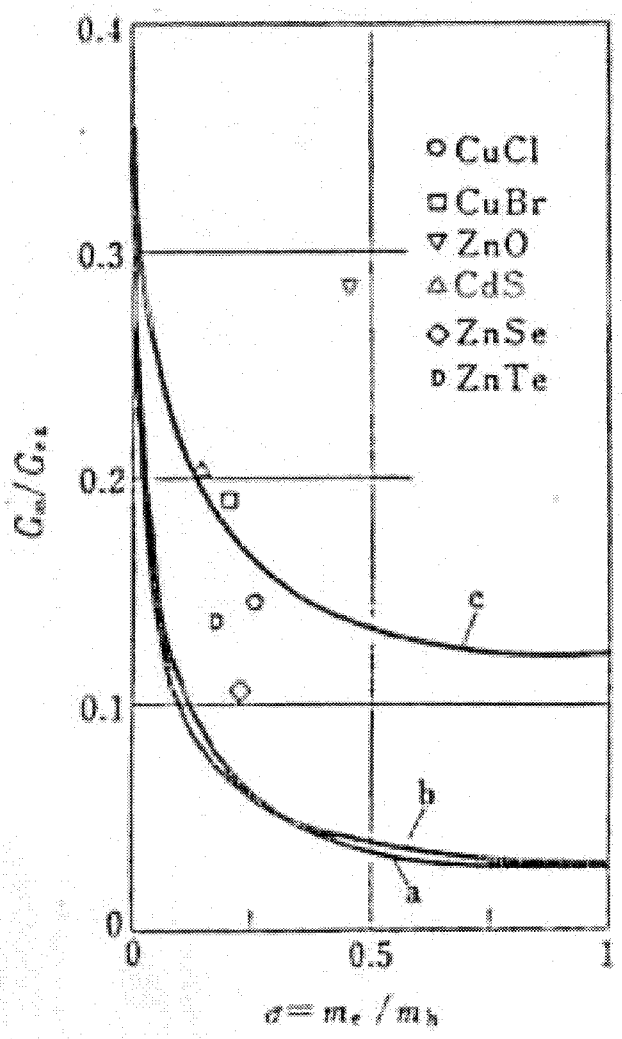

Figure 1-1. Ratio of a biexciton binding energy G_m and an exciton binding energy G_{ex} as a function of the effective mass ratio of an electron and a hole σ. Experimental values for some typical semiconductor are marked, respectively. The solid lines are obtained by theoretical calculations according to a: Akimoto [44], b: Brinkman [45] and c: Huang [46], respectively.

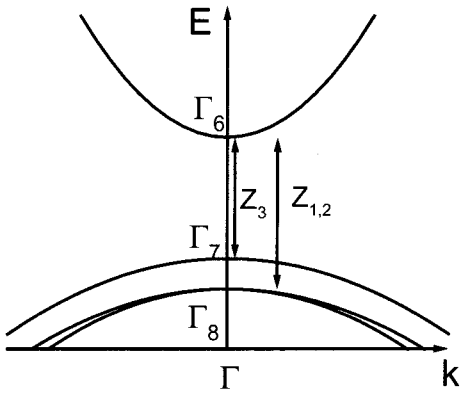

Figure 1-2. Band structure of CuCl crystal.

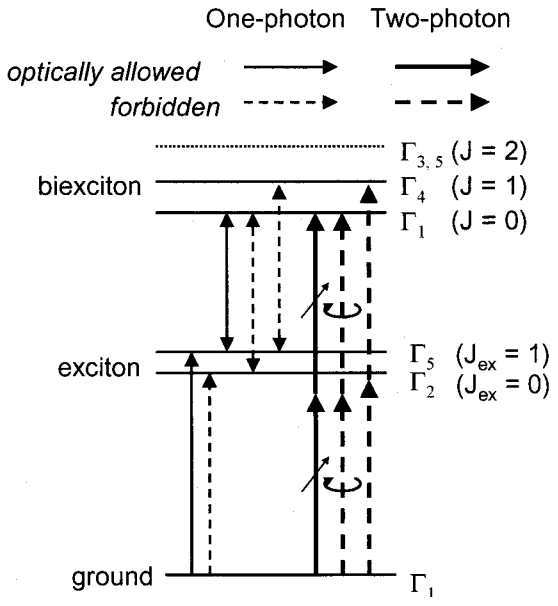

Figure 1-3. Energy diagrams and the selection rules of excitons and biexcitons in CuCl. The thick (thin) arrows show the two- (one-) photon transitions and the solid (broken) lines represent optically allowed (forbidden) transitions. In the case of two-photon absorption of Γ_1 biexciton state with use of single laser beam, the transition is allowed by only the linearly polarized beam [48].

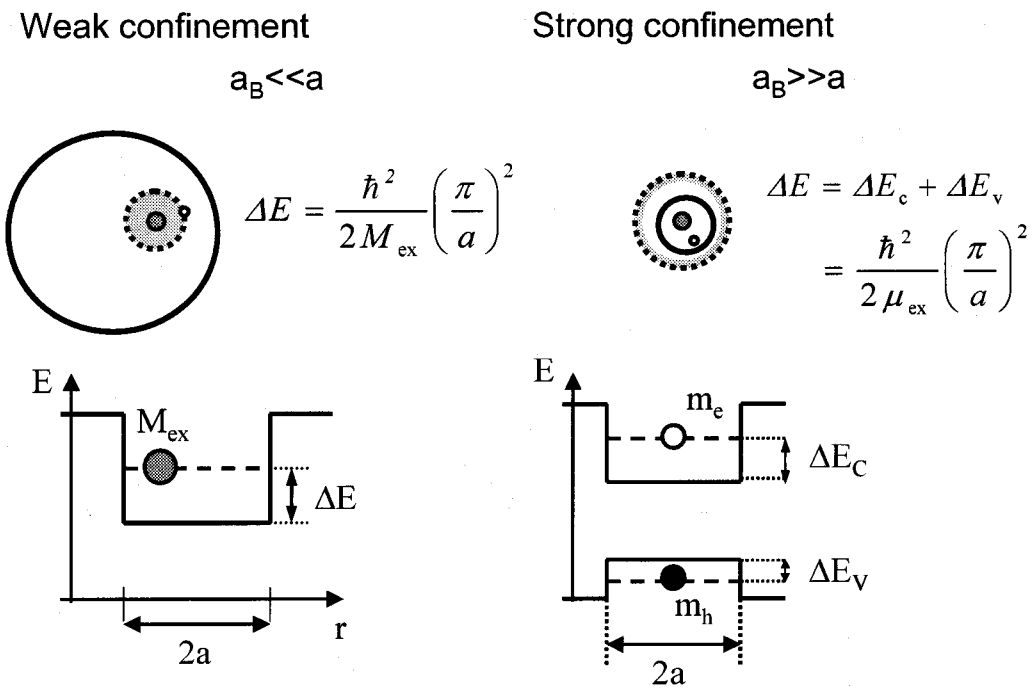

Figure 1-4. Typical regimes of quantum size confinement on an electron–hole pair in a spherical potential well.

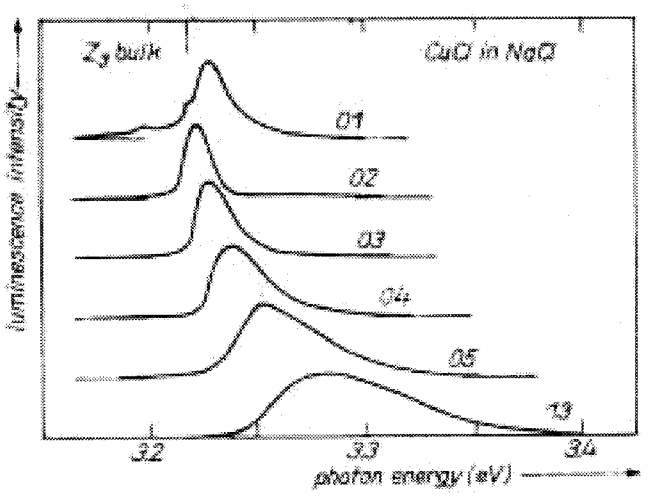

Sample number	R_g (nm)
01	>3.95
02	4.40
03	3.82
04	2.59
05	2.08 ± 0.03

Figure 1-5. PL spectra of CuCl quantum dots with use of a variety of samples (left side). Table on the right side shows the radius of gyration of the samples [11].

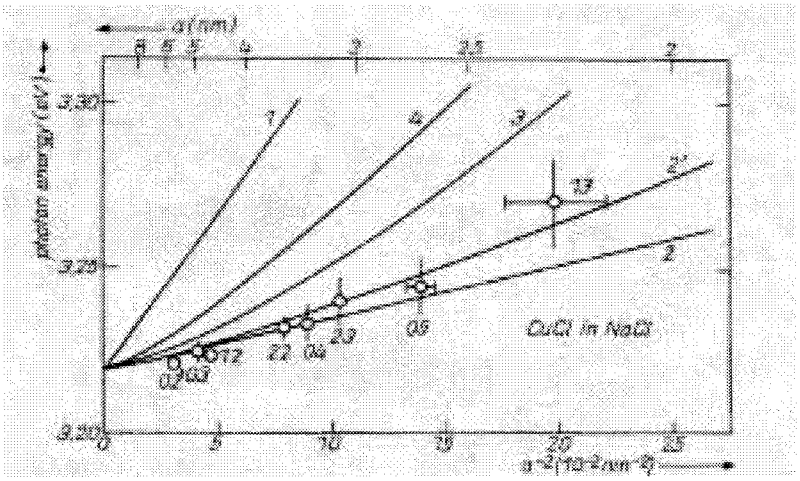

Figure 1-6. Relation between the peak energy of the exciton luminescence and the squared reciprocal radius of the CuCl quantum dots obtained by assuming the spherical shapes [11]. The open circles and solid curves are experimental results and calculated one, respectively. The curves *1* and *2* are obtained by the assumption of "strong confinement" and "weak confinement", which obey Eq. (1.16) and (1.14), respectively. The line *2'* shows the weak confinement model taking a dead layer effect into account, represented by Eq. (1.22). The curves 3 and 4 are obtained according to the variational calculations for three- and one-dimensional confinement, respectively.

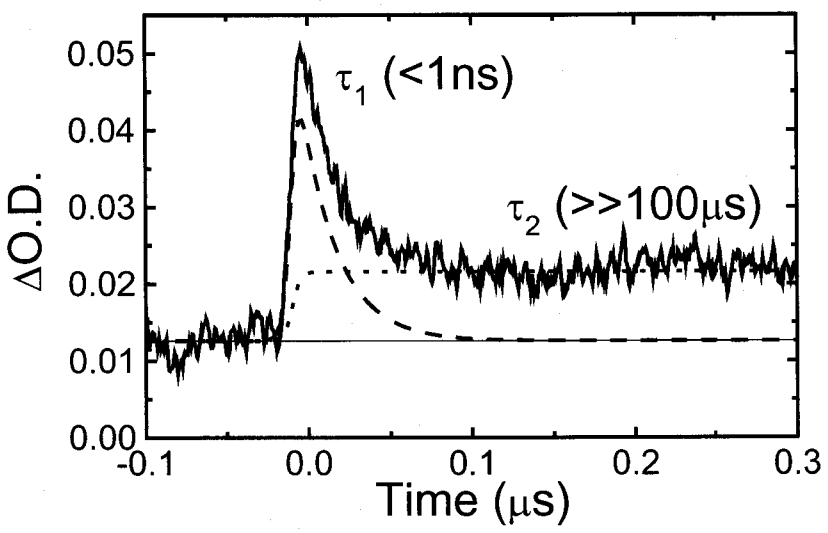

Figure 1-7. Temporal profile of the transient absorption for CuCl qunatum dots at 77 K reported in doctor thesis of Yamanaka [53]. Pump photon energy (wavelength) is 3.230 eV (383.4 nm) that corresponds to the resonant excitation energy of confined exciton in quantum dots with effective radius of ~3.9 nm. Probe photon energy (wavelength) is 210 meV (5.9 μm). Solid line shows the experimental result. The dashed and broken curves shows the fast and slow decay components obtained by the line shape fitting, respectively.

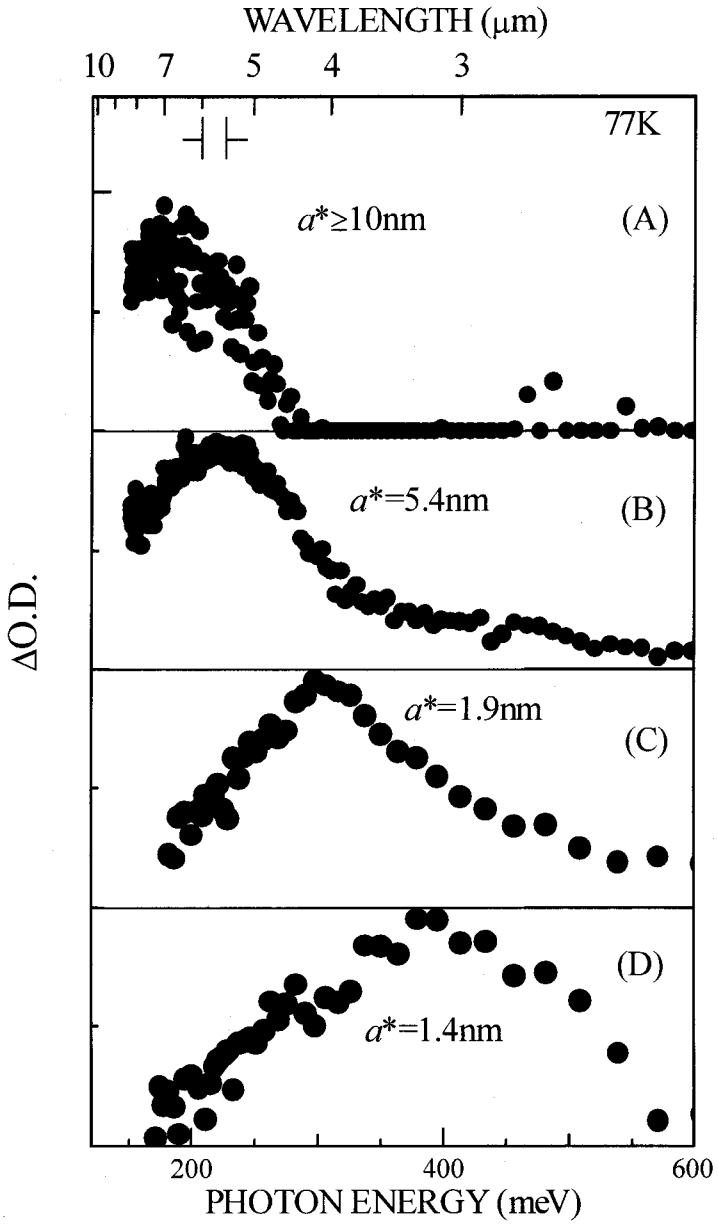

Figure 1-8. IRTA spectra of the fast decay componenet of CuCl quantum dots with different size-selective pumping reported by Yamanaka *et al* [53]. a^* indicates the effective radius of the quantum dot.

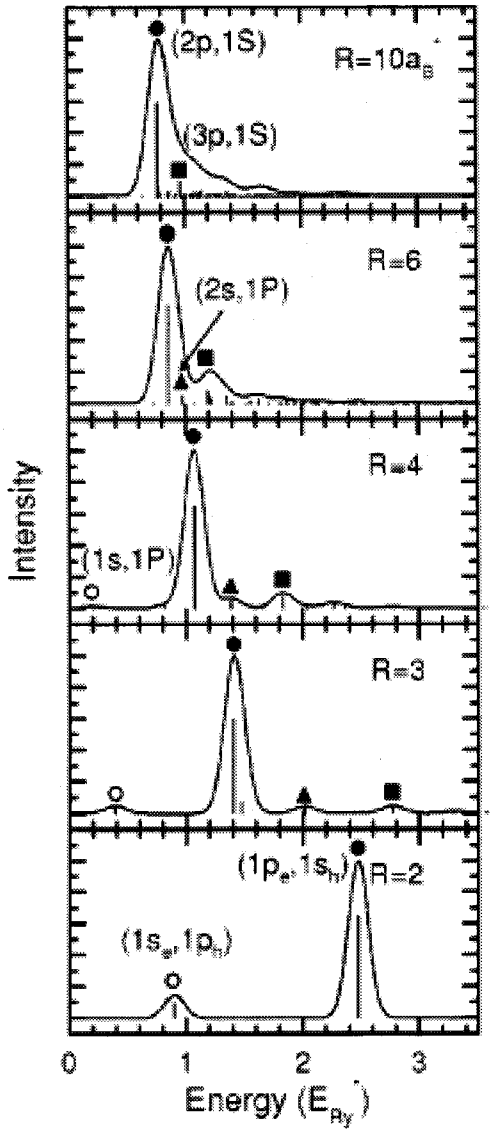

Figure 1-9. Dot-size dependence of IRTA spectra of spherical quantum dots obtained by theoretical calculation [55]. The transition energy is normalized by exciton Rydberg energy E_{Ry}^*. The dot radius, R, is normalized by the exciton Bohr radius, a_B^*. The effective ratio is taken as $m_e/m_h = 0.3$.

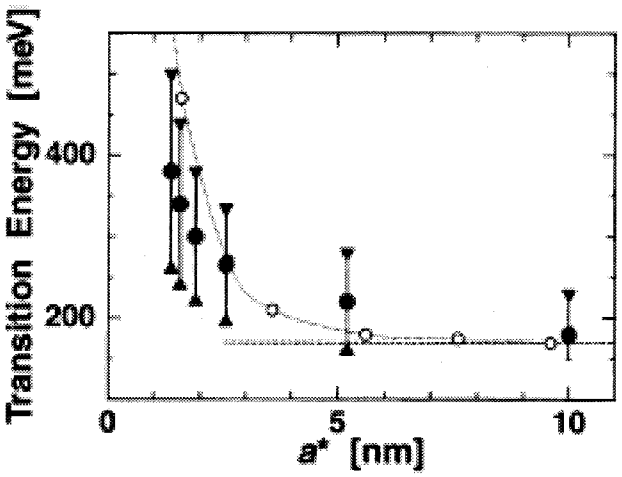

Figure 1-10. The peak energies (solid circles) and bandwidths (distance between a pair of triangles) of the IRTA for the fast component as a function of dot radius a^* [53]. The open circles shows the 1s-2p transition energies obtained by theoretical calculation [54]. The dotted line is a guide to the eye. The broken line indicates the energy separation between 1s and 2p exciton states for CuCl bulk crystal (170 meV) reported in Ref. [20].

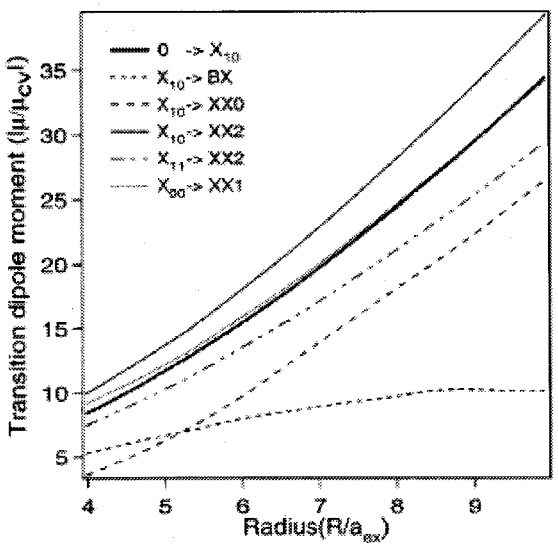

Figure 1-11. Dot radius dependence of the transition dipole moments for the ground-to-exciton and exciton-to-biexciton transitions. The ground, exciton and biexciton states are denoted by 0, $X_{j,Jz}$ and XX*J*. [37]

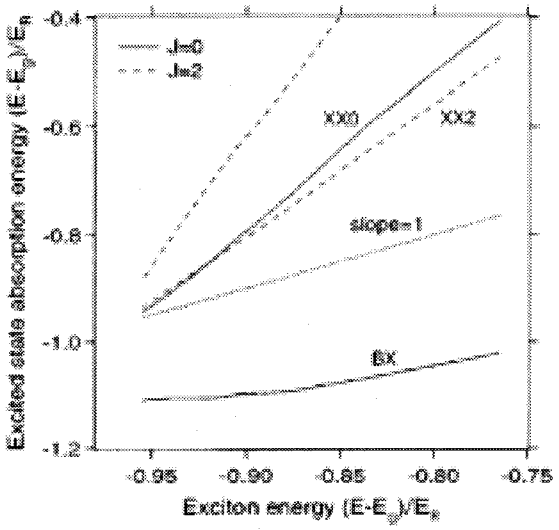

Figure 1-12. The induced absorption energies of the two-exciton states as a function of the exciton energy obtained by theoretical calculation. E_R and E_g indicate the exciton Rydberg energy and band gap energy, respectively [37].

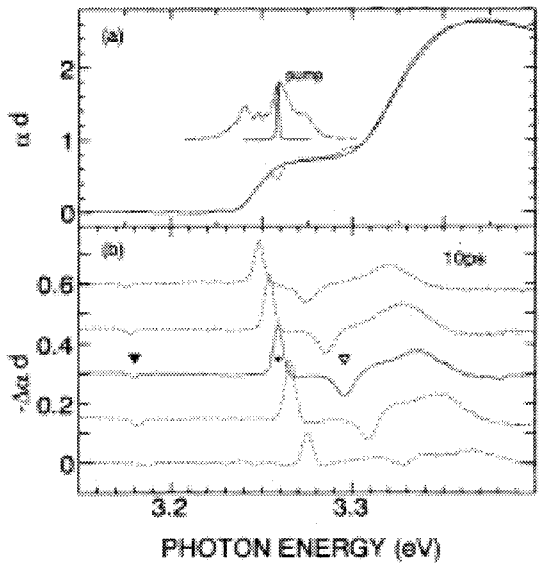

Figure 1-13. (a) The solid and dotted line show the absorption specta without and with pump light, respectively. (b) The change of the absorption spectra induced by the pump light. The closed and opened circles indicate the induced absorption to the lowest and excited-biexciton states [31].

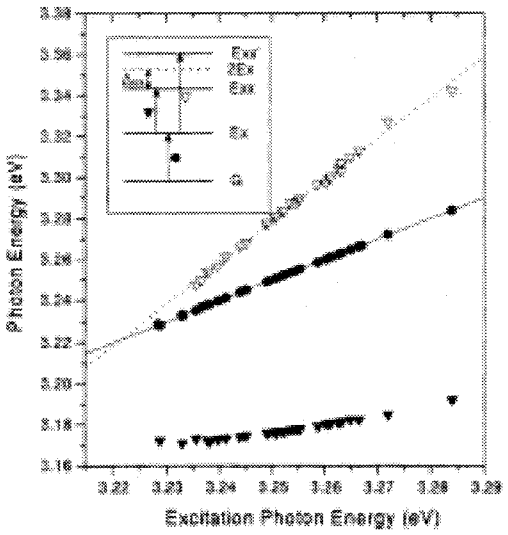

Figure 1-14. The induced absorption energies of the lowest biexciton (closed inversed triangles) and excited biexciton (opened inverted triangles) as functions of excitation photon energy. The closed circles indicated the excition energy [31].

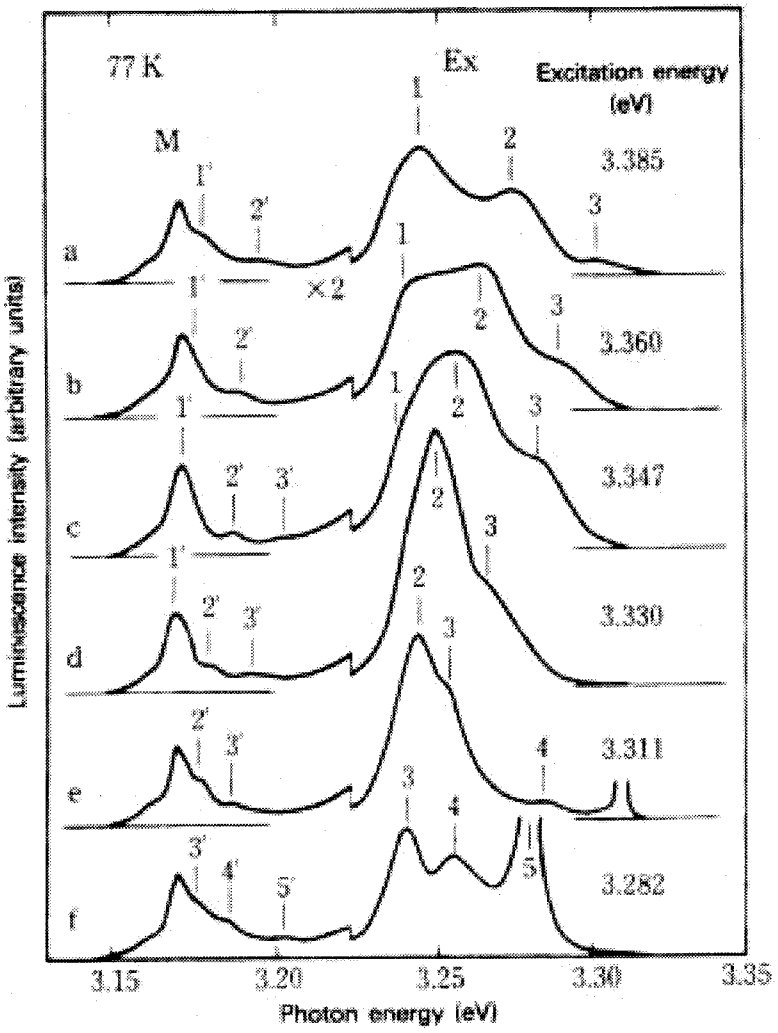

Figure 1-15. The excitation energy dependence of the PL spectra of the biexcitons (M) and the excitons (Ex) for CuCl quantum dots at 77 K. The excitation energy is shown on the right. 1 and 1'. 2 and 2', etc. represent the peak energy appearing as pairs in the M and Ex PL bands [32].

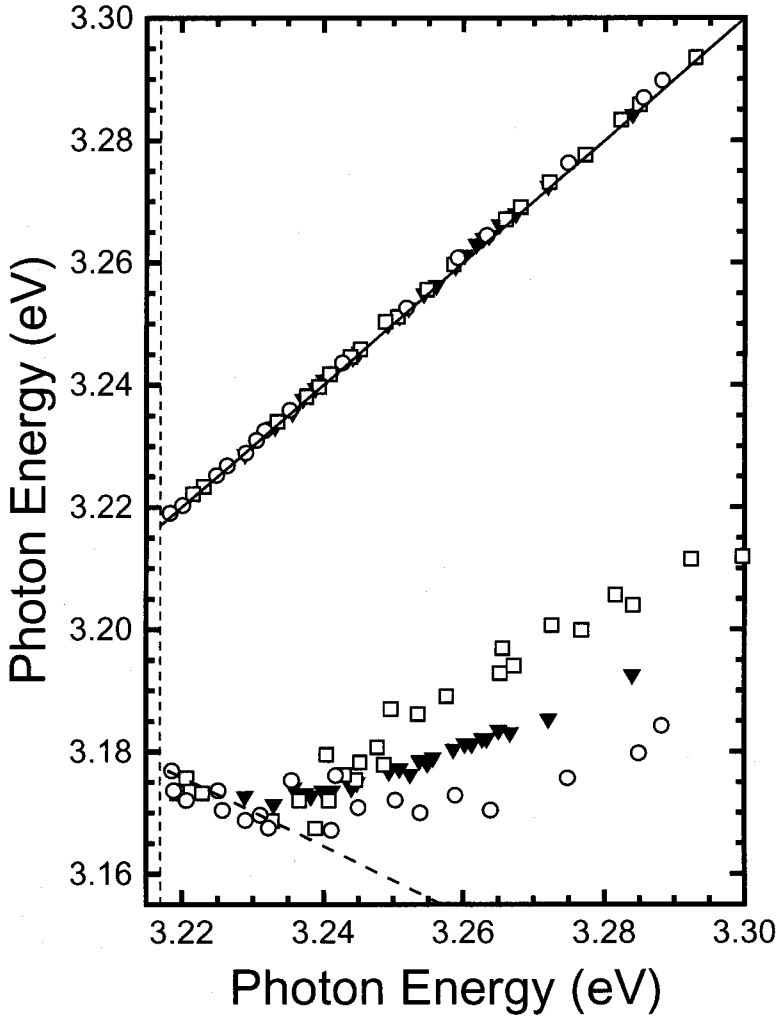

Figure 1-16. The relationship between the peak energy in the PL bands of the exciton (Ex) and the biexciton (M), which are reported by Itoh [32]. The open squares and circles show the data obtained with the band-to-band excitation and the selective excitation, respectively. The dashed line shows the energy relationship calculated under the assumption of confinement model for the center-of-mass motion of the biexcitons. The closed triangles show the transient absorption energies as a function of the excitation energies, which were reported by Masumoto *et al* [31].

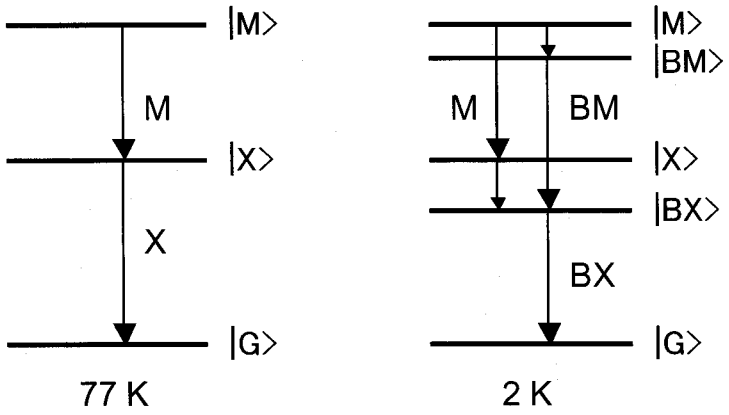

Figure 1-17. Energy diagrams of the excitons and biexcitons confined in CuCl quantum dots at 77 K (right side) and 2 K (left side). Symbols |G⟩, |X⟩, |BX⟩, |M⟩, |BM⟩ represent the states of a ground, free exciton, bound exciton, free biexciton, and bound biexciton, respectively. The vertical and dotted lines represent the radiative and non-radiative relaxation.

77K

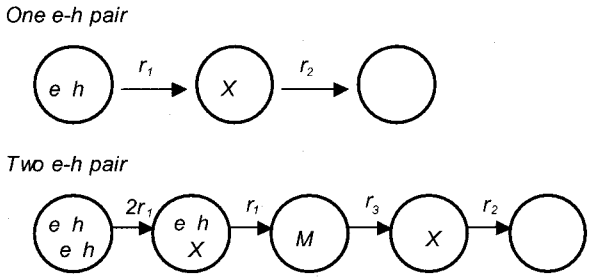

2K

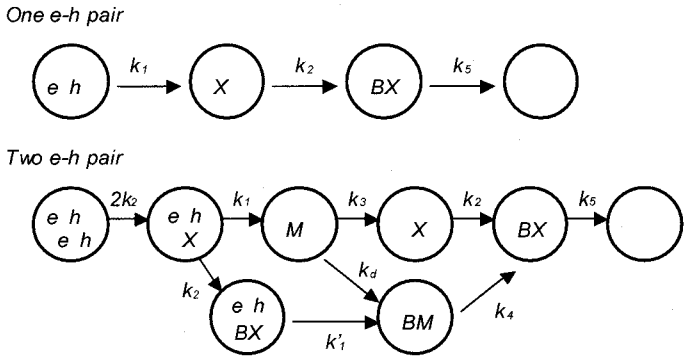

Figure 1-18. The scheme of the cascade relaxation process at 77 K and 2K when one or two *e–h* pairs are initially created in a nanocrystal. The characters, e, h, X, M, BX and BM, denote an electron, a hole, an exciton, a biexciton, a bound exciton and bound biexciton, respectively. r_1, r_2, r_3, in the case of 77 K denote the transition rates of e–h pair state to the X state, of the X state to the ground state, and of the M to the X state, respectively. k_i (i = 1 – 6 and d) and k_1' in the case of 2 K denote relaxation rates from a high state to a low state, similarly to the case of 77 K. For the average effective radius ~4.2 nm, these relaxation rate was reported as follows: $1/r_1$ = 1.6 ps, $1/r_2$ = 400 ps, $1/r_3$ = 70 ps at 77 K, and $1/k_1$ = 1.3 ps, $1/k_1'$ = 1.8 ps, $1/k_2$ = 1.4 ps, $1/k_3$ = 120 ps, $1/k_4$ = 30 ps, $1/k_5$ = 800 ps, and $1/k_d$ = 30 ps at 2K, respectively [35].

Table 1-1. Physical constant of CuCl bulk crystal

lattice constant	a_L	0.54 nm (298 K) [56]
band gap energy	E_g	3.399 eV (4 K) [20]
effective masses		
electron (Γ_{6c})	m_e	$0.5m_0$ [57]
hole (Γ_{7v})	m_h	$1.8m_0$
dielectric constant	ε_∞	3.6 [58]
Z_3 exciton states		
1s	E_{1s}	3.218 eV (77 K) [59]
3.202 eV (2 K)		
2s	E_{2s}	3.266 eV (2 K) [20]
2p	E_{2p}	3.372 eV (2 K) [20]
exciton binding energy		
Z_3(1s)	G_{ex}	197 meV [20]
effective exciton Rydberg energies for $n \geq 2$		
Z_3 s-series	E_{Ry}	131 meV [20]
Z_3 p-series	E_{Ry}	109 meV [20]
effective exciton Bohr radius		
Z_3(1s)	a_B	0.7 nm (4.2 K) [60]
effective masses of transverse Z_3 exciton		
translational mass	M_{ex}	$2.3m_0$ [61]
reduced mass	μ_{ex}	$0.39m_0$ [62]
biexciton binding energy		
	E_b	32 meV [39]

Chapter 2

Experimental Setup

2.1 Sample preparation

The samples used in this experiment were CuCl quantum dots embedded in NaCl matrix, which were produced by Itoh *et al.* [11], and aged for about fifteen years old to stabilize the supersaturation. The preparation method was already described in the reference, so that it will be described simply as follows.

1. NaCl powder placed in a quartz tube was heated with vacuum pumping to get rid of gaseous impurities to purify NaCl which is used as a matrix. In addition, it was melt at 820 °C in sealed quartz tube with 0.9 atm Cl_2 gas, so that NaCl ingot free from water was obtained.
2. CuCl flakes were added to the NaCl ingot at 1 mol% concentration and they were sealed together with H_2 gas of 0.3 atm in the quartz tube.
3. CuCl flakes and NaCl ingot were melted in a transverse Bridgman furnace, and NaCl was crystallized from one end by moving the furnace slowly (2 cm/day). As a result, single crystals of NaCl doped with Cu^+ were grown.
4. The prepared crystals were quarried out to be about 5×5×5 mm, then a subsequent annealing process makes the coagulation of Cu^+ ions to form small crystallites of the order of several nm in size.

During the annealing process, it is possible to control the average size of the dots by changing annealing temperature and time. The average size becomes larger (~ 10 nm)

when the annealing temperature is low, that is 200 ~ 300 °C, whereas it becomes smaller (~ a few nm) when the temperature is raised to 500 ~ 600 °C. The samples were annealed for several hours in Ar gas atmosphere of 0.3 atm which was used to prevent the evaporation of CuCl from NaCl matrix.

The obtained crystals were cleaved to be suitable for the optical measurement. Optical density of the samples is 1 ~ 2 at the peak energy of the absorption band of Z_3 exciton.

2.2 Tunable *ps* pulse laser system

I have studied confined biexcitons in quantum dots by means of two-photon excitation spectroscopy and mid-infrared transient absorption spectroscopy, so that the excitation light has been required to possess following specifications for these experiments. First, it is necessary that the excitation light intensity is strong enough to excite at least one biexciton in considerable amounts of the quantum dots. The estimation of the light intensity for exciting one biexciton in all of the quantum dots on average will be discussed later. Second, a short pulse width is required in order to resolve the decay components attributable to the excitons and biexcitons in the transient absorption spectroscopy. The decay times of the excitons and biexcitons confined in the CuCl quantum dots are reported to be about several hundreds and tens of picoseconds [33]. Accordingly, the pulse width is necessary to be less than ten ps. Furthermore, a narrow spectral width is required for the size-selective excitation of the excitons and/or the biexcitons because the absorption band of the confined excitons is broadened due to the size distribution of the quantum dots. It is desirable that the spectral width of the laser is nearby the Fourier transform limit of the pulse width.

I have used the laser system based on *ps* dual optical parametric amplifiers (OPAs) pumped by a regeneratively amplified mode-locked Ti:sapphire laser pulses, which meet aforementioned requirements as the pump and probe light sources for my research work.

The *ps* dual OPA system comprises the lasers and amplification systems provided by Spectra Physics. OPA systems have been now introduced in many laboratories but most

of them are, in general, *fs* OPA systems. The *ps* OPA requires higher pump power for stable operation in comparison with *fs* OPA operate since the wavelength-conversion efficiency of the *ps* pulse is lower than that of the *fs* pulse due to the low peak intensity. In addition, the higher pump power is necessary to operate two OPAs simultaneously. Therefore, the amplification system is figured out to generate higher pump power than the ordinary one. I will explain functions of this laser system, outline of which is shown in Fig. 2-2.

2.2.1 Amplification system

The laser light from a mode-locked Ti:sapphire laser (Tsunami, wavelength: 799nm, repetition rate: 82 MHz, pulse width: ~100 fs) pumped by a diode-pumped cw visible laser (Millennia, wavelength: 532 nm, output power: ~5 W) is used as a seed light in this laser system. The spectral width of the seed light is more than 10 nm, and the output power is about 1 W.

The laser light from the mode-locked Ti:sapphire laser is amplified by a Ti:sapphire amplifier (Spitfire) pumped by intra-cavity doubled Nd:YLF pump laser (Merlin, wavelength: 527 nm, repetition rate: 1 kHz, pulse width: ~250 ns, output power: ~20 W).

Spitfire comprises three main parts, so-called, Ti:sapphire amplification system, optical pulse stretcher and optical pulse compressor. The technique of chirped pulse amplification, the principle of which is shown in Fig. 2-3, is used to remove the limitation of the amplification, which comes from self-focus destructivity of the amplified pulse for a Ti:sapphire crystal. The peak energy of the pulse is reduced significantly by stretching the pulse width, then the stretched pulse with lower-peak intensity is amplified. After the amplification, the pulse is recompressed to the short pulse width.

Pulse stretching and compression are achieved with the use of diffraction gratings. In the pulse stretcher, the input beam is incident on a diffraction grating, causing the light with different wavelengths to disperse. The grating can be configured in such a way that the shorter wavelength components have to travel longer through the stretcher than the longer wavelength components. A single grating is used in the stretcher, and spatially reconstruction of the stretched pulse is ensured by passing the grating four times. Pulse compression is essentially the reverse of the pulse stretching, in which, however, the

grating is arranged so that the shorter wavelength components travel shorter path and catch up the longer components.

In the *ps* amplifier, the spectral mask is placed inside the pulse stretcher to select the small portion ($\Delta\lambda$: ~1 nm) of the seed spectrum to achieve the narrow spectral width, as shown in Fig. 2-4. The stretched pulse with the narrower spectral width results in a few ps pulse after the compressions, which is close to the Fourier transform limit.

The amplification system comprises two parts, that is, a Ti:sapphire regenerative amplifier and Ti:sapphire external amplifier. The layout of these amplifiers is shown in Fig. 2-5. Pump laser beam from Merlin is split into two beams, then both beams is used for pumping the Ti:sapphire crystals in the regenerative amplifier and external amplifier, respectively.

The principle of the regenerative amplification is first the confinement of a single pulse selected from a mode-locked pulse train by polarization rotation followed by the amplification to an appropriate power level, and finally the production of cavity dumped output.

The seed pulses coming from the pulse stretcher are injected into the cavity of the regenerative amplifier through the reflection at the Ti:sapphire rod (R1). The pulse passes through a $\lambda/4$ wave plate (WP) and an input Pockels cell (PC1), and it is reflected by mirror and thus retraces its path. Because it doubly passes the WP, the polarization has undergone a $\lambda/2$ rotation and is transmitted by the R1 and other optical components with Brewster angle with respect to the optical path. When the PC1 is deactivated, a pulse makes a single round-trip and exits again. On the other hand, when the incident single pulse is amplified, the quarter-wave voltage is applied to PC1 as soon as the pulse leaves PC1. The PC1 is now effectively a $\lambda/4$ wave plate and cancels the effect of WP. Thus, the pulse is trapped in the cavity.

After a number of round trip, usually about 20, and that the pulse energy reaches the appropriate power level, a quarter-wave voltage is applied to the output Pockels cell (PC2), causing a half wave rotation to the pulse polarization after it has doubly passed the PC2. The pulse is thus ejected from the cavity by the polarizing beam splitter (P1).

The amplified pulse is amplified further in the external amplifier, by passing though the Ti:sapphire crystals twice to acquire the higher power enough to pump the two OPAs simultaneously.

After the amplification system, the amplified pulse is recompressed in the pulse

compressor, to obtain the pulse width of ~2 ps. The output energy of the Spitfire is ~3 mJ and the repetition rate is 1 kHz. Amplified laser beams is split into two beams and they pump the OPAs, respectively.

2.2.2 Optical parametric amplifier

Figure 2-6 shows the simple layout of the OPA-800P. The amplified input beam is split into two beams by a beam splitter (BS1). Approximately 96 % of the energy is reflected by BS1 and used as a pump beam, and the remains passes through BS1 and used to generate a white light continuum that provides the seed pulse for OPA. A half wave plate (WP) and a cube polarizer (P) are used to polarize the beam horizontally and the stable white light generation is provided by attenuating the beam intensity by an iris. After passing through a delay stage, the generated seed pulse is incident on BBO crystal, which is used for optical parametric amplification.

In the other leg, the major portion of the amplified beam is split into two pump beams by the beam splitter (BS2), then ~15 % of the beam is reflected by BS2, which is used as a pre-amplifier beam in the first stage, and the remainder passed through BS2 is used as a main-amplifier beam in the second stage. In the first amplification stage, the pre-amplifier beam is steered to BBO crystal by using a dichroic mirror D1, which is a high reflector for 750 – 850 nm and highly transmissive for the longer wavelengths. The signal and idler beams generated in the BBO crystal in the first amplification stage pass through the dichroic mirror D2, then the idler beam is diffracted back to the BBO crystal by the grating, which is mounted on a rotation stage on the delay line. The main-amplifier beam is steered to BBO crystal by using D2, where it is overlapped co-linearly with the returning idler beam into BBO crystal in the second amplification stage. As a result, the amplified signal and idler beams are generated co-linarly. The residual 800 nm beam is separated from the amplified signal and idler beam by the dichroic mirror D4.

The wavelengths of the signal or idler beam can be tuned by rotating the BBO crystal for changing the phase-matching condition and by rotating the grating to make an appropriate diffraction angle for the idler beam. Tables 2-1 and 2-2 show the specification of the OPA-800P at the pump energy of 1 mJ/pulse.

In my research work, one OPA which is pumped by ~2 mJ is used as the pump light source. Fourth harmonic generation (FHG) of the signal beam is achieved by using two

BBO crystals, and the wavelength was tuned in the ultraviolet region. On the other hand, another OPA is used for the probe light source in the pump-probe spectroscopy. The wavelength is tuned at the mid-infrared region, which is obtained by an idler beam or differential-frequency-mixing (DFM) of the idler and signal beam by using $AgGaS_2$ crystal.

2.3 Estimation of excitation intensity for creation of excitons and biexictons

For measurements of the two-photon excitation and mid-infrared transient absorption of the biexcitons in the quantum dots, the high power of the excitation light is required. I will describe how to estimate the light intensity which is necessary to excite one biexciton in the quantum dots. Although the samples used or the excitation conditions are not equal for some of the experiments, here I will explain the estimation by adopting the sample thickness to be 1 mm, the mean radius of the dots to be 4 nm, and irradiated spot size to be 300 μm.

The concentration of the CuCl quantum dots in NaCl is 1mol%, so that it results in 3.37×10^{16} /cm^3 by taking account of the dot radius of 4 nm. Since the irradiated volume is 7.07×10^{-4} cm^2 which is calculated by using the spot size and sample thickness, the number of the quantum dots in the irradiated volume is estimated to be $\sim 2.37 \times 10^{12}$. Namely, the number of photons is needed to be 2.37×10^{12} in the irradiated volume to create one exciton in one quantum dot, by assuming that one photon was converted to the exciton with probability of 100%. By assuming that the excitation light wavelength is 384 nm and O.D. is 1.8 at this wavelength, excitation intensity of 1.3 μJ/pulse is necessary. In addition, to excite two excitons in a quantum dot in average, the power of ~3 μJ/pulse is necessary.

2.4 Two-photon excitation spectroscopy

2.4.1 Absorption and PL spectra at 77 K

The sizes of the quantum dots can be estimated by the absorption and photoluminescence (PL) spectrum. Figures 2-7 and 2-8 show the experimental setups for the measurement of the absorption and PL spectrum, respectively. The samples were fixed on the sample holders in a cryostat and the sample temperature was kept at 77 K. For the absorption measurement, I used the tungsten lamp as a light source. The transmitted light from the sample was focused on an optical fiber, which was connected to the slit of a spectrometer. For the PL measurement, a continuous wave He-Cd laser (wavelength: 325 nm) was used as the excitation light source. The laser light was focused on the sample, and PL from the sample was collected into the optical fiber with the backward-scattering geometry.

The detection was made by the spectrometers with focal length of 150 mm and grating of 1200 g/mm (Acton Research Corporation, hereafter denoted by ARC ; SpectraPro-150) equipped with a charge-coupled device (CCD) (Hamamatsu; C7042), or that with focal length of 500 mm and a grating of 1200 or 2400 g/mm (ARC; SpectraPro-500) with a liquid nitrogen cooled CCD array (Prinston Instruments ; LN/CCD-1340/100-EB).

2.4.2 Two-photon excitation spectroscopy at 4 K

The experimental setup for two-photon excitation of the biexcitons at 4 K is shown in Fig. 2-9. The excitation light is obtained from FHG of the signal beam of OPA, and the wavelength is tuned in the range of 384 – 390 nm (3.195 – 3.220 eV). The maximum output power of the laser was ~3 μJ/pulse. The excitation light was focused by the quartz lens and the irradiated spot size on the sample was ~100 μm. The excitation light was normally incident on the samples, and the polarization is chosen by using the λ/4 plate (luceo; RETAX-λ/4·3900) which is placed in front of the focus lens. The polarizer was placed in front of the optical fiber to remove the scattering light of the excitation laser. PL was collected with the forward-scattering geometry and was detected by using the spectrometer (ARC; SpectraPro-500) equipped with liquid nitrogen cooled CCD array.

The average of the effective radius of the CuCl quantum dots is ~6 nm, which is estimated from the one-photon absorption spectrum. The samples was cleaved with the

thickness of ~0.5 mm. The sample was placed in the He flow cryostat and the temperature is kept at 4.2 K.

2.4.3 Two-photon excitation spectroscopy at 70 K

Figure 2-10 shows the experimental setup of two-photon excitation of the biexcitons at 70 K. The excitation light source was obtained by FHG of the signal beam from the OPA, and the wavelength (photon energy) was tuned from 382.3 nm (3.242 eV) to 388.6 nm (3.189 eV). The maximum output power of the laser was about ~3 μJ/pulse. The excitation light was focused by a quartz lens and the irradiated spot size on the sample was ~180 μm. The PL was collected with the backward-scattering geometry to acquire the PL due to the excitons and was detected by using the spectrometer (ARC; SpectraPro-500) equipped with liquid nitrogen cooled CCD array.

The average of the effective radius of the CuCl quantum dots is ~3.7 nm, which is estimated from the one-photon absorption spectrum. The samples was cleaved with thickness of ~0.5 mm. The sample was placed in the He flow cryostat and the temperature is kept at 70 K.

2-5 Mid-infrared transient absorption spectroscopy

2.5.1 Experimental setup

Pump-probe spectroscopy was performed with using the dual OPA system. The experimental setup is shown in Fig. 2-11.

The pump pulse was obtained by FHG of the signal beam from one OPA and wavelength was tuned at 383 – 388 nm (3.236 – 3.194 eV) for the resonant excitation of the exciton or biexciton state in CuCl quantum dots in NaCl matrices. The pump pulse was focused on the sample with the spot size of ~300 μm. The maximum excitation intensity was 4 μJ/pulse, and with this intensity, it was estimated that on average 2.5 e–h pairs would be created in a dot.

On the other hand, the probe pulse was obtained by an idler beam or the DFM of the signal and idler beam from another OPA. The probe pulse intensity was reduced by

neutral-density filters to ~0.1 μJ/pulse and focused on the sample with spot size of ~200 μm by using the parabolic reflector. The relative angle between the pump and probe pulse was ~11°.

PL spectrum was measured simultaneously with the transient absorption spectroscopy. The PL retraced the optical path of the excitation light was collected by using the reflection of a quartz plate and was detected by using the spectrometer (ARC; SpectraPro-150 or SpectraPro-500) equipped with the CCD.

The samples were held in a He gas flow cryostat with the BaF_2 windows. The sample temperature was kept to 70 K in the measurements in order to avoid the influences from the trapping states of the carriers at the interfaces of the dot, which contributes the IRTA signals at the low temperature [48].

2.5.2 Detecting system

The transmitted probe light was detected by a liquid nitrogen cooled HgMnTe photodiode (Broward Infrared Detector Corporation, MCTLNE-0.2-10.6 (hereafter denoted by MCT)) after a monochromator with focal length of 100 mm and grating of 120 g/mm (JASCO: M10). Some important characteristic parameters of MCT are shown in Table 2-4.

Output signals of MCT were amplified by a pre-amplifier circuit and introduced a lock-in amplifier (EG & G Instruments, 7260) or a digital oscilloscope (Tektronix, TDS3032). The differential transmitted signal (ΔI) was obtained with the lock-in amplifier synchronized with the chopping frequency (~80 Hz) of the pump light. On the other hand, the reference intensity of the transmitted probe light (I_0) was obtained by chopping the probe light with cutting the pump light.

The transient absorption intensity (ΔO.D.) was obtained as follows;

$$\Delta\text{O.D.} = -\log_{10}\left(\frac{I_0 - \Delta I}{I_0}\right) \qquad (2.1).$$

For this measurement, the stability of the laser output during collecting the signals is very important because the fluctuation of the laser light gives rise to noise in the signal. Therefore, before and after collecting the signals by changing the delay time, I checked the stability of the light intensity by observing the fluctuations of waveforms of the signals by using the digital oscilloscope, which is triggered by TTL signal from the

regenerative amplifier.

2.5.3 Origin of delay time

The origin of the delay time for this pump-probe spectroscopy was determined by cross-correlation of difference frequency mixing (DFM) of the pump and probe light, which is obtained by using a $LiIO_3$ crystal (4×4×4 mm, cutting angle: 24°). The generated DFM light was collected by the lens and focused on the optical fiber, and the spectrum of the DFM light was measured by the spectrometer (Acton Research Corporation SpectraPro-150) and the liquid nitrogen cooled CCD (Hamamatsu: C7557). Figure 2-13 shows the obtained temporal profiles of the DFM of the pump light of 386.9 nm and probe light of 4.5 μm, which was denoted as solid circles. The wavelength of the DFM was 423.4 nm. The solid curve shows result of fitting to the experimental values with a Gaussian function. The obtained temporal width of the correlation from the fitting curve was 1.7 ps, and this value was defined as the temporal resolution of this measurement.

We may note, in passing, that the pulse width was estimated to be 1.3 ps by the assumption that temporal profiles of the pump and probe light are approximated by Gaussian functions with the same width. However, I have not confirmed the pulse widths of them individually.

For the longer wavelength of the probe light than 5 μm, the DFM intensity decreases and the temporal width becomes extended since the wavelength region for the transparency of $LiIO_3$ is 300–5000 nm. Consequently, the origin of the delay time was necessary to be determined by using the probe wavelength shorter than 5 μm, before the measurement of transient absorption spectra. It was confirmed that origin of the delay time is constant regardless of the changes of the probe wavelength from 3 μm to 5 μm.

2.5.4 Transient absorption spectra

Transient absorption spectrum was obtained by changing the probe wavelength from 2.5–10 μm. The output direction of the light from OPA varies with changing the output wavelength. Consequently, the realignment of the optical pass was necessary to make the light incident on the same point on the sample surface every time the wavelength was tuned.

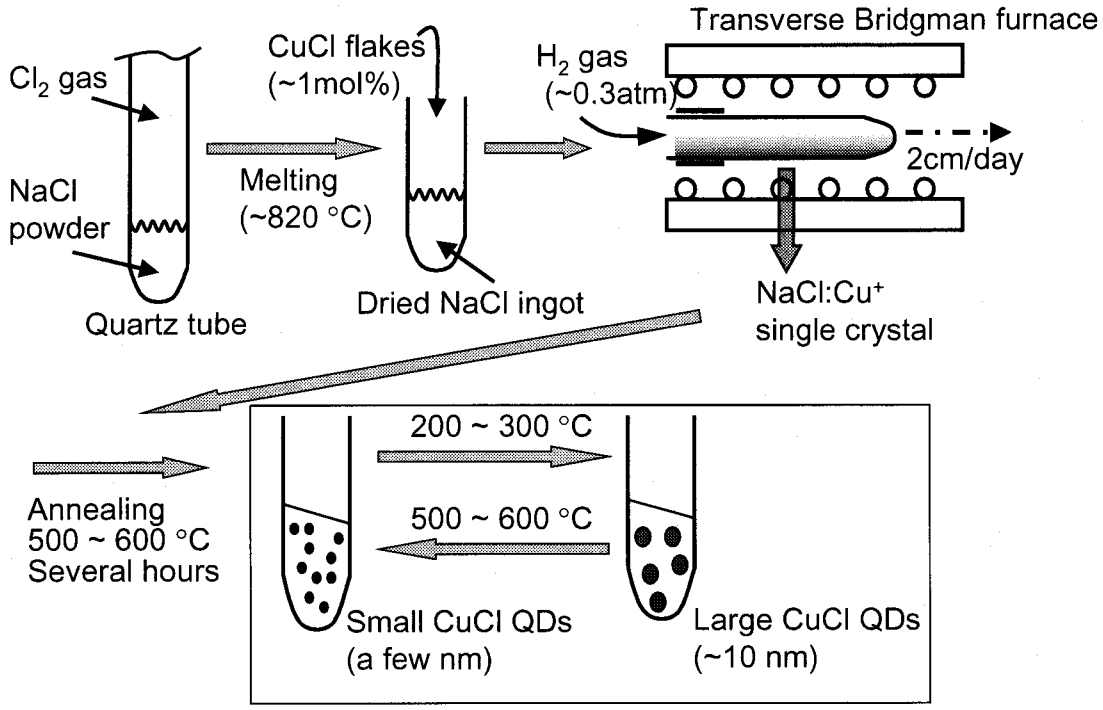

Figure 2-1. Procedure for the sample preparation of CuCl quantum dots embedded in NaCl matrix by means of transverse Bridgman method followed by subsequent annealing processes [11].

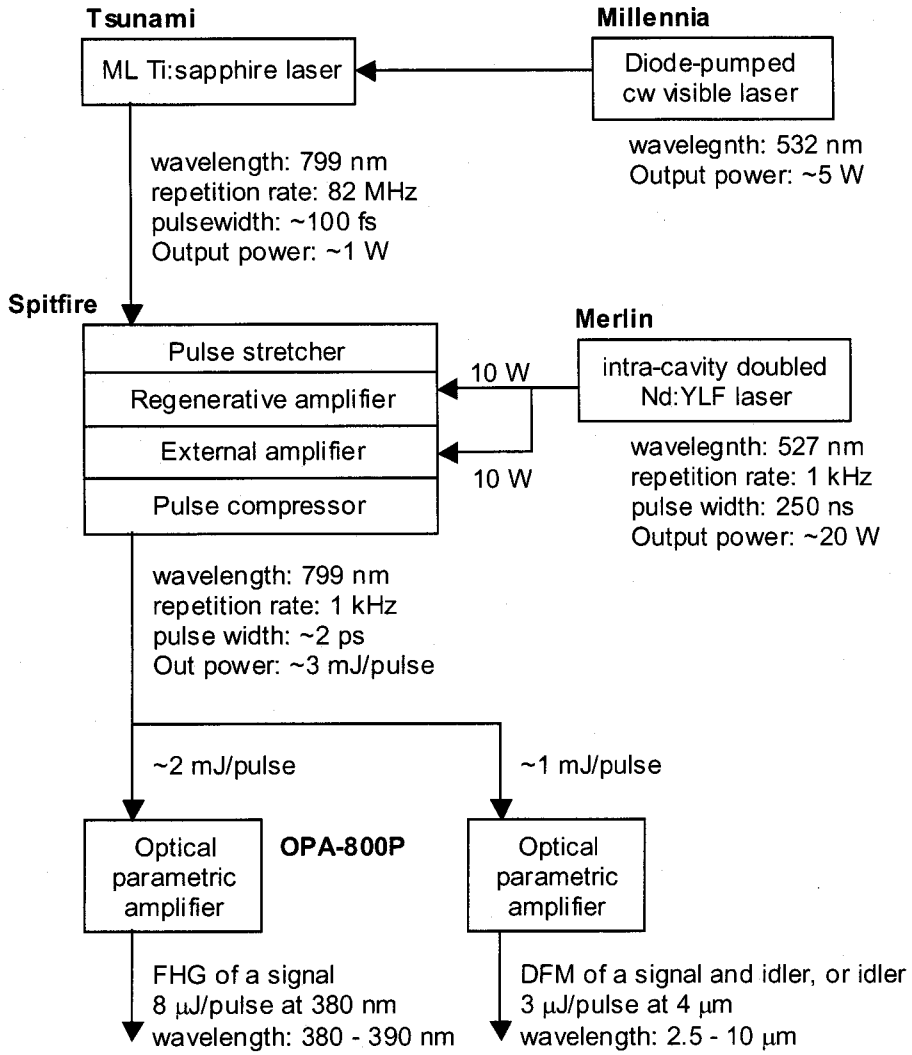

Figure 2-2. Outline of the *ps* OPA system which was used for my research work. Output powers from the OPAs indicate typical values.

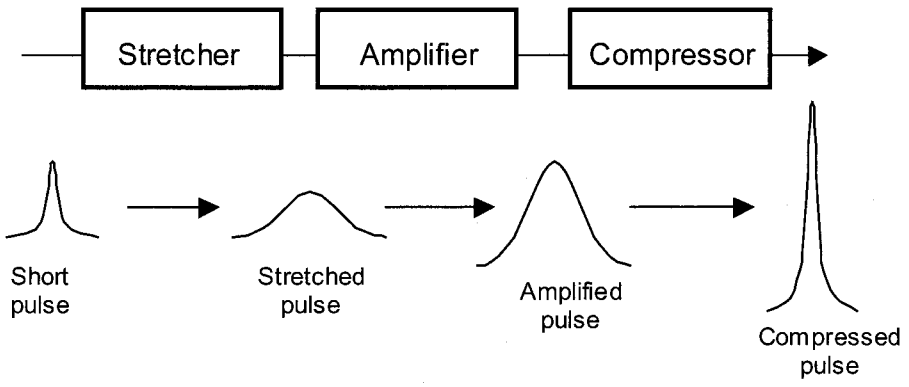

Figure 2-3. Principle of chirped pulse amplification.

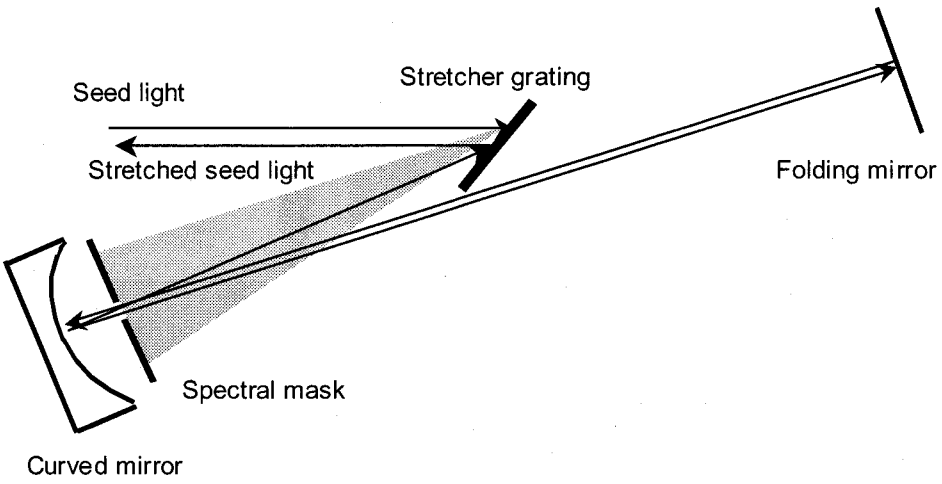

Figure 2-4. Scheme of a grating stretcher with a *ps* mask.

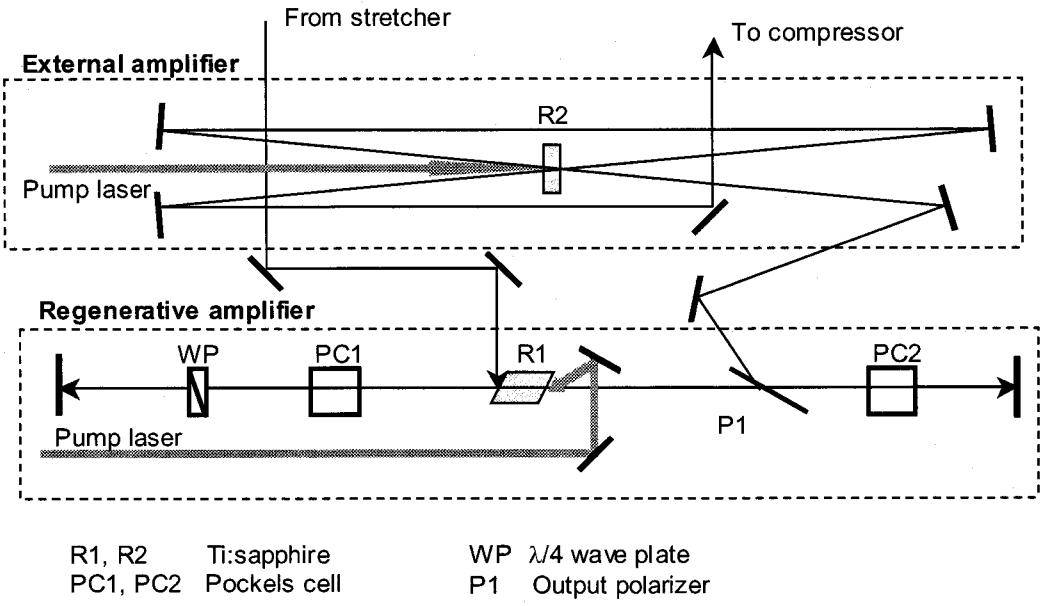

Figure 2-5. Layout of the Ti:sapphire amplification systems.

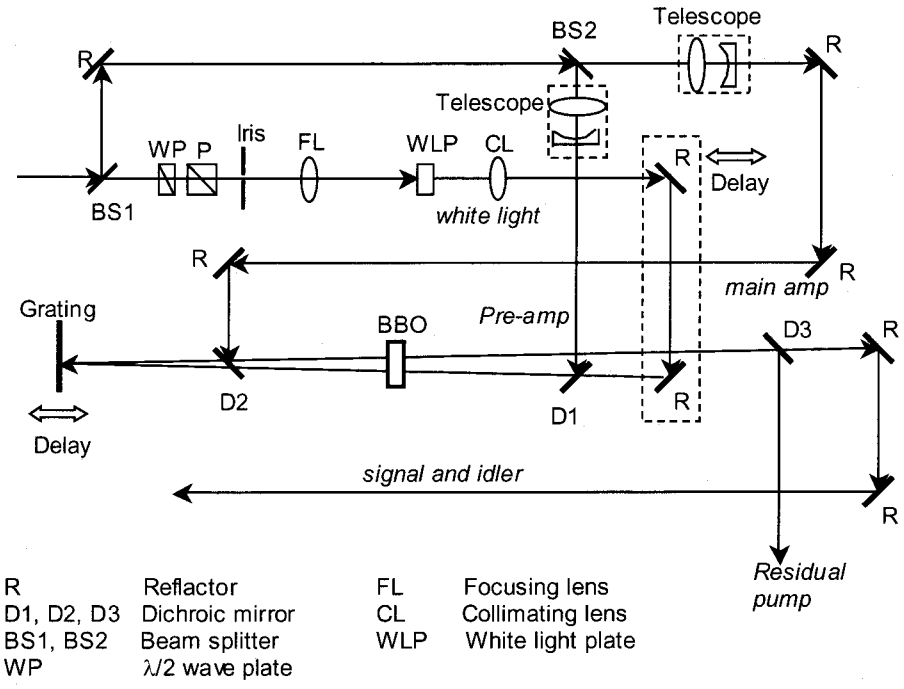

Figure 2-6. Layout of optical parametric amplifier system.

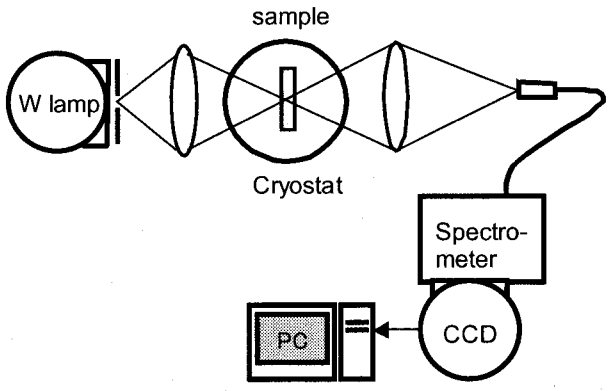

Figure 2-7. Experimental setup for absorption measurement at 77 K.

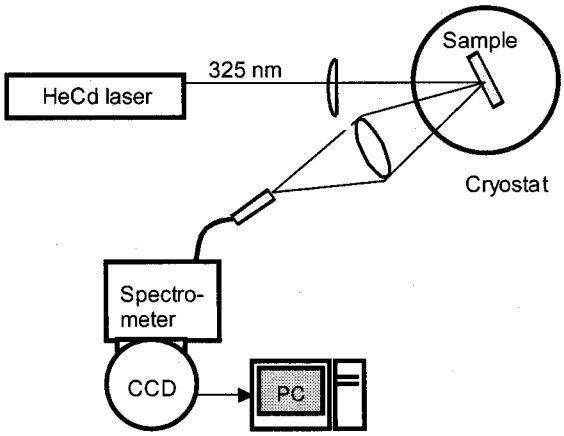

Figure 2-8. Experimental setup for photoluminescence measurement at 77 K.

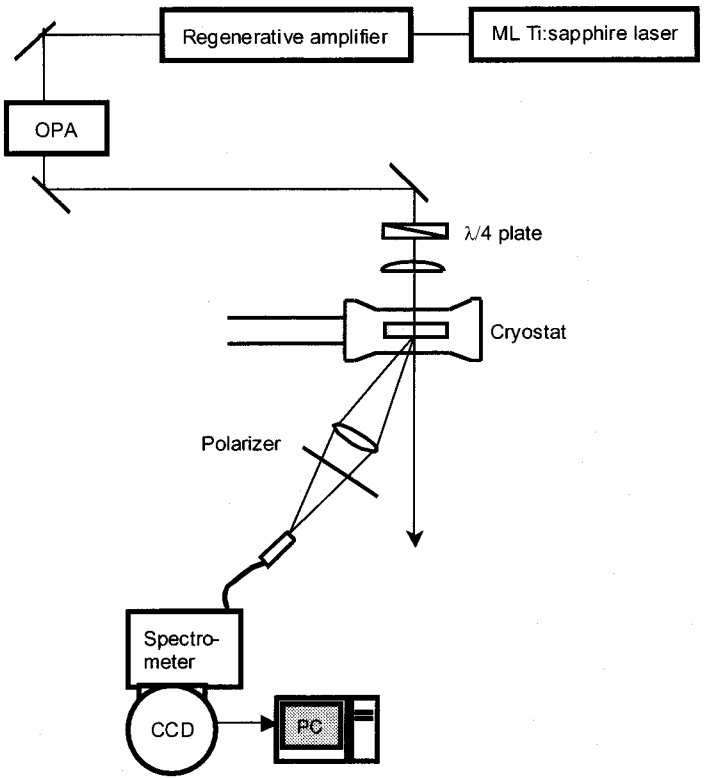

Figure 2-9. Experimental scheme for the two-photon excitation of biexcitons at 4 K.

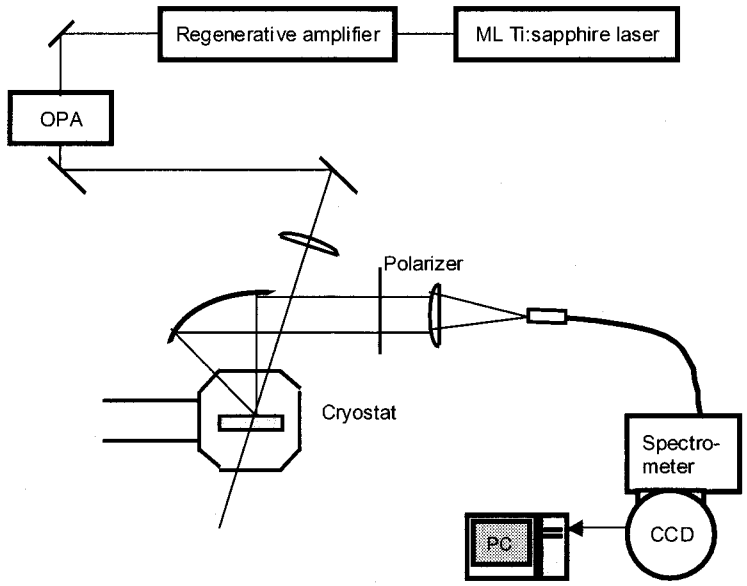

Figure 2-10. Experimental setup for the two-photon excitation of biexcitons at 70 K.

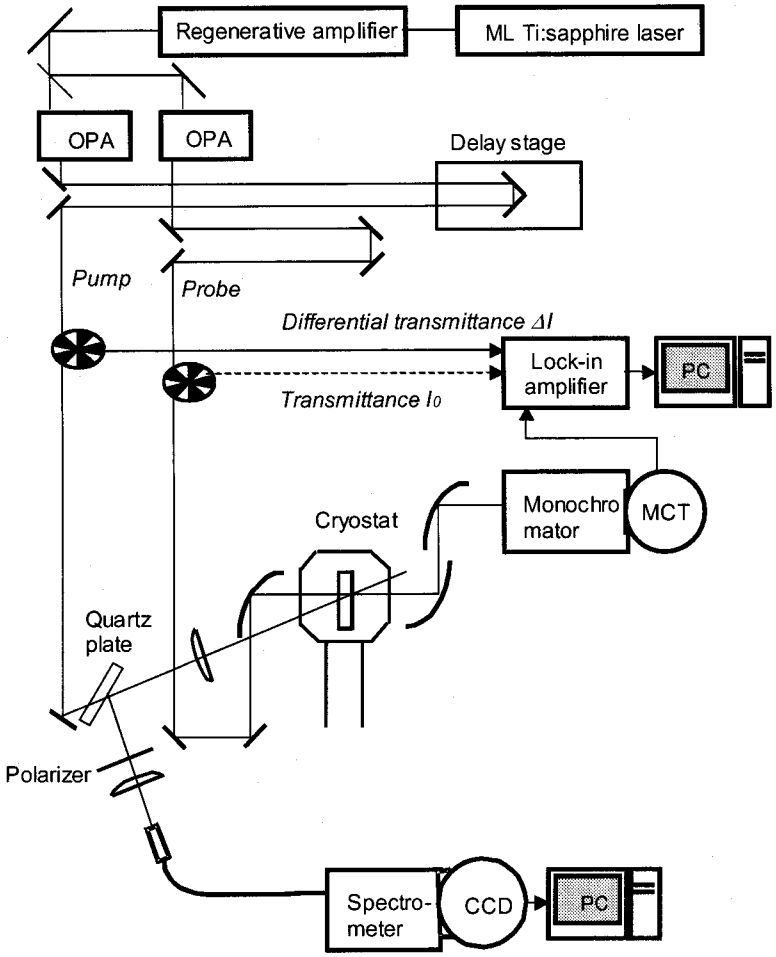

Fig. 2-11. Experimental setup for pump-probe spectroscopy.

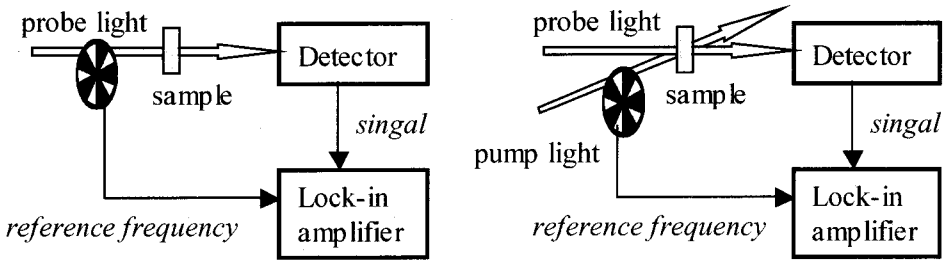

Figure 2-12. Outline of the method of obtaining the reference intensity I_0 (right hand side) and differential intensity ΔI (left hand side) of the transmitted probe light.

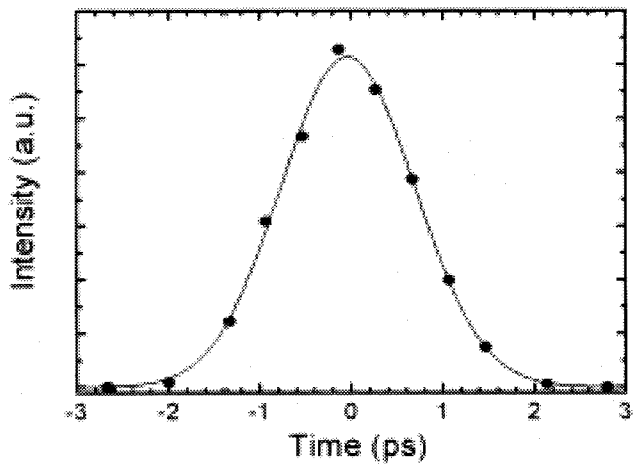

Figure 2-13. Temporal profile of the cross-correlation between pump and probe pulses, which is obtained by difference-frequency-mixing (DFM). The pump and probe wavelengths were 386.9 nm and 4.5 μm, and the generated DFM wavelength was 324.6 nm. The solid line shows the fitted curve to the experimental points with a Gaussian function.

Table 2-1. OPA-800P Specification

Input Characteristic		Output Performance	
	Pump Energy	Signal (λ_s= 1.3 μm)	ider (λ_i= 2.08 μm)
Pulse Energy	1.0 mJ	60 μJ	25 μJ
Pulse Width	≤ 1.5 ps	< 1.5 ps	< 1.5 ps
Line Width	≤ 22 cm^{-1} @800 nm	< 25 cm^{-1}	< 25 cm^{-1}
Tuning Range		1.10 – 1.60 μm	1.60 - 3.00 μm
Repetition Rate		1 kHz	
Energy Stability		< 3 %	

Table 2-2. Specification of OPA-800P Wavelength Extension Output

Option	Wavelength Range	Pulse Energy	Pulse Width	Energy Stability
ω_i	1.6 – 1.6 μm	25 μJ at 2.0 μm	< 25 cm^{-1}	< 3 %
ω_s	1.1 – 1.6 μm	60 μJ at 1.3 μm	< 25 cm^{-1}	< 3 %
4 ω_s	300 – 400 nm	4 μJ at 330 nm	< 30 cm^{-1}	< 7.5 %
DFM ω_s–ω_i	3.0 – 10.0 μm	3 μJ at 4.0 μm	< 25 cm^{-1}	< 5 %

Table 2-3. Estimation of excitation intensity to excite the excitons and biexcitons.

Radius of CuCl quantum dots	4 nm
Concentration of the CuCl quantum dots	3.37×10^{16} /cm^3
Irradiated spot size (diameter)	300 μm
Thickness of the sample	1 mm
Wavelength of the pump light	384 nm
Minimum of the photon numbers to excite an exciton per dot	2.37×10^{12} 1.3 μJ/pulse
Minimum of the photon numbers to excite a biexciton per dot	4.74×10^{12} 2.6 μJ/pulse

Table 2-4. Characteristic parameter of MCT.

Cutoff wavelength	11.84 μm
Spectral responsibility	6.0 A/W
Quantum efficiency	> 50 %
Response frequency	> 100 MHz
Active areas	4.0×10^{-4} cm^2
Window	ZnSe

Chapter 3

Two-Photon Excitation of Confined Biexcitons

3.1 Introduction

The biexciton (excitonic molecule), which is formed by the combination of two excitons, has provided us the huge information of basic properties of the interactions between the excitons. In addition, it plays the important role for the optical nonlinear response of the semiconductors. The biexcitons have been considered as a candidate for the high-efficient semiconductor lasers [18], since their luminescence has in essential quasi-three-level-system and the inverse population can be realized easily between the biexcitons and longitudinal exciton states. The binding energy of the biexcitons in low dimensional materials is increased because of the confinement effects, so that the biexciton become stable even at elevated temperature. Therefore, in the thin films or nanoparticales, the biexciton state has been studied very much.

In most experiments, the biexcitons are generated through the thermalization of hot carriers or exctions generated by the band-to-band excitation or the exciton resonant excitation. However, the direct creation of the biexcitons is possible by the giant two-photon absorption involving quasi-resonant intermediate states of the exictons. Experimentally, the giant two photon absorptions of the biexciton were reported in some II-VI and I-VII semiconductors [39, 43, 50 - 52, 63, 64]. For the two-photon absorption process, the total angular momentum of the biexciton state determines the optical selection rule [48]. In the case of CuCl, the direct creation of the lowest biexciton (Γ_1 state) is forbidden for co-circularly polarized lights because the total angular momentum is zero. This selection rule was confirmed experimentally [51]. The two-photon

absorption process of the biexcitons was investigated extensively for CuCl bulk crystal [39, 50 - 52].

However, in the case of the quantum dots, there is no report on the two-photon resonant excitation of the biexciton states, although the study of it is very interesting and important. First, a two-photon absorption coefficient is the important parameter associated with the optical nonlinearity. In general, the nonlinear susceptibility of quantum dots increases compared to the bulk crystal. However, the confinement effect on the two-photon absorption of the biexcitons has not been revealed. Second, the confinement effect on the polarization selection rule of the biexciton creation by the two-photon absorption is still unknown. In the confinement system, the interaction between the electrons and holes is modulated, and it may affect the selection rule of the biexcitons. Furthermore, for the development of the quantum dot lasers, one of the important problems to be solved is how to prevent the Auger ionization of the dots, which originates from mutual interactions between the isolated excitons. The direct creation process of the biexciton would give the stable and efficient system for the laser applications since the excess energy of the biexciton in the generation process is suppressed.

The energy levels of the biexciton confined in the quantum dots, taking account of the correlation between two excitons, were investigated [37]. According to the previous investigations, when one exciton already exist in a quantum dot, the second exciton can not be created at the same energy as that of the first exciton because of the influence of the large correlation between the two excitons. In other words, one can not create the two exciton state by the step-by-step process of one-photon absorption under the resonant excitation of the confined single exciton. This result makes the investigation of the quantum size effect on the biexciton more difficult and complicated. If the direct creation of the confined biexciton by two-photon absorption is successful, the details of the quantum size effect of the biexciton will be clarified.

3.2 Motivations and purpose

According to the previous study on the confined biexciton states in semiconductor

quantum dots, the second exciton is created at the absorption energy different from that of the first exciton in the creation process of the biexciton. However, the photoluminescence (PL) band of the biexciton has been observed even in the case of exciting the confined exciton level size-selectively [32]. This report does not agree with the former reports and it has been unresolved question. In order to resolve this discrepancy, I tried to investigate the existence of the two-photon resonant absorption process of the confined biexcitons. I propose that two-photon absorption process of the biexciton is capable of a new tool to study the confined biexciton states.

To date, there is no report on the direct creation process of the confined biexciton states in CuCl quantum dots by the two-photon resonant excitation, to my knowledge. It is perhaps because of the wide size distribution of the quantum dots in one sample. The large size distribution of the dots results in the extension of the one-photon absorption band to the lower energy side. In the photoluminescence excitation (PLE) spectrum of the biexciton, consequently, it is difficult to clearly discriminate the two-photon absorption band from the one-photon absorption band.

To resolve this problem, I examined the dependence of the PLE spectrum of the biexciton on the polarization of the excitation light. If the polarization selection rule of the biexction survives even in the confined system like the quantum dot, the PL intensity of the biexciton is expected to decrease for the circularly polarized light in comparison with the linearly polarized one. It must be a clear evidence of the two photon resonant excitation of the confined biexciton state. By means of this method, the observation of the biexciton state in the GaAs quantum dots was succeeded for single quantum dot by using microspectroscopy [65].

Furthermore, it should be possible to observe the transition not only to the lowest biexciton state ($J = 0$) but also the excited biexciton state ($J = 0$, $J = 2$) by the two-photon absorption process.

I will discuss the possibility of the two photon resonant absorption of the confined biexciton states in reference to the one-photon induced absorption from the exciton to biexciton state.

3.3 Results and discussion

3.3.1 PL spectra

Figure 3-1 shows the PL spectra with the excitation photon energy of 3.228 eV (thick line) and 3.184 eV (thin line), respectively. These excitation photon energies are higher and lower than the exciton energy in the bulk crystal (indicated by dotted vertical line), respectively.

The photon energy of 3.228 eV corresponds to the resonant excitation of the confined excitons in the dots with the effective radius of 2.5 nm. The observed PL bands are the same as the case of the band-to-band excitation [34]. The PL bands denoted by M, BM and BX are originated from free biexcitons, bound biexcitons, and bound excitons, respectively. The sharp line denoted by I_1 is the PL originating from the exciton trapped to the some neutral donar, the energy of which is not dependent on the dot radius. The energy diagram and the relaxation process associated with the free and bound biexcitons and the bound excitons are shown in Fig. 3-2.

Although the excitation photon energy of 3.228 eV corresponds to the resonant energy of the excitons in the dot with effective radius is 2.5 nm, the larger dots than 2.5 nm is also excited since it is possible that the excitation photon energy corresponds to the higher confinement states of the excitons in larger dots. Such kind of creation process for excitons and biexcitons will be discussed in next chapter.

On the other hand, in the case of the excitation photon energy lower than the exciton energy for the bulk crystal, the PL bands of M, BM and BX were also observed. In this excitation condition, the excitons are not created by the one-photon absorption process, but by some nonlinear process. Consequently, the biexciton can be created through the two-photon absorption process. In the M and BM bands, a few structures appeared in the case of the two-photon excitation. The origin of these structures is considered as follows.

For the biexciton luminescence in the bulk crystal, the two bands were observed, which are associated with the longitudinal and transverse excitons as the final states [49]. It might be possible to observe these bands even in large quantum dots although the mixing of the transverse and longitudinal modes of exciton occurres for smaller quantum dots [66]. Furthermore, by the two-photon absorption, the size-selective excitation of the biexcitons would be possible. As a result, fine structures of the biexciton luminescence would appear. More detailed discussion is necessary to clarify the origin of the fine structures.

In summary for the PL spectrum under the excitation at the photon energy lower than the exciton energy for the bulk crystal, it was confirmed that the biexcitons were created in the quantum dots since the M and BM bands were observed. This result seems to show the two-photon absorption process of the confined lowest biexciton state.

3.3.2 PLE spectra of confined biexcitons

Next, I examined the PLE spectra of the M and BM bands with linear and circular polarizations of the excitation light in order to confirm the two-photon absorption process. Figure 3-3 shows the PLE spectra of the M and BM bands with excitation photon energy between 3.179 and 3.228 eV. For the linearly polarized excitation shown in the Fig. 3-3 (A), the PLE spectrum has a peak around 3.21 eV and continuous structure in the higher energy side. In addition, the PLE intensity is decreased monotonously toward the lower energy side. The isolated peak structure due to the two-photon resonant absorption, which was clearly observed in the bulk crystal, was not observed, perhaps because of the inhomogeneous size distribution of the dots.

On the other hand, for the circularly polarized excitation, however, the PL intensities of the M and BM band reduced abruptly beneath the 3.204 eV, as shown in Fig. 3-3 (B). This value almost coincides with the transverse exciton energy (3.202 eV) in the bulk crystal which corresponds to the lowest energy edge of the one-photon absorption band of the free exicitons. According to this result, the biexcitons confined in the quantum dots are not be created by the two-photon absorption with the circularly polarized excitation light. This feature of the PLE agrees with the polarization selection rule for the lowest biexciton ($J = 0$).

This polarization dependency of the PLE is more explicitly shown by the ratio spectrum of the PLE as shown in Fig. 3-4. The ratio spectrum was obtained by dividing the PLE curve with circularly polarized excitation by that with linearly one. Beneath the excitation photon energy of 3.202 eV, the PL intensities of the M and BM decrease for the circularly polarized excitation compared to the linear one. This is direct and clear confirmation of the existence of the direct creation process of the biexciton confined in CuCl quantum dots by the two-photon resonant absorption.

3.3.3 Two-photon absorption of excited biexciton states

In the ratio spectra of the PLE shown in Fig. 3-4, the ratio exceeds unity above the excitation photon energy higher than 3.204 eV. That is to say, the biexcitons are created more efficiently with the circularly polarized excitation light than with the linearly one. This polarization dependency is quite opposite to the selection rule of the biexciton with J = 0. In order to clarify the difference of the PL intensities of the M and BM bands, I examined the differential PL spectrum, shown by a thin line in Fig. 3-5. It is obtained by subtracting the PL spectrum for the linearly polarized excitation light (thick dotted line) from that for the circularly one (thick solid line). The increase of the PL intensities of the M and BM bands and the decrease of the PL intensity of BX band are observed clearly in the differential spectrum.

I will discuss this peculiar nature of the polarization dependence. When the excitation photon energy is higher than the exciton energy of the bulk crystal, one can assume the two kinds of the creation processes of the biexciton. One process is that the biexcitons are collisionally created from two excitons after they are created by one-photon absorption process and then thermalized. However, the one-photon absorption of the excitons has no polarization dependency for the excitation light. Therefore, the creation process of the biexcitons also has no polarization dependency, so that the ratio of the PLE should be 1. Other possibility is the two-photon absorption process for the direct creation of the biexcitons. However, in the case of the generation process of the biexcitons of J = 0, the biexcitons would not be created by the circularly polarized light as mentioned before.

In order to explain the observed polarization dependency of the PLE above 3.207 eV, I assumed the two-photon absorption of the excited biexciton states, the energies of which are larger than twice the creation energy of the isolated excitons. According to previous reports on the pump-probe spectroscopy [31], two of the excited biexciton states (J = 0, 2) are optically allowed for the transition from the exciton state with J_{ex} = 1, and the transition dipole moment for J = 2 biexciton state is much larger than that for J = 0 biexciton state. Since the two-photon absorption process of the biexciton utilize the exciton state as the virtual immediate state, the giant transition dipole moment between the exciton and biexciton affects efficiently to the two-photon absorption coefficient. Under this assumption, it is reasonable to consider that resonant two-photon absorption of the excited biexciton of J = 2 has a larger dipole moment than that of J = 0. Since the excited biexciton with J = 2 are created by the circularly polarized light more

efficiently than by linearly one, the polarization dependency of PLE above 3.204 eV can be explained. The energy diagrams for the two cases that the excitation photon energy is higher and lower than the exciton energy are shown in Fig. 3-6.

3.3.4 Excitation intensity dependence of PL intensity of biexcitons

At the photon energy for the resonant excitation of the confined excitons, it was supposed that the excitons and biexcitons of J = 2 are excited at the same time. In this case, the one-photon absorption process of the excitons might reduce the efficiency of the biexciton creation. Nevertheless, the PL intensities of M and BM bands in this excitation energy region are larger than the case of the creation process of the lowest biexciton of J = 0, as shown in the Fig. 3-3 (A). This fact indicates that the two-photon absorption of the excited biexciton (J = 2) has the transition dipole moment larger than that of the lowest biexciton (J = 0).

One can compare the two-photon absorption coefficient between the lowest and excited biexciton states from the result of the excitation intensity dependence of the biexciton PL intensity. The PL intensities of the M and BM bands increase superlinearly with the excitation intensity. Figure 3-7 shows the excitation intensity dependence of them at the excitation photon energy of 3.230 eV, which corresponds to the resonant excitation of the confined excitons for the dot with the size of 2.4 nm. The PL intensities of M and BM bands increase in proportion to the excitation intensity to the power 1.4 and 1.2, respectively.

On the other hand, in the case of the excitation photon energy of 3.189 eV, which corresponds to the two photon absorption of the lowest biexciton state, the dependencies of M and BM bands show the excitation intensity to the power 1.9 and 1.7, shown in Fig. 3-8. In order to explain the difference in the excitation intensity dependencies between the two different excitation photon energies, I will discuss about the net absorbed light intensity by the two-photon absorption processes.

One- and two-photon absorption coefficients, α and β, are defined as

$$dI = -(\alpha I + \beta I^2)dz . \qquad (3\text{-}1).$$

Here, I is a beam flux and z is a length for the beam propagation. By solving this equation with respect to the incident beam intensity I_0, and the sample thickness l, the transmitted light intensity I is given as

$$I = \frac{I_0 e^{-\alpha l}}{1 + \frac{\beta}{\alpha}\left(1 - e^{-\alpha l}\right) I_0} \quad . \qquad (3\text{-}2)$$

When one considers only the two photon absorption process, by assuming that α in (3-2) is negligible small compared with $1/l$, the transmitted light intensity is obtained as

$$I = \frac{I_0}{1 + \beta l I_0} \qquad (3\text{-}3).$$

Consequently, the absorbed light intensity I_{abs}, by the two-photon absorption process is

$$I_{abs} = I_0 - I$$

$$= I_0 \left(1 - \frac{1}{1 + \beta l I_0} \right)$$

$$\approx \begin{cases} \beta l I_0^2 & (\beta l I_0 << 1) \\ I_0 & (\beta l I_0 >> 1) \end{cases} . \qquad (3.4)$$

Namely, for a small β or a low incident light intensity, the absorbed light intensity increases in proportion to the square of the incident light intensity. On the other hand, for a large β or a high incident light intensity, the dependency becomes nearly linear.

As shown in Fig. 3-7 and 3-8, the nonlinearlity of the PL intensities of the M and BM bands is smaller for the excitation of the excited biexciton compared to that of the lowest biexcitons. This result indicates that β associated with the excited biexcitons is considerably larger than that associated with the lowest biexcitons. This assumption agrees with the PLE spectrum in which the biexcitons are created more efficiently than the excitons with the excitation energy of the excited biexciton, in spite of the occurrence of the one-photon absorption of the excitons at the same energy.

3.3.5 Lasing action of biexciton luminescence

Here, I introduce an interesting phenomenon related to the two-photon excitation of confined biexciton in CuCl quantum dots. With the excitation intensity is increased under the two-photon excitation of the lowest biexcitons, successful achievement of stable and efficient lasing of the biexciton luminescence is realized.

Figure 3-9 shows the PL spectra under the two-photon resonant excitation of the biexcitons at two different excitation intensities. The lower curve was taken at the

excitation power just below the lasing threshold I_{th}. The upper curve shows the durable laser emission of the biexcitons around 3.173eV where the excitation power is somewhat above the lasing threshold. The observed mode distance and the direction of lasing clearly show that the cleaved parallel surfaces of the NaCl matrix act as an effective optical cavity in spite of the low reflectivity which is only 5%. This fact implies that the optical gain should be extremely high and. On the contrary, in case of the resonant one-photon excitation of excitons, the laser action stops within a few seconds. Therefore, the direct two-photon resonant creation of biexcitons is essential to prevent the Auger ionization of the quantum dots, that dramatically improves the quantum efficiency and long durability of lasing.

3.4 Summary

I have investigated the direct creation process of the confined biexciton states in CuCl quantum dots by resonant two-photon absorption at 4 K.

The PL bands of the free and bound biexcitons (M and BM) were observed when the excitation photon energy was lower than the one-photon absorption band of the confined excitons. From this result, the two-photon absorption process of the biexciton has been proposed.

Furthermore, I have measured the photoluminescence excitation (PLE) spectra of the M and BM bands with the linearly and circularly polarized excitation lights. When the excitation photon energy is lower than the lowest energy edge of the exciton absorption band, the PL intensities of the M and BM bands were decreased clearly with the circularly polarized light in comparison with the linearly one. This feature agrees with the polarization selection rule of the lowest biexciton state with $J = 0$. As a result, the direct creation process of the biexcitons by the two-photon absorption was confirmed.

In addition, when the excitation photon energy falls inside the one-photon absorption band of the confined excitons, the PL intensities of the M and BM bands were larger with the circularly polarized light than with the linearly polarized light. This polarization dependence for the excitation light was quite opposite to the selection rule of the biexcitons with $J = 0$. I proposed that this feature is attributable to the two-photon

absorption process for the excited biexcitons with J = 2. Based on this assumption, the circularly polarized light is found to create the biexcitons more efficiently than the linearly polarized light.

From these experimental results, the existence of the characteristic of the two-photon absorption process of the confined biexcitons in the semiconductor quantum dots was clarified for the first time. This two-photon absorption process will be a novel tool for the study of the quantum size effect on the biexcitons. The dot-size dependence of the two-photon absorption coefficient and the optical nonlinearlity associated with the biexciton states will be revealed in the near future. Furthermore, it will be possible to realize hyper parametric scattering process utilizing the resonant two-photon excitation of the biexcitons confined in single quantum dots. The process has been observed in the bulk crystal and will be the useful candidates for the applications of the quantum dots to the quantum information.

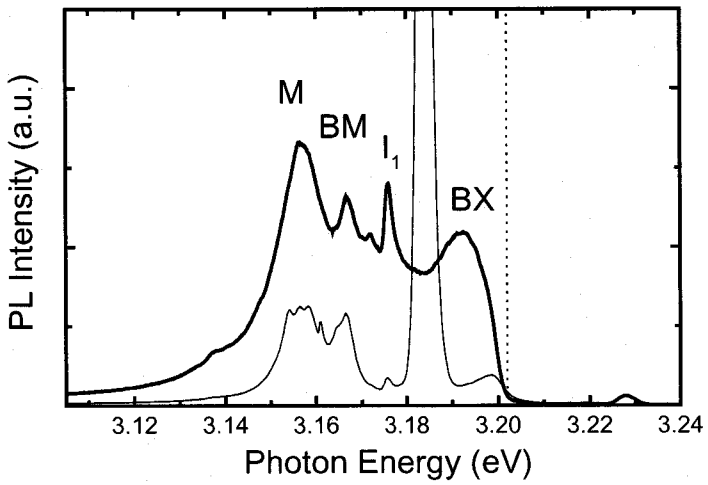

Figure 3-1. PL spectrum under the excitation photon energy of 3.228 eV (thick line) and 3.184 eV (thin line). The dotted vertical line indicates the exciton energy in the bulk crystals.

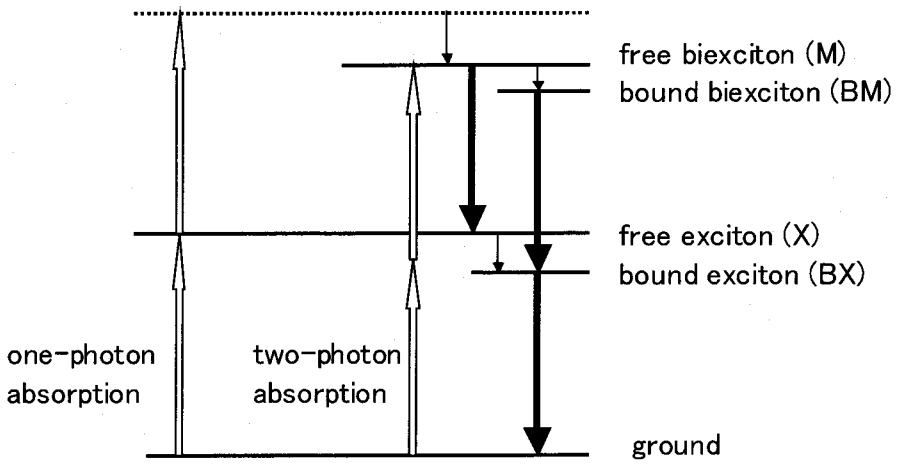

Figure 3-2. The energy diagram of the relaxation process.

(A)

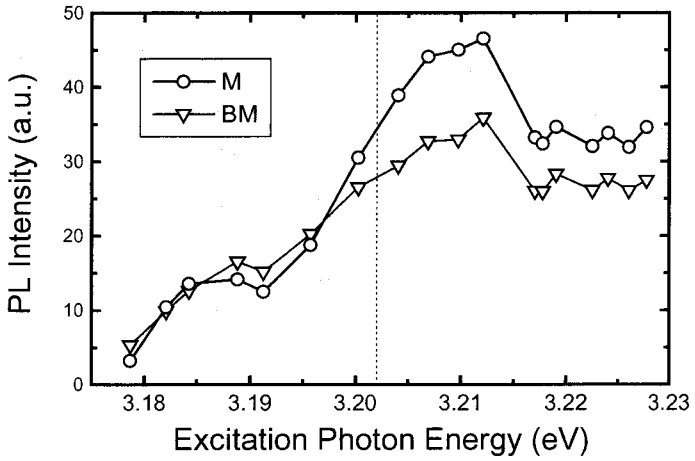

(B)

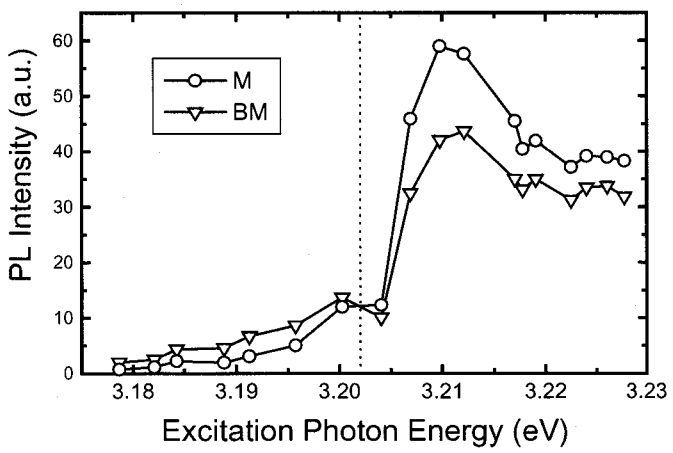

Figure 3-3. PLE spectra of biexciton and bound biexciton with linearly (A) and circularly (B) polarized excitation light.

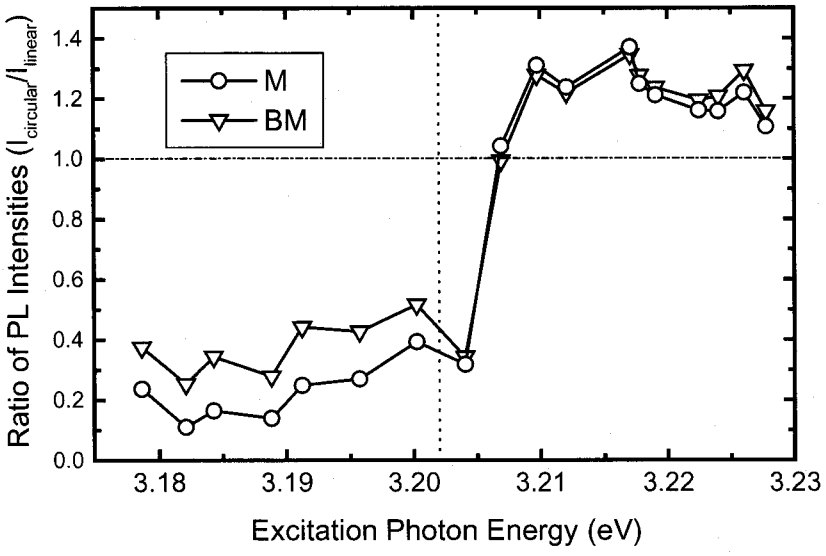

Figure 3-4. Ratio of PLE spectra for different polarized excitations.

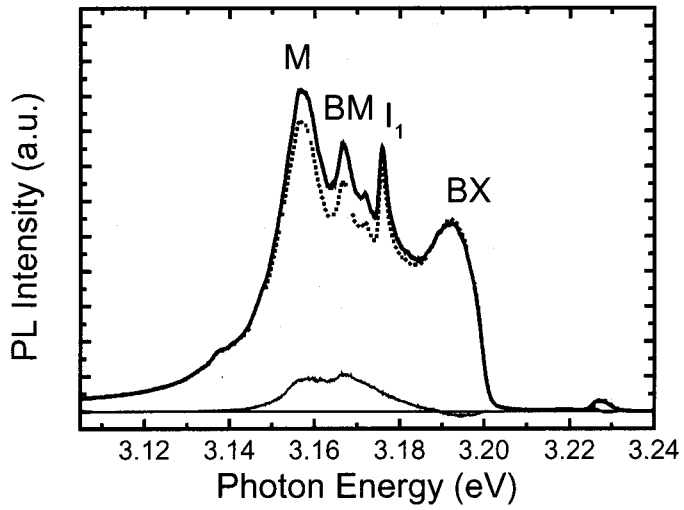

Figure 3-5. PL spectra with linearly (thick dotted line) and circularly (thick solid line) polarized excitation light. The excitation photon energy was 3.228 eV. The thin line indicates the differential spectra between them.

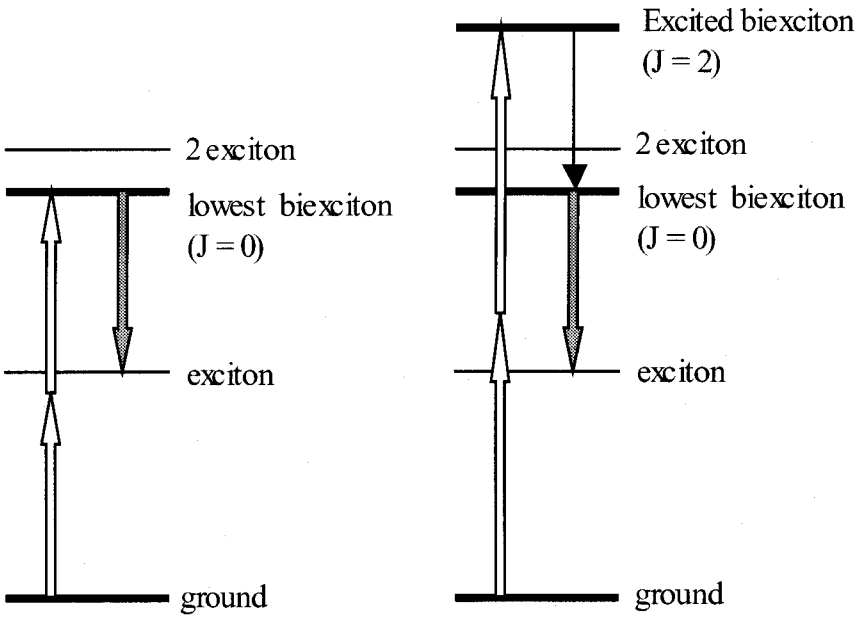

Figure 3-6. Energy diagrams of the two photon absorption processes of the lowest biexciton (left) and the excited biexciton (right) states. The open and closed arrows show the absorption and emission processes. Non-radiative relaxation from the excited to the lowest biexciton state is expressed by a thin arrow.

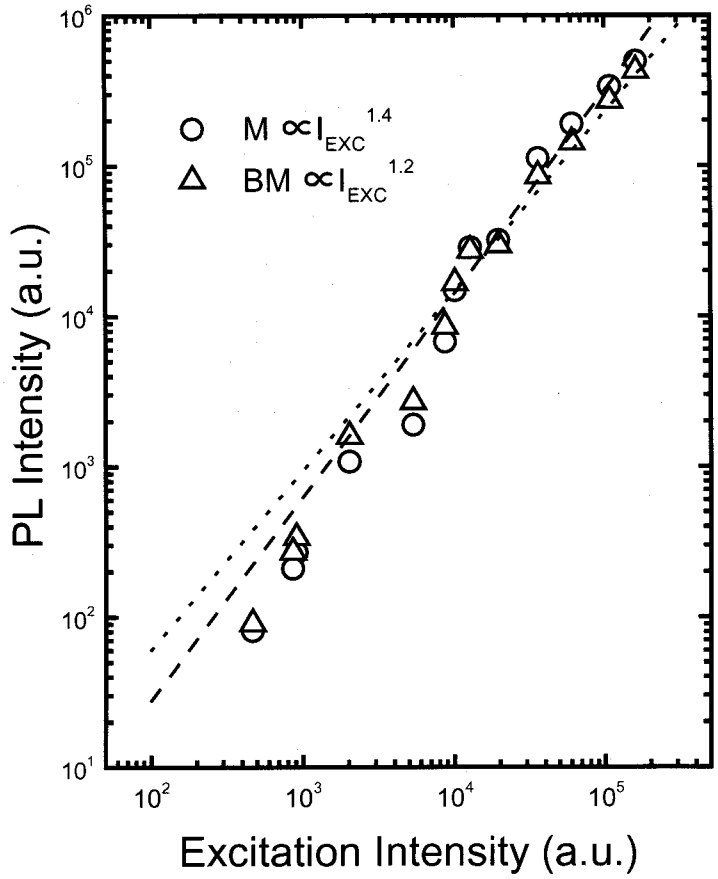

Figure 3-7. Excitation intensity dependence of the PL intensities of the M and BM bands at the excitation photon energy of 3.230 eV. The open circles and triangles indicate the PL intensities of the M and BM bands, respectively.

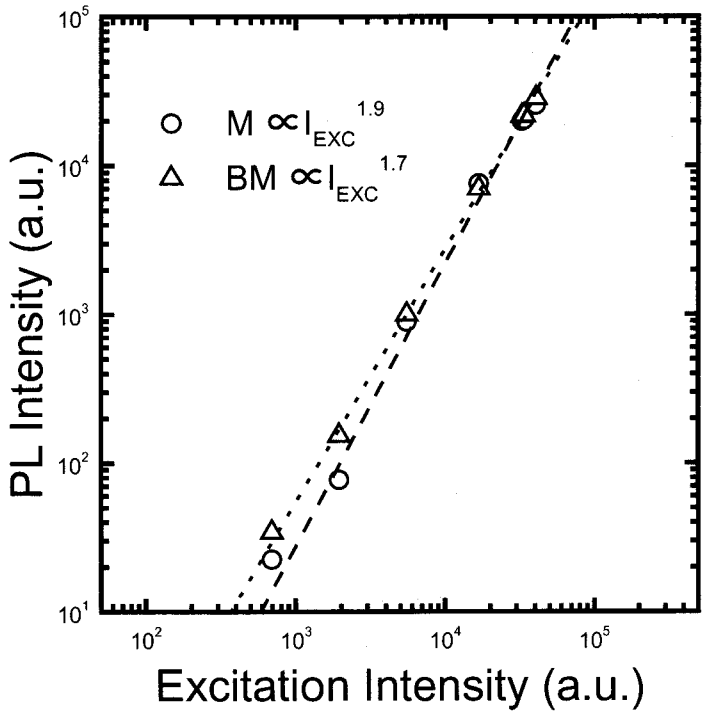

Figure 3-8. The excitation intensity dependence of PL intensities of the M and BM bands at the excitation photon energy of 3.189 eV. The open circles and triangles indicate the PL intensities of the M and BM bands, respectively.

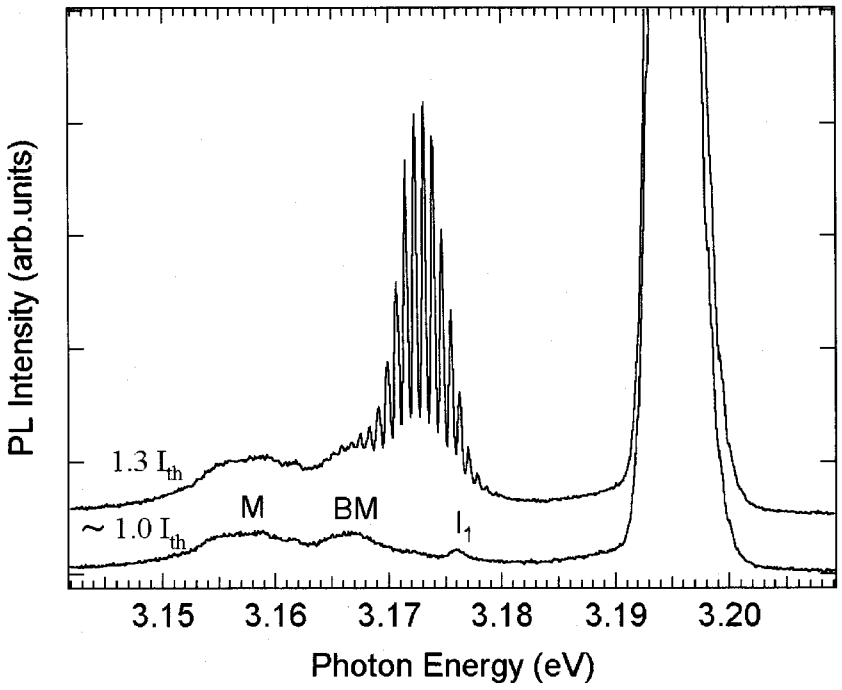

Figure 3-9. Luminescence spectra of CuCl quantum dots at the excitation power below (lower curve) and above (upper curve) the lasing threshold (I_{th}) under the two-photon resonant excitation of confined biexcitons at 4K. The excitation energy of 3.195eV is about 10meV below the one-photon resonance of confined excitons.

Chapter 4

Photoluminescence under Two-Photon Excitation of Biexcitons

4.1 Introduction

The study of the quantum size effect on the confined biexcitons in semiconductor quantum dots is very important and interesting from view of their distinctive features from those of the confined excitons because of larger effective radius and large correlation between electrons and holes. For CuCl quantum dots embedded in NaCl matrices, the studies on the confined biexciton states have been carried out by means of two experimental methods. One is the measurement of the PL spectra of the biexcitons obtained by the size-selective intense excitation of the confined excitons [32], and another one is the transient absorption from the excitons to the biexcitons by means of the pump-probe spectroscopy [31]. However, the reported size-dependence of the PL energy and that of the transient absorption energy are not equal. Therefore, the confined biexciton states in CuCl quantum dots still have many unknown properties to be solved.

Here, I propose for the investigation into the confined biexciton properties that one has to consider strictly the size-selective excitation condition of the biexciton states in the quantum dots. For the confined excitons, the size-selective excitation can be realized by tuning the excitation photon energy. However, the biexcitons would not be created in the quantum dots of the same sizes as in the case of the excitons since the second exciton is created by absorbing somewhat different photon energy from that for the first exciton due to the mutual correlation between two excitons. The stepwise creation

process of the biexciton via a real state of the exciton by the use of two beams can be realized but the method is rather complicated and unconventional.

In former Chapter, the direct creation process of the biexcitons by the two-photon absorption was confirmed. This excitation process is proposed to be a novel technique for the study on the quantum size effect on the biexciton states since it can be realized conventionally by using only one excitation beam. In addition, since there is no excess energy originating from the stabilization energy for the bound two excitons in the creation process of the biexcitons, the simple creation and cascade relaxation process of the biexcitons and excitons can be considered. It has been very difficult to estimate the size of the quantum dot possessing the biexcitons from the PL energy because it is nearly constant in the large dot sizes (a > ~3 nm) [32]. However, the PL energy of the excitons, which are created after the radiative relaxation of the directly created biexcitons by the two-photon absorption, indicates the excited dot size more exactly.

PL of the free excitons can not be observed at low temperature since the excitons are bound to impurities strongly. Therefore, it is necessary to measure the PL spectra at the elevated temperature to confirm the size-selective excitation by two-photon excitation of the biexciton.

4.2 Motivations and purpose

In Chapter 3, the direct creation process of the biexcitons by the two-photon absorption has been clarified by means of polarization dependence of the PL intensity on the excitation light. The question which we must consider next is the confirmation of the sizes of the quantum dots where the biexcitons are created. Although it is prospected that the size-selective excitation of the biexcitons are achieved by the two-photon absorption process, the estimating the excited dot size from the PL energies of the free or bound biexcitons could not be successful because PL energy observed at low temperature showed almost no dependence on the excitation photon energy. This fact agrees with the previous report, in which the PL energy of the biexciton shows nearly constant with changing the effective dot radius larger than 3 nm [32].

In order to resolve this question, it is suggested that the observation the PL energy of

the excitons is an available method to estimate the selected dot size. When the biexcitons are created directly by the two-photon absorption, the excitons are not created directly by the excitation light because the excitation energy is lower than the exciton absorption band. Therefore, the excitons are created only through the de-excitation of the biexcitons. Consequently, we can estimate the selected dot size for the biexciton creation from the PL energy of the excitons by utilizing well-known relation of the exciton energy and the effective dot radius.

Furthermore, when the excitation photon energy corresponds to the one-photon absorption bands, the creation process of the excited biexciton state with J = 2 is observed. In this case, the biexcitons are created in the quantum dots of larger sizes in comparison with that for the resonantly excited excitons by one-photon absorption. Consequently, it is expected to observe the PL peaks due to the exciton, which are associated with the two-photon absorption of the biexcitons, at the lower energy side of that due to the excitons, which are associated with the one-photon absorption.

In this chapter, I report the PL spectra with changing the excitation photon energy corresponding to the both regions of the one-photon absorption band of the excitons and the two-photon absorption band of the biexcitons at 70 K. With using the excitation energy dependence and intensity dependence of the PL spectra, I tried to confirm the possibility of the size-selective excitation of the confined biexcitons.

4.3 Results and discussion

4.3.1 PL spectra under one-photon absorption of excitons

Figure 4-1 shows the PL spectra with changing the excitation photon energy from 3.224 eV to 3.213 eV, together with the PL spectrum obtained by using a continuous wave HeCd laser (325 nm) and the absorption spectrum at the bottom. The excitation photon energy corresponds to the resonant excitation of the confined excitons size-selectively.

When the excitation energy was 3.242 eV as in curve (a), two PL bands of the confined exciton (X, X_1) and a PL line of the bound exciton trapped to the neutral donors (I_1), the free and bound biexciton (M, BM) were observed. Since the peak

energy of the X_1 band is the same as the excitation photon energy, it is associated with the excitons which are created size-selectively in the dots of the effective radius a = 2.8 nm by the resonant excitation. The spectral width of the X_1 band is ~5 meV, which is broader than that of the excitation light (2.7 meV) because of the interaction with the acoustic phonons. On the other hand, the X band is located on lower energy side at peak energy of the absorption band and the PL peak energy shows no dependence on the excitation energy. When the excitation energy was decreased, the PL intensity of the X band decreased relatively to that of the X_1 band, and finally, the X band was overwhelmed by the X_1 band. Accordingly, it is suggested that the X band originates from the excitons which are created by the resonant excitation of the higher confinement states of exciton in larger dots.

Figure 4-2 shows the excitation intensity dependence of the PL intensities of X_1, X, BM and M bands at the excitation photon energy of 3.237 eV which corresponds to resonant energy of the confined excitons in the dot radius of ~3.1 nm. The PL intensity of the X_1 band shows a linear dependence at low excitation intensity and then tends to saturate as the excitation intensity is increased. On the other hand, the BM and M band increased superlinearly ($\propto I_{exc}^{1.5}$) as the excitation intensity increased. The X band also shows sublinear dependence like the X_1 band. However, the PL intensity relative to the X_1 band became larger with increasing the excitation intensity.

To show the change of the relative PL intensities clearly, the excitation intensity dependence of the PL spectra, which are normalized by the PL intensity of the X_1 band, are shown in Fig. 4-3. The numbers of the created excitons in the dots by the resonant excitation follows a Poisson distribution. Therefore, when the excitation intensity is increased, the PL intensity of the X band should saturate. On the other hand, in the case of the resonant excitation of the higher confinement states, the two or three excitons can be created in the dots. Therefore, the relative PL intensity of the X band may be larger than that of the X_1 band. When the excitation energy was changed, the excitation intensity dependence of the PL intensities of these bands was changed slightly, but overall feature was nearly the same.

On the other hand, the M band shows, in principle, the superlinear dependence on the X band intensity, which is a typical feature of the PL bands due to the biexcitons.

4.3.2 Two-photon absorption of excited biexciton states

In Chapter 3, the two-photon absorption of the excited biexciton states with J = 2 has been proposed by the polarization dependence of the PLE of the biexcitons for the excitation light. Under this excitation condition, the PL band of the excitons which are created after the relaxation of the biexcitons was expected to appear at the lower energy side of the excitation photon energy.

In Fig. 4-3, the new PL structure denoted by X' appears around 3.23 eV, which is overlapped with X band, as the excitation intensity is increased. It is suggested that the X' band is attributed to the excitons which are created by nonlinear excitation process. According to Eq.(B-5) in Appendix B, when the exciton is created in the quantum dots of ~3.1 nm, the dot radius where the excited biexciton is created is estimated to be ~3.7 nm. The PL energy of the exciton in the quantum dot of ~3.7 nm is 3.231 eV. Therefore, X' band is thought to be the PL band of the excitons which are created after the relaxation of the biexcitons created directly into J = 2 state by the two-photon absorption process.

However, I could not succeed in the observation of the X' band clearly in all cases of the excitation energy since the spectral width of the PL bands were broader so that it hide the fine structures of the expected exciton bands. If the measurements will be performed with the excitation laser with the narrower spectral width, there is a possibility that we can discuss the dot size where the biexcitons are created at J = 2 state by the two-photon absorption process.

4.3.3 PL spectra under two-photon absorption of biexcitons

Figure 4-4 shows the PL spectra with changing the excitation photon energy which corresponds to the resonant two-photon absorption of the lowest biexciton. At 70 K, the exciton resonant energy of the CuCl bulk crystal is 3.215 eV. In the PL spectra, two PL bands, which are attributed to the biexcitons and excitons, appeared on the lower and higher energy sides of the excitation photon energy, respectively. Since the excitation photon energy was lower than the one-photon absorption band, the excitons are not directly excited by the excitation light. Consequently, the creation process of the excitons originated from the radiative-cascade relaxation from the biexcitons which are created directly by the two-photon absorption.

At the lower energy side of the excitation energy, there are the PL peaks of the free and bound biexcitons (M and BM). In addition, M band has two fine structures which are denoted by open squares and diamonds. The origins of these fine structures have been still ambiguous. However, it can be reasonable that these are associated with the several excitonic modes as the final states of the transition from the biexciton states. In the case of the bulk crystal, the two PL bands were observed, which are associated with transition from the lowest biexciton to the longitudinal and transverse excitons, respectively [49]. In the nanocrystal or quantum dots, L-T modes of the biexciton couple and form new modes [66]. In addition, the surface mode of the exciton will appear, which shows almost constant energy for the change in the dot size. There is a possibility that the fine structures in the biexciton band are related to these modes which, however, have not been observed experimentally until now.

On the other hand, at the higher energy side of the excitation energy, the PL band (X) of the excitons was observed. Figure 4-5 shows the excitation intensity dependence of the PL intensities of X, BM and M bands (solid circles, squares and triangles) at the excitation photon energy of 3.198 eV. The PL intensities of both the X and M bands increased superlinearly ($I_{EXC}^{1.7}$) with the excitation intensity. Namely, the PL intensity of the exciton showed the excitation intensity dependence similar to that of the biexcitons. As a result, it is concluded that the excitons are created after the relaxation of the biexciton which are created by the two-photon absorption.

Based on this evidence, the number of the exciton should be the same as that of the biexciton. However, the PL intensity of the M band is larger than that of the X band. When the excitation photon energy corresponds to the one-photon absorption band, only the quantum dots near the surface of the sample are excited due to the attenuation of the excitation light inside the sample. However, in the case of the two-photon excitation condition, the excitation light pass through the whole thickness of the sample, and the quantum dots inside the sample were excited. Since the PL of the exciton was affected by reabsorption process, the PL intensity of the exciton is weaker than that of the biexcitons although it is thought that the created numbers of the biexcitons and the excitons are the same. Some difference in the quantum yields of luminescence between the exciton and biexciton might be the additional factor.

4.3.4 Energy relation between confined biexcitons and excitons

Figure 4-6 shows the PL peak energies of the excitons (solid circles), the bound biexcitons (open triangles) and two peaks of the free biexcitons (open squares and diamonds) plotted as a function of the excitation photon energies. The PL energies of three peaks associated with the biexcitons showed almost no dependence on the excitation photon energy. This feature is consistent with the previous reports, in which the PL energy of the biexciton is almost constant in the quantum dot of the larger sizes. On the other hand, the PL energy of the exciton was changed very sensitively with the change in the excitation photon energy. Since the excitons are created after the radiative relaxation of the biexcitons which are created directly by the two-photon absorption, the PL energy of the excitons can be concluded to indicate directly the dot-size where the corresponding biexciton are created. In other words, it is confirmed that the biexciton were excited size-selectively by the two-photon absorption although the biexciton luminescence peaks do not shift in energy.

When the excitation photon energy was decreased, the satellite peaks at the lower energy side of the X band appeared. I speculate that these satellites may be originated from the two-photon absorption of the higher confinement states of the biexcitons confined in the larger dots. It would be possible that the excitation photon energy corresponds not only to the resonant excitation of the lowest confinement state but also to the higher confinement states of the biexcitons. In this case, the exciton PL will appear at the lower energy side of the fundamental PL of the X band.

Here, I examined the energy relation of the exciton and biexciton PLs obtained by the two-photon absorption, and compare it with that of the previous reports. The two-photon excitation energy is half the energy of the biexciton state, that is, it must appear just at the middle energy between the PL energies of the biexciton and exciton. Based on this assumption, I calculate the expected energy values for the transition between the exciton and biexciton, which were obtained by subtracting the exciton PL energy from twice the excitation energy. They are plotted as a function of the exciton PL energy as open circles in Fig. 4-7, together with the transition absorption energies (solid triangles) reported by Masumoto *et al* [31]. Here, the calculated transition energies were recalibrated by 2 meV with taking account of the temperature difference between 70 and 77 K of the band gap. As a result, the calculated transition energy coincides well with the transient absorption energy. On the other hand, in Fig. 4-8, the PL energies of the

free biexcitons (open squares and diamonds) obtained by the two-photon absorption are shown, together with the PL energies of the biexcitons reported by Itoh [32]. The lower PL peak energies (open diamonds) are almost the same as those obtained by the band-to-band excitation (solid triangles). However, the higher energy peaks (open squares) do not corresponds to any reported structures. Analysis of the features of the excitation energy dependence of the PL spectra of the biexcitons is rather difficult and complex because one can not deny the possibility that there are further structures in the PL bands, which are unresolved due to the band-width of the excitation laser or the spectral broadening owing to high temperature in the PL band.

In Figures 4-7 and 4-8, the energy values obtained by the present experiment (open circle in Fig. 4-7, and open diamonds in Fig. 4-8) around the exciton energy of 3.223 eV deviated away from the aforementioned explanations. The reason is not well known, but these energy values were obtained at the two-photon excitation energy of 3.194 eV, and it is much lower than the two-photon absorption energy for the bulk crystal, which is 3.200 eV at 70 K [52]. Therefore, it is speculated that the unknown mechanism is involved in the two-photon excitation process for larger dot sizes.

As a result of the investigation of the energy relation between the excitons and biexcitons obtained by the present two-photon absorption measurement, it was clarified that the behavior of the PL energy of the excitons coincides well with the result of the transient absorption measurement, and the PL of the biexcitons agreed nearly with the result of the previously reported one. Therefore, it may be concluded that the transition energy between the excitons and biexcitons may be different between the absorption and emission processes. It is still open to question.

4.4 Summary

I have measured the PL spectra of CuCl quantum dots with changing the excitation photon energy which corresponds to the one-photon absorption band of the excitons and the two-photon absorption band of the biexcitons, at 70 K. As a result, I have succeeded in the confirmation of the size-selective excitation of the confined biexcitons which are created by the two-photon absorption process.

When the excitation photon energy falls inside the one-photon absorption band of the exciton, the PL bands due to the excitons (X_1, X) and the free and bound biexciton (BM and M) were observed. The X_1 band is due to the excitons which were created size-selectively by the resonant excitation of the excitons because the PL energy was the same as the excitation photon energy. On the other hand, the X band is associated with the excitons which are created at the higher energy confinement states in the quantum dots with larger dot sizes than that for the X_1 band. In addition, the PL intensities of M and BM bands increased superlinearly with respect to that of the exciton band. This is the typical feature of the PL bands attributable to the biexcitons.

When the excitation energy is 3.237 eV which corresponds to confined exciton energy in the quantum dot of the radius ~3.1 nm, the new PL band (X') appears at the lower energy side of X_1 band with increasing the excitation intensity. PL energy of the X' band is consistent with the exciton energy which is estimated from the assumption that the excitons are created after the relaxation of the biexcitons which are created directly into excited state of $J = 2$ by the two-photon resonant excitation. This assumption supports the dependence of PLE spectra of the biexciton on polarization of the excitation light in Chapter 3. As a result, the two-photon absorption process of the excited biexciton states is confirmed.

In the case that the excitation photon energy corresponds to the two-photon absorption of the biexcitons, the PL band of the exciton, which are created after the relaxation process of the biexcitons, were observed at the higher energy side of the excitation energy. The PL energies of the excitons were quite sensitive to the excitation energy. From the PL energy of the excitons, we can deduce the excited dot size for the biexcitons by the two-photon absorption. Therefore, it was confirmed that the size-selective excitation of the biexcitons was successful by the resonant two-photon absorption.

The relation between the PL energy of the excitons and the excitation photon energy shows that the biexciton state calculated from energy difference between the exciton and biexciton obtained by the two-photon absorption measurement is consistent well with the previously reported energy obtained by the transient absorption measurement. On the other hand, the PL energy of the biexcitons agrees with that obtained by the size-selective excitation. As a result, it seems reasonable to conclude that the biexciton states observed by the absorption process does not coincide with the PL transition

energy from the biexciton to excitons. In order to clarify the difference of the transition energies obtained by the absorption and luminescence processes, further experiments will be necessary. For example, the measurement of transient absorption measurement with use of pump-probe spectroscopy or time-resolved PL spectra under the excitation condition of the two-photon absorption of the biexcitons, will provide us more detailed information about the energy levels of the confined biexciton and exciton states.

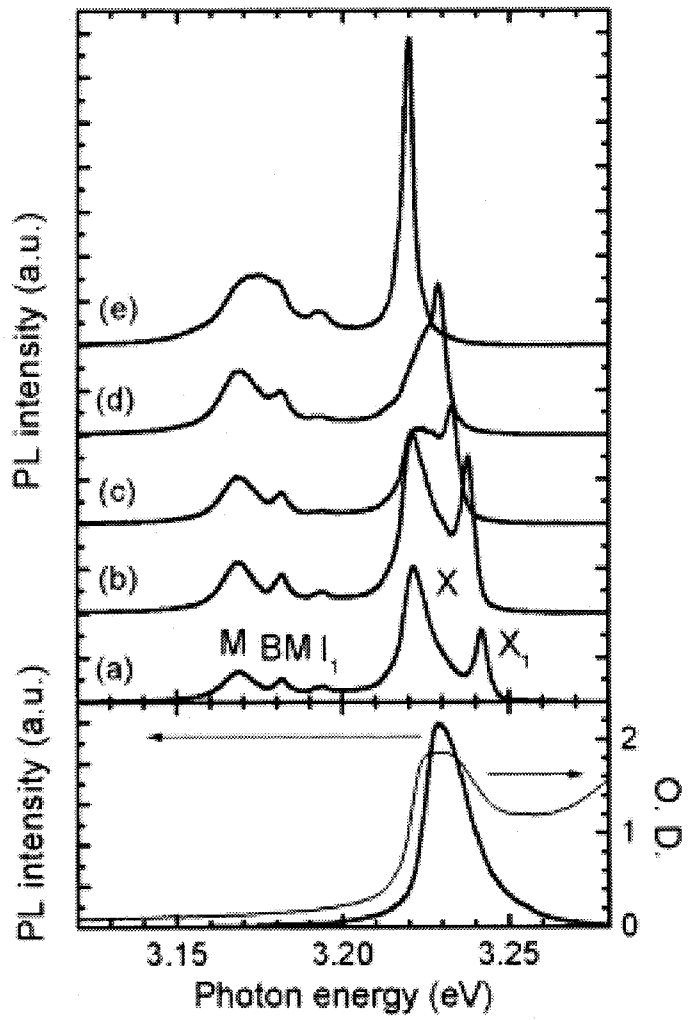

Figure 4-1. Lower traces show the PL spectrum (thick curve) obtained by using a cw HeCd laser (325 nm) and absorption spectrum (thin curve) at 77 K. Upper traces show the PL spectra obtained by using a FH light of a signal beam from an OPA. The excitation photon energies are 3.242 eV (a), 3.237 eV (b), 3.235 eV (c), 3.228 eV (d) and 3.220 eV (e), respectively.

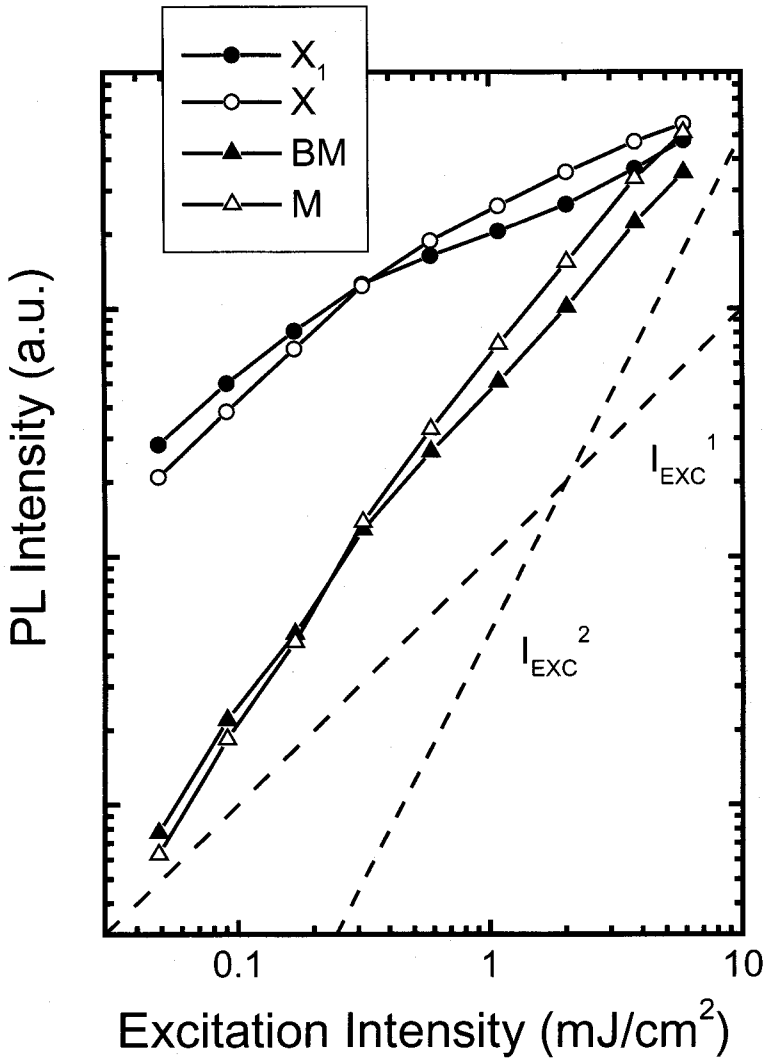

Figure 4-2. The excitation intensity dependence of the PL intensities of X_1 (solid circles), X (open circles), M (open triangles) and BM (solid triangles) bands when the excitation photon energy is 3.237 eV.

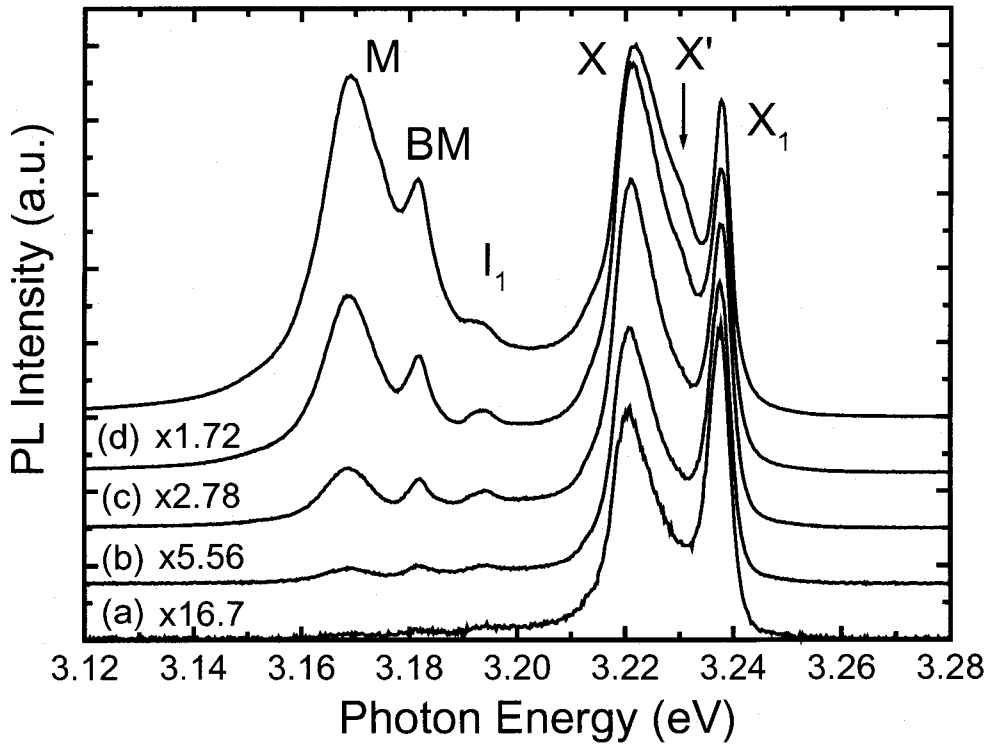

Figure 4-3. The excitation intensity dependence of the PL spectra with the excitation photon energy of 3.237 eV. The PL intensities were normalized for that of the X bands. The excitation intensities were (a) 0.05, (b) 0.17, (c) 0.58, (d) 2.0 and (e) 5.8 mJ/cm^2, respectively.

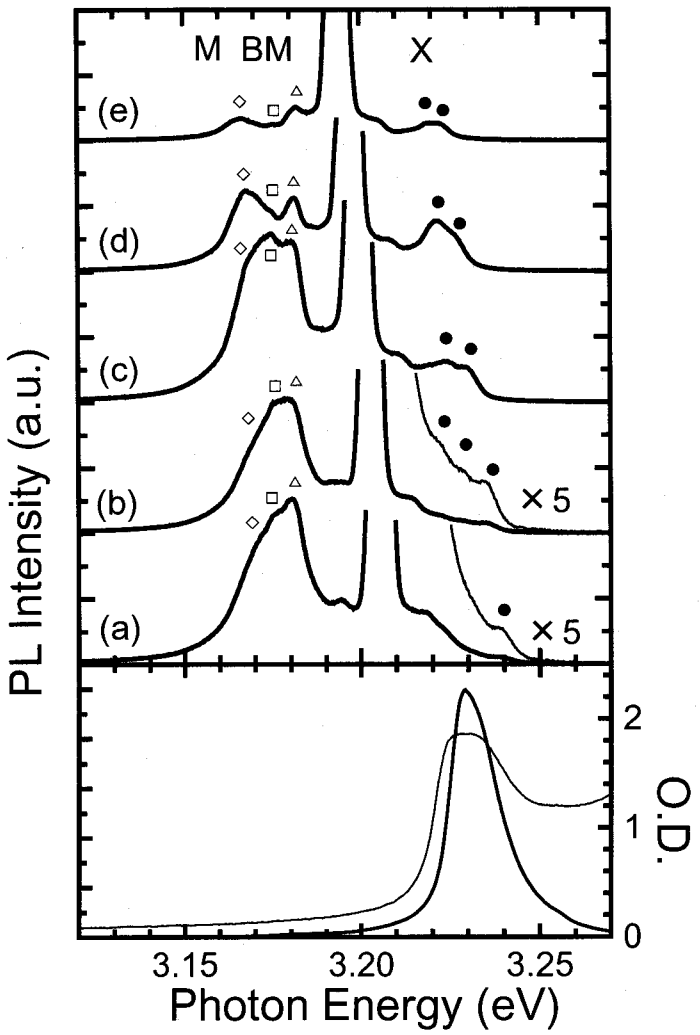

Figure 4-4 Lower traces show the PL spectrum (thick curve) obtained by using a cw HeCd laser (325 nm) and absorption spectrum (thin curve) at 77 K. Upper traces show the PL spectra obtained by using a FHG of a signal beam from an OPA. The excitation photon energies are 3.205eV (a), 3.203 eV (b), 3.199 eV (c), 3.197 eV (d) and 3.194 eV (e), respectively. The solid circles show the PL peaks in the X band due to the excitons. The open triangles, squares and diamonds show the PL peaks of the bound biexcitons (BM) and two of the structures in free exciton band (M).

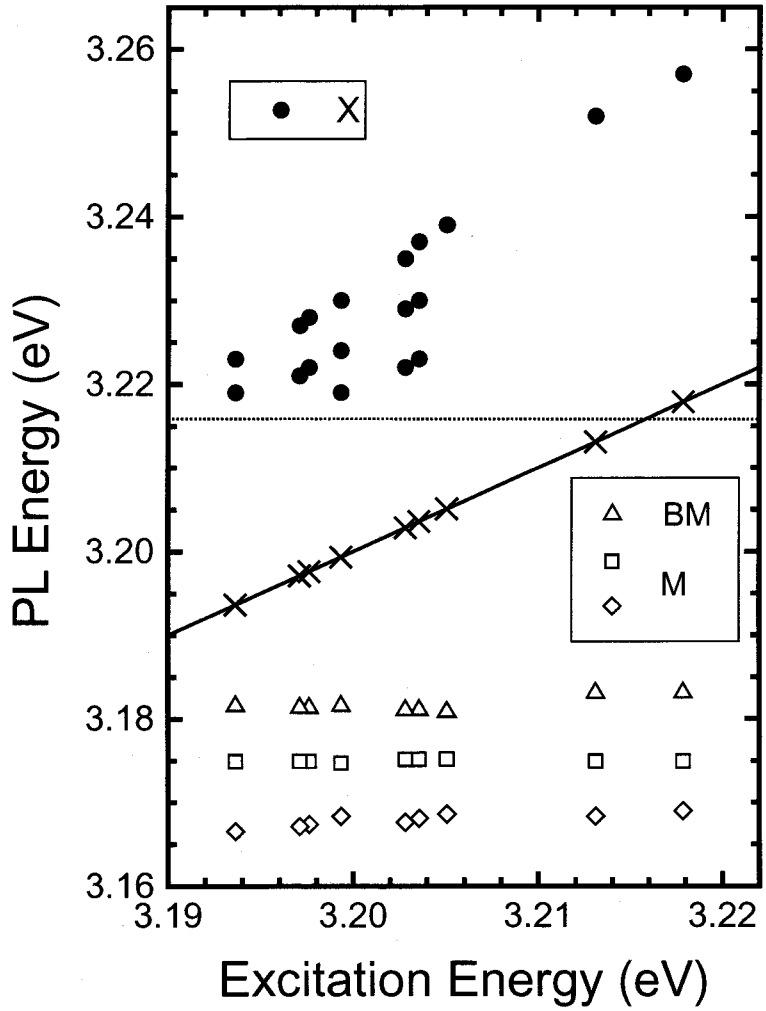

Figure 4-6. The excitation photon energy dependence of the PL energies of the X (solid circles), M (open triangles and diamonds) and BM bands (open squares), respectively. The crosses indicate the excitation energy, and the dotted line indicate the exciton energy in the bulk crystal.

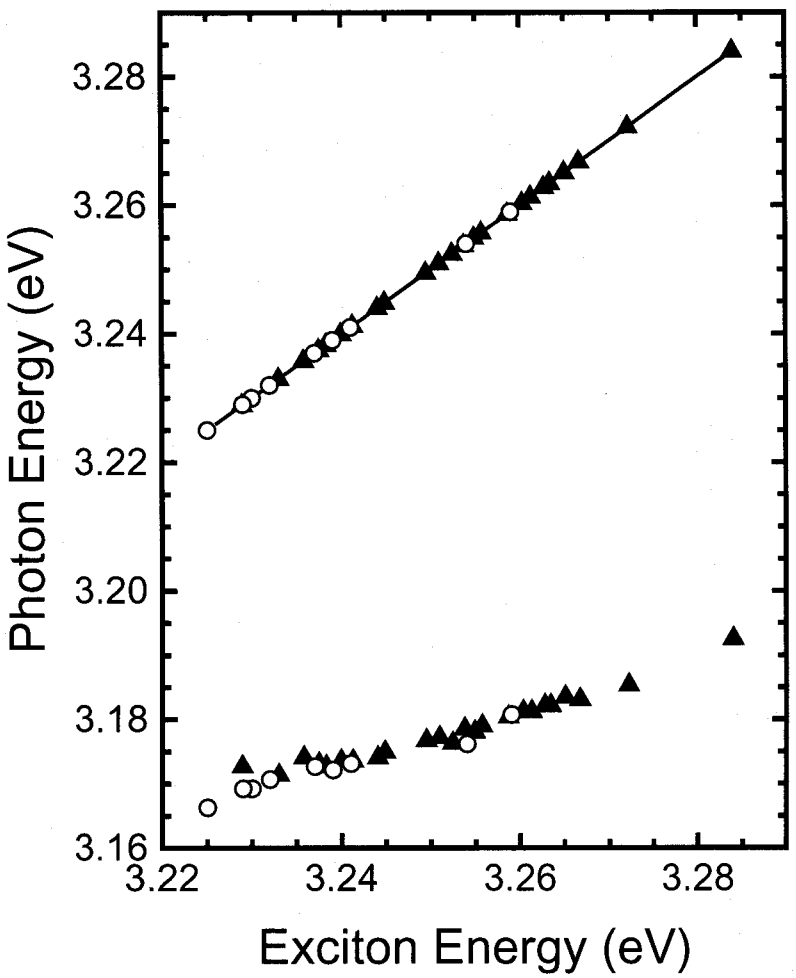

Figure 4-7. Energy relation between the excitons and the transition between the exciton and biexciton. The open circles were obtained by subtracting the exciton energy from twice the excitation photon energy under the two-photon excitation of the biexcitons. The solid triangles show the previously reported values obtained in the transient absorption measurement.

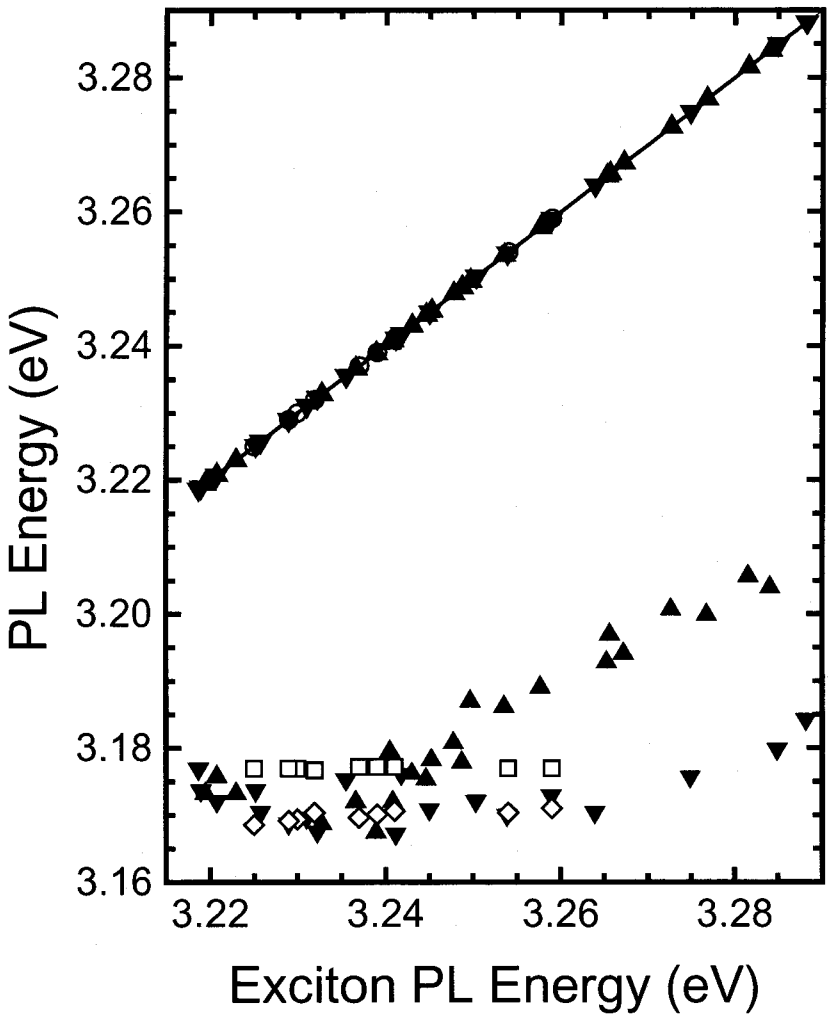

Figure 4-8. The PL-energy relation between the excitons and biexcitons. The open squares and diamonds show the PL energy of the biexcitons, which were obtained in the two-photon absorption measurement. The solid triangles and inverted triangles were previously reported values obtained in the size-selective excitation of the excitons.

Chapter 5

Mid-Infrared Transient Absorption Spectroscopy

5.1 Introduction

In recent years, optical investigations of semiconductor nanocrystals or quantum dots have been performed extensively. The electronic structure in the quantum dots shows atomic-like discrete energy levels by the three dimensional confinement of electrons and holes. To date, previous studies on the quantum size effect have been concentrated on their lowest state properties. However, it is interesting to study the excited state properties because of wider and anisotropic wavefunctions compared to that of the lowest state. Consequently, the quantum size effect on the excited states is expected to be different from that on the lowest state. In addition, the optical nonlinearlity associated with the transitions between sublevels of the electron – hole pairs (exciton) are expected to be available for the novel infrared devices. In fact, utilizing the sublevel transition, the developments of the quantum cascade lasers [6] or infrared photodetectors [8] have been investigated in recent years. Therefore, it is important to study the optical properties not only of the lowest state but also of the higher excited states of confined excitons and multi-excitons.

Transient absorption measurement is very useful for the study of the excited state properties, since it provides us much information about the transition dynamics between the sublevels, which can not be observed by the conventional photoluminescence (PL) or one-photon absorption spectroscopy. Up to now, an infrared transient absorption (IRTA) of the quantum dots was reported mainly for the strong confinement regime, for example, InAs/GaAs dots [67], CdSe colloids [68, 69] and Si/Ge quantum dots [70]. In

these researches, the reported IRTA were attributable to the transitions between 1s and 1p quantum confined states or from-bound-to-continuum states of the electron or hole. On the other hand, for the weak confinement regime, the IRTA of CuCl quantum dots embedded in NaCl was reported [53, 54]. For this material, IRTA is ascribed mainly to the transition from Rydberg 1s to 2p state of the confined exciton. Thus, there were the reports on the IRTA only of one electron-hole pair or exciton for both of the weak and strong confinement regimes.

However, there is no report on the IRTA of the biexciton states. Up to now, "excited biexciton states" described generally in the previous reports have indicated the anti-bounding states of the two 1s excitons. The quantum size effect to such state was investigated already for CuCl quantum dots [31, 37], as described in Chapter 1. However, the excited biexciton states, which are composed of higher Rydberg states (2s, 2p, 3s, 3p...) of the exciton, have not been investigated. Molecular orbitals of a hydrogen molecule is well-known, including not only the pairs of Rydberg 1s state but also that is related with the higher Rydberg state (n = 2) of hydrogen atom [71]. Since the biexcitons in the semiconductor can be considered to have the comparable energy levels of the hydrogen molecule, it is reasonable to suppose the existence of the excited biexciton states including the excited exciton with the higher Rydberg state.

The quantum confinement effects to such excited biexcitons have strong possibilities to induce the specific properties which have not been observed. First, the excited biexciton has the larger correlations between two electrons and holes compared to the lowest one because of the wider wave functions. Therefore, quantum confinement affects not only on the translational motion of the biexcitons but also on the relative motions of the electrons and holes. This is the unknown regime of the quantum size confinement. Next, two excitons in one quantum dot have to be spatially confined, so that they can not dissociate completely even if they absorb the larger photon energy than the dissociation energy, namely biexciton binding energy. Therefore, the transition dynamics are expected to show the specific features that never appear in the bulk crystal.

CuCl quantum dot is an appropriate material to study the excited states of the confined biexciton since the quantum confinement affects on the translational motion of the lowest biexciton in the case of the larger quantum dots (a > 3 nm). In this work, I report the IRTA originating from the biexciton confined in CuCl quantum dots. To our

knowledge, the IRTA of the biexciton confined in the semiconductor quantum dots is the first observation. The transition energies from the lowest to higher excited biexciton states will be discussed in comparison with that of the confined exciton.

5.2 Motivations and purpose

As the aforementioned description, the IRTA due to the confined exciton for CuCl quantum dots was reported. However, there still remain many unresolved questions.

Firstly, the temporal resolution is not sufficient to resolve the fast decay time of the IRTA, so that the assignment of the confined exciton to the fast component is still ambiguous. Thus, it is necessary to confirm that the transient absorption is actually induced by the exciton, and to examine the possibilities of other origins for the transient absorption. Among them, it is interesting to study the excited states of the confined biexciton state under the high excitation intensity. No one has even reported the IRTA of the biexciton confined in the semiconductor quantum dots.

Secondly, the observed IRTA spectra had large spectral widths due to the rack of spectral resolution and the absorption band corresponding to the individual higher excited states were not resolved. Therefore, it is also interesting to observe the transient absorption with higher spectral resolution in order to examine the influence of the higher excited states.

In order to solve these questions, I have performed the IRTA measurement by means of ultrafast pump-probe spectroscopy with the use of a dual OPA system. The pulse duration of ~2 ps from the OPAs is sufficient to resolve the decay components of biexciton (several tens ps) and exciton (several hundreds ps) confined in the CuCl quantum dots [33]. In addition, the higher peak energy of the short pulse laser can create larger amounts of electron-hole pairs efficiently, compared to the previous experiment, where the effective numbers of created exciton per a quantum dot are ~0.15 by taking account of the pulse duration. Therefore, the IRTA associated with the biexciton may be expected to be observed in this experiment. Furthermore, in the previous measurement, the poor spectral resolution was caused by the large slit width of the monochromator, which was necessary to collect weak differential absorption signals. By adopting the

pulse lasers for both of the pump and probe lights, however, the IRTA spectrum is expected to be obtained with higher spectral resolution which is determined by the band width of the probe pulse.

In this section, I report on the IRTA of CuCl quantum dots with higher temporal and spectral resolutions by means of pump-probe spectroscopy using the dual OPA system.

5.3 Results and discussion

5.3.1 PL spectrum

Figure 5-1 shows a typical PL spectrum at 70 K. The excitation wavelength was 383.9 nm (3.229 eV) that corresponds to resonant excitation of the excitons confined in the quantum dots with the radius a = 3.9 nm. The excitation intensity was 2 mJ/cm^2. The resonant PL from the exciton is not separable from the scattered excitation light. The M band, which appeared in the lower-energy side of the excitation light, is due to the radiative relaxation from the biexciton state to the exciton state. Thus, it is evident that biexcitons were created in a considerable amount of the quantum dots under the present excitation condition.

As discussed in Chapters 3 and 4, when the excitation energy falls inside the absorption band of the confined excitons, the biexcitons are created in the quantum dots by two-photon absorption process for the excited state of J = 2. Consequently, the dot size for biexciton creation is different from that for exciton creation (3.9 nm). By using the size relation of Eq. (B-5), it is suggested that the biexcitons exist in the quantum dots of a = 4.6 nm

5.3.2 Temporal profile of IRTA

Figure 5-2 shows the temporal profile of the IRTA measured at the probe photon energy of 250 meV (4.9 μm) with pump photon energy of 3.227 eV (384.1 nm). At this pump photon energy, the dot radius in which the excitons and biexcitons were created is estimated to be 4.2 nm and 5.5 nm, respectively.

The IRTA exhibits two decay components in a sub-nanosecond region. This result

clarifies that previously reported faster decay component (<1 ns) was decomposed further into two kinds of components. The decay curve was fit by calculated curve assuming two exponentially decay components as follows:

$$I_{\mathrm{IRTA}}(t) = C_1 \cdot \exp\left(-\frac{t}{\tau_1}\right) + C_2 \cdot \exp\left(-\frac{t}{\tau_2}\right) \qquad (5.1)$$

where C_1 and C_2 are absorption intensities at $t = 0$. As a result, the faster decay time (τ_1) was obtained to be ~56 ± 15 ps and the slower one (τ_2) was ~490 ± 200 ps. These decay times are almost the same as those previously reported for the biexciton (~65 ps) and exciton (~380 ps) in the quantum dots, respectively [33].

Figure 5-3 shows the excitation intensity dependences of the intensities of the two decay components at $t = 0$. The faster decay component increases superlinearly with the excitation intensity ($\propto I_{EXC}^{1.3}$), while the slower one has a linear dependence ($\propto I_{EXC}^{1.0}$). From these results, it is suggested that the observed IRTA components with the faster and slower decay times are induced from the confined biexciton and exciton, respectively.

Here, the calculated curves are obtained under the assumption that the biexcitons and excitons are created simultaneously at $t = 0$ and the effect of the excitons which are created after the relaxation of the biexcitons is neglected. It is impossible to fit the calculated curve including such effect to the experimental data. Therefore, the estimated IRTA intensity of the slow decay component includes approximately the effect of both the excitons which are created directly by the excitation light and created after the relaxation of the biexcitons.

5.3.3 PL and IRTA under two-photon excitation of biexcitons

In order to confirm that the IRTA is caused by the biexciton, I examined the IRTA under the two-photon resonant excitation of the confined biexciton. In chapter 3, it is clarified that selection rule of the biexciton with lowest state (J = 0) is available in the quantum dot.

Figure 5-4 shows the PL spectra (A) and IRTA temporal profiles (B) under the excitation with the photon energy of 3.204 eV, which is lower than the resonant energy of the exciton for the bulk crystal. Therefore, the biexciton of J = 0 is created directly by the excitation light and the creation process of the exciton is only the cascade relaxation

process from the biexciton. In the PL spectra, I clearly observed the PL bands of the biexcitons (~3.18 eV) on the lower energy side of the excitation light and even the excitons (3.235 eV) on the higher energy side. The dot radius for the biexciton creation is estimated to be 3.5 nm from the PL energy of the exciton. In addition, the PL intensities of the biexciton and exciton decreased under the circularly polarized excitation light compared to the linearly polarized one. This feature of the polarization dependence coincides with that of the low temperature measurement in Chapter 3, so that it is evident that the biexcitons of the lowest state are created in the quantum dots by the two-photon resonant excitation.

On the other hand, the existence of the fast decay component of the IRTA suggests that it is originating from the biexciton state. In addition, the IRTA of the fast component decreased for the circularly polarized light, which is similar to the case of the biexciton PL spectra. As a result, I concluded that the fast decay component of IRTA is originated from the lowest biexciton state. To our knowledge, this is the first observation of the IRTA attributable to the biexciton state confined in semiconductor quantum dots.

The solid and dashed curves are obtained by calculation fitted to the experimental decays with the linearly and circularly polarized excitation lights, by using the equation:

$$I_{\mathrm{IRTA}}(t) = C_1 \cdot \exp\left(-\frac{t}{\tau_1}\right) + C_2 \cdot \left[\exp\left(-\frac{t}{\tau_2}\right) - \exp\left(-\frac{t}{\tau_1}\right)\right] \qquad (5.2).$$

Here, the first and second terms on the right hand side of Eq. (5.2) show the contributions of the biexcitons and excitons, respectively. As a result, the IRTA of the biexciton is much larger than that of the exciton although the number of the exciton should be the same as that of the biexciton.

5.3.4 IRTA spectra

Figure 5-5 (A) presents the IRTA spectra originating from the biexciton (closed circles) and the exciton (open circles) under the excitation photon energy of 3.227 eV (384.1 nm). The dot radius in which the excitons and biexcitons were created is estimated to be 4.2 nm and 5.5 nm, respectively. The transient absorption is dominated by the biexciton absorption at this excitation intensity (~2 mJ/cm^2). The absorption spectrum has a main peak at 225 meV (spectral width ~50 meV) with a tail to the higher

energy side. On the other hand, in the absorption spectrum of the exciton, one could not observe any structure because of the insufficient signal to noise ratio. The peak energy of the biexciton is almost same as that of the exciton previously reported, shown in Fig. 5-5 (B) [53]. In the following, we focus on the IRTA originating from the confined biexciton state and discuss it in comparison with that due to the confined exciton discussed in the previous reports [54, 55].

For the exciton confined in spherical dots, the transition energies from the lowest (1s, 1S) state to the P-like states (np, n'S), (ns, n'P), etc. have been calculated [54, 55]. Theoretical IRTA spectrum of CuCl quantum dots with the radius of $a = 5.6$ nm is shown in Fig. 5-5 (C). Here, the vertical lines indicate the energies and strengths of the transitions to the p-like states. The theoretical spectrum with broadening was obtained by convoluting the line spectral width Gaussian functions with an arbitrary width (~40 meV). It has a main peak at 190 meV that originates from the transition to the (2p, 1S) state, and several small peaks due to (np, 1S) ($n > 2$) and others in the higher energy side. The calculated transition energy to the (2p, 1S) state as a function of the dot size is plotted by the solid curve in Fig. 5-6, together with our experimental point (closed circle), the experimental data from Ref. [53] (open circles) and separation energy between 1s and 2p states of the exciton for bulk crystals [20] (dashed line). The peak energy of the IRTA originating from the biexciton (closed triangle) eventually almost coincides with the transition energy of 1s–2p state of the confined exciton. Also, the spectral shape of the IRTA has a wide tail in the higher energy side, suggesting the absorption to the higher excited states.

In order to explain these features, we consider the following assumption. The lowest state of the biexciton is composed of two 1s excitons. The excited-biexciton states are supposed to be mainly composed of one 1s lowest exciton and one excited exciton (e.g. 2p state). The speculated energy diagrams are shown in Fig. 5-7. In general, such states would not to be stable in bulk crystal and the biexciton would separate into the two excitons since the excess energy of the excited state is considerably larger than the biexciton binding energy (~50 meV). In the three-dimensional confinement as in the case of quantum dots, however, the two excitons do not separate so that the excited biexciton states become stable. Under this assumption, it is reasonable that the observed IRTA spectrum of the biexciton is very similar to that of the exciton.

In addition, it is interesting that the observed IRTA from the biexciton state is much

stronger than that of the exciton. Taking account of the fact that the decay of one biexciton remains one exciton, we suppose that the absorption cross section of the biexciton is more than two times larger than that of the exciton (giant oscillator strength).

5.3.5 Energy levels of hydrogen molecule

By the experimental results of the mid-infrared transient absorption, the excited biexciton states which comprise the lowest state and excited states of the excitons have been proposed. I will discuss such excited biexciton states in aspect of the energy levels of the hydrogen molecule.

The electronic energies of diatomic molecules have been investigated. Figure 5-8 shows the electron states of the H_2 molecule reported by Mulliken [72]. The vertical axis indicates the potential energy and the literal axis shows the distance between two nucleuses. Namely, the limitation of the distance toward 0 results in He atom. On the other hand, for further distance, there are two isolated H atoms. The molecular orbital of lowest state of H_2, which is expressed by $^1\Sigma_g^+$, is composed of two H(1s) atoms. The higher states which are composing of one H(1s) and one H(2s or 2p state) are expressed by $^1\Sigma_u^+$, $^1\Pi_u$,...., where Σ means total orbital momentum, which is denoted as Σ, Π, Δ,... ,and upper symbol + (or –) expresses sign on reflection in a plane passing through the nuclei and lower symbol g (or u) indicates symmetry of parity respect to the operation of inversion of the wave function.

The transition from $^1\Sigma_g^+$ state to $^1\Sigma_u^+$, $^1\Pi_u$ states have been observed experimentally and its energy is called "second dissociation energy" of H_2 [71]. Consequently, it is reasonable to consider that IRTA of the biexciton observed in my measurement is associated with the excited biexciton states composing of one 1s exciton and one 2p exciton. Replacing this fact into the IRTA absorption energy of the biexciton, the transition energy of biexciton is expected to be larger than that of the excitons.

When H_2 atom absorbs the photon, which of energy corresponds to the transition energy to higher excited state, it separates into two H atom. In the case of the confined biexciton in semiconductor quantum dots, it never dissociate into two excitons. Therefore, It is interesting to study the confinement effect on the transition energy of the biexciton in semiconductor quantum dots.

5.4 Summary

I have measured the mid-infrared transient absorption for the CuCl quantum dots embedded in NaCl matrix by pump-probe spectroscopy with picosecond temporal resolution. I have observed two decay components of the IRTA, which decay times are ~56 ps and ~490 ps, respectively. The faster component is increased superlinearly with the excitation intensity, on the other hand, the slower component shows linear dependence. As a result, the faster and slower decay components are attributed to the confined exciton and biexciton, respectively.

The existence of IRTA contributed by the biexcitons is confirmed by the measurement under the two-photon excitation of the lowest biexcitons; the IRTA intensity decreased with the circular polarized excitation light compared to with the linearly polarized light. The IRTA of the confined biexciton in semiconductor quantum dots is the first observation.

The IRTA of the biexciton shows the similar spectrum to that of the confined excitons. From these results, it is supposed that the excited biexciton states may be not much different from those composed of one exciton at the lowest state and the other at the excited states. The observation of the IRTA of the biexciton is an essential in spatially confined system like the quantum dots. In the bulk crystal, such excited biexciton would dissociate into two isolated excitons because transition energy from the lowest to excited biexciton state is much larger than the biexciton binding energy. However, observed absorption spectrum of the biexciton similarly to that of the excitons suggests that the excited biexciton states are stable in the confinement system.

Our results open a new concept on the excited states of the confined biexcitons and multiexciton states. Next interest in the excited biexciton poperties is dot size dependence of the IRTA. Since the biexciton has effective radius larger compared to that of the exciton, the IRTA energy of the biexciton is expected to be larger than that of the exciton due to the strong confinement effect and distinctive features of the transition dynamics in the quantum dots are expected to be appear.

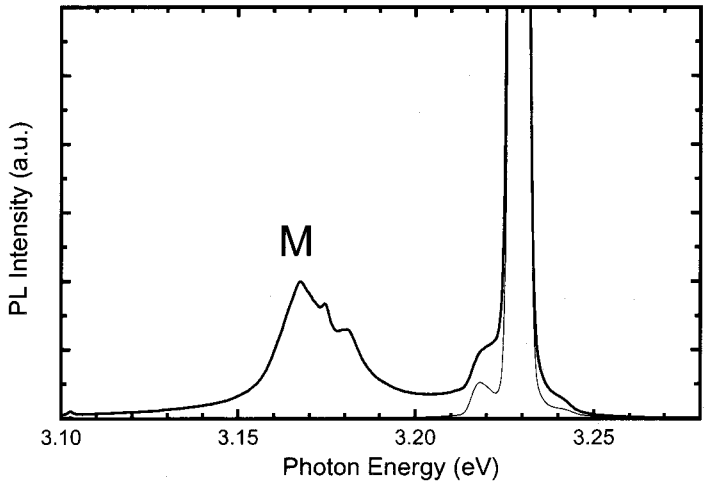

Figure 5-1. PL spectrum with excitation photon energy of 3.229 eV, which corresponds to resonant excitation of the confined exciton in the quantum dots with a = 3.9 nm, and biexciton in that of 4.6 nm (thick line). The thin line shows the spectral profile of the excitation light.

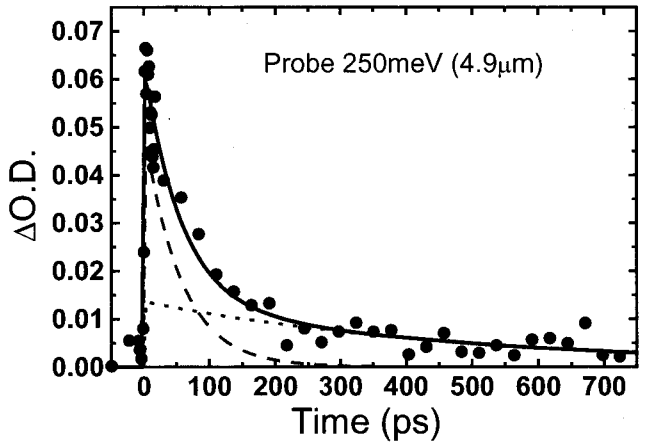

Figure 5-2. Temporal profile of the IRTA measured at the probe photon energy of 250 meV. The excitation was made at 3.227 eV. The solid curve is a fit to the experimental data assuming two decay components; ~56 ps (dashed line) and ~490 ps (dotted line).

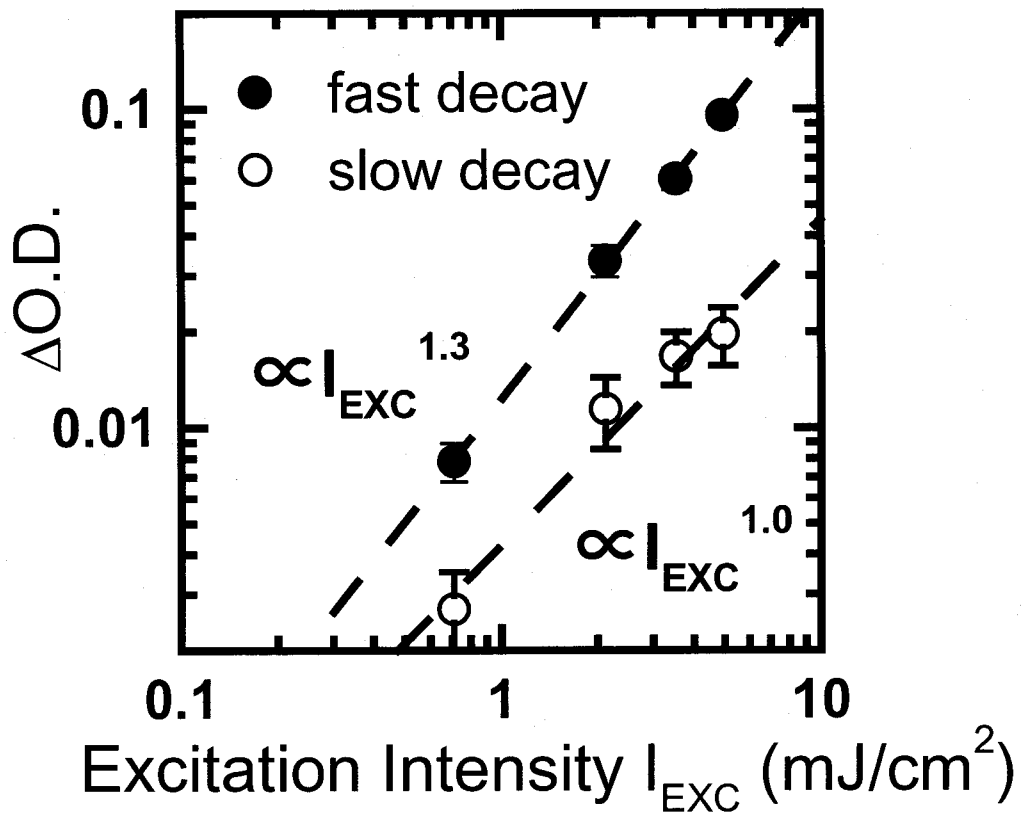

Figure 5-3. Excitation intensity dependence of initial intensities of the fast and slow decay components of the IRTA.

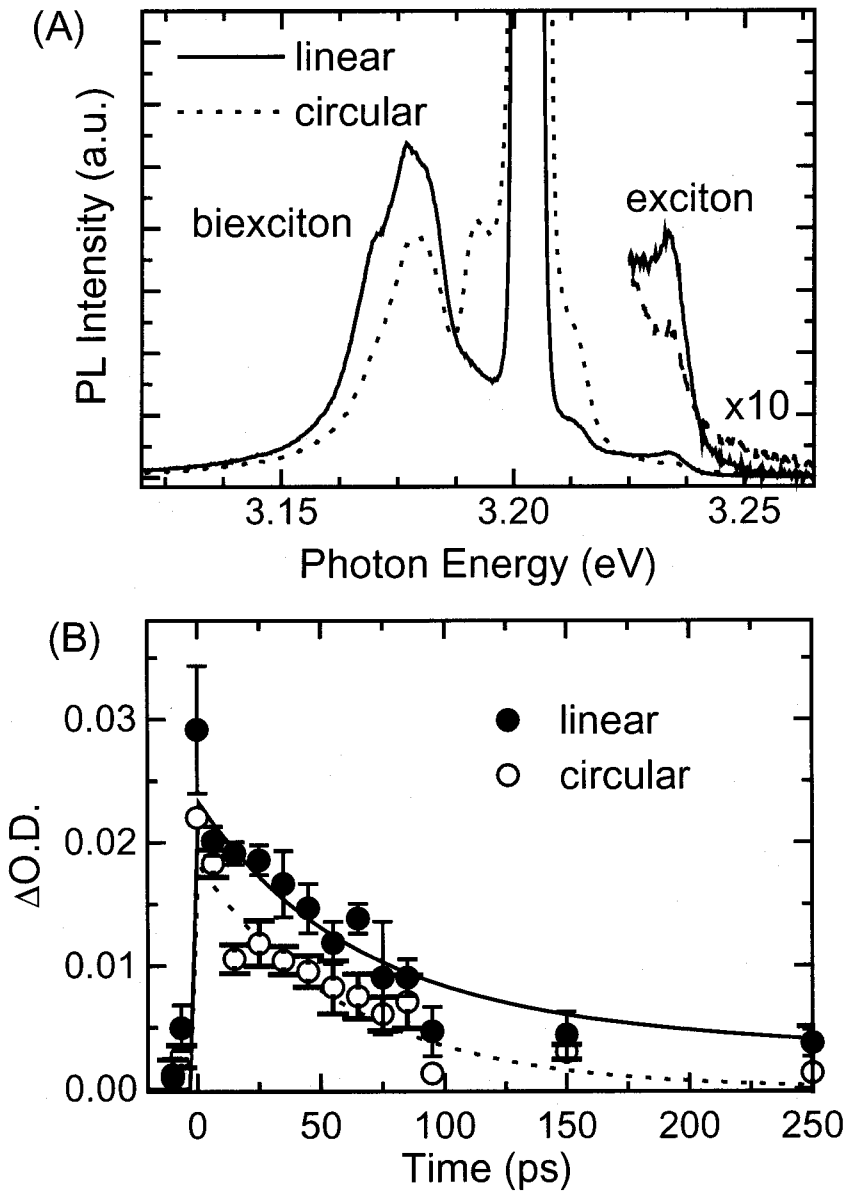

Figure 5-4. PL spectra (A) and temporal profiles of the IRTA (B) under the two photon resonant excitation of the confined biexcitons with linearly (solid) and circularly (dashed line) polarized lights.

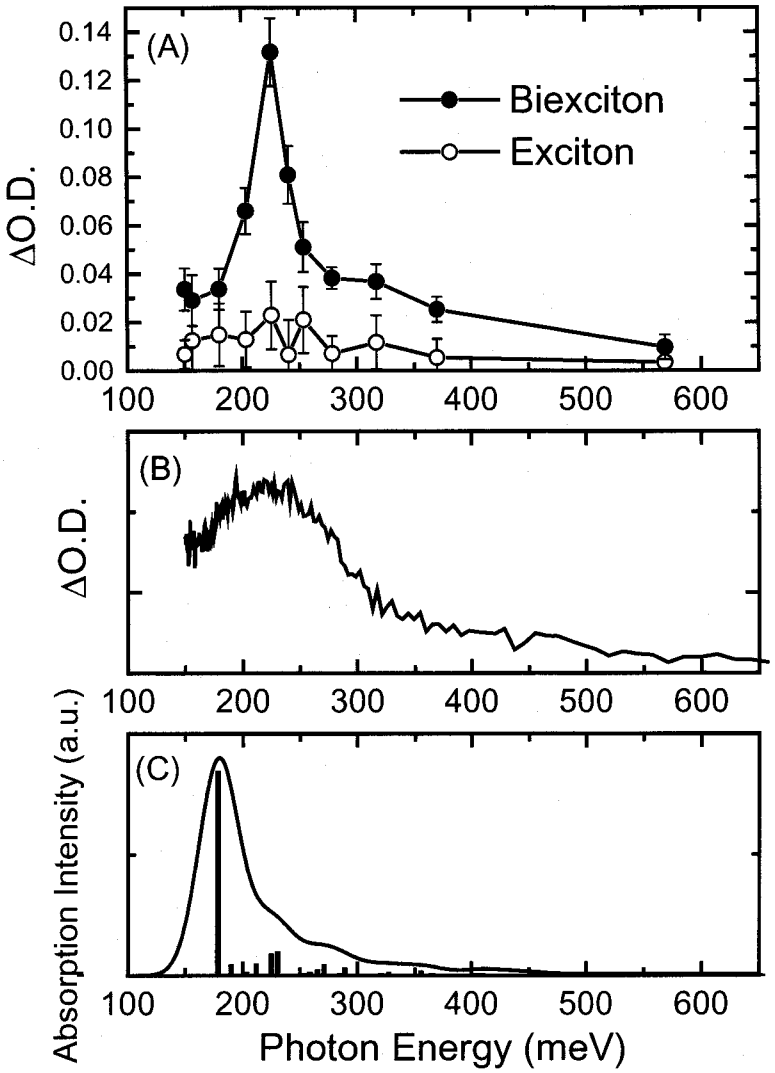

Figure 5-5 A) The IRTA spectra due to the biexciton (closed circles) and the exciton (opened circles). B) The IRTA spectra due to the exciton with dot radius of 5.6 nm, previously reported [53]. C) Theoretical IRTA spectrum due to the exciton confined in the quantum dots with the radius of ~5.6 nm [55].

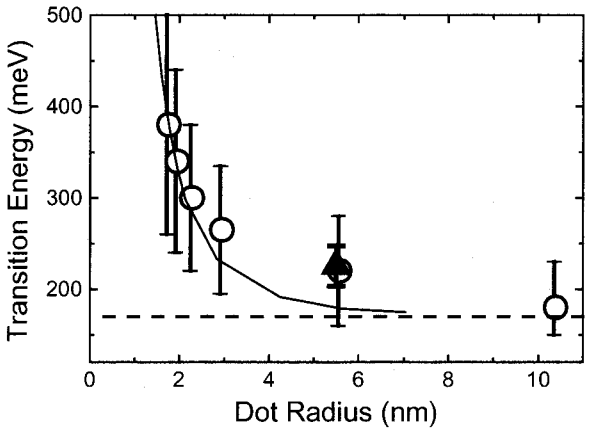

Figure 5-6. Dot-size dependence of the IRTA peak energy. The opened circles and closed triangle indicate the IRTA peak energies due to the exciton [53] and the biexciton (the present result), respectively. The solid line indicates the theoretical transition energy from 1s to 2p exciton states [54, 55]. The broken line indicates that for the bulk crystals [20].

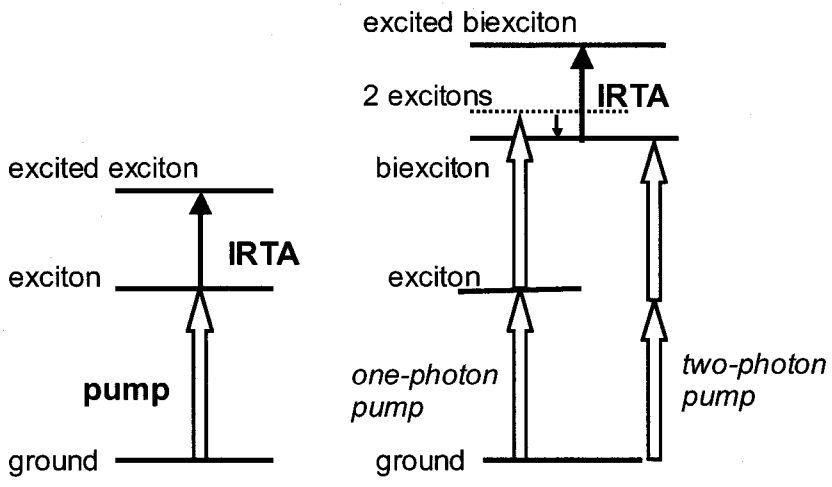

Figure 5-7. Energy diagram of observed transient absorption originating from the confined exciton (left) and biexciton (right).

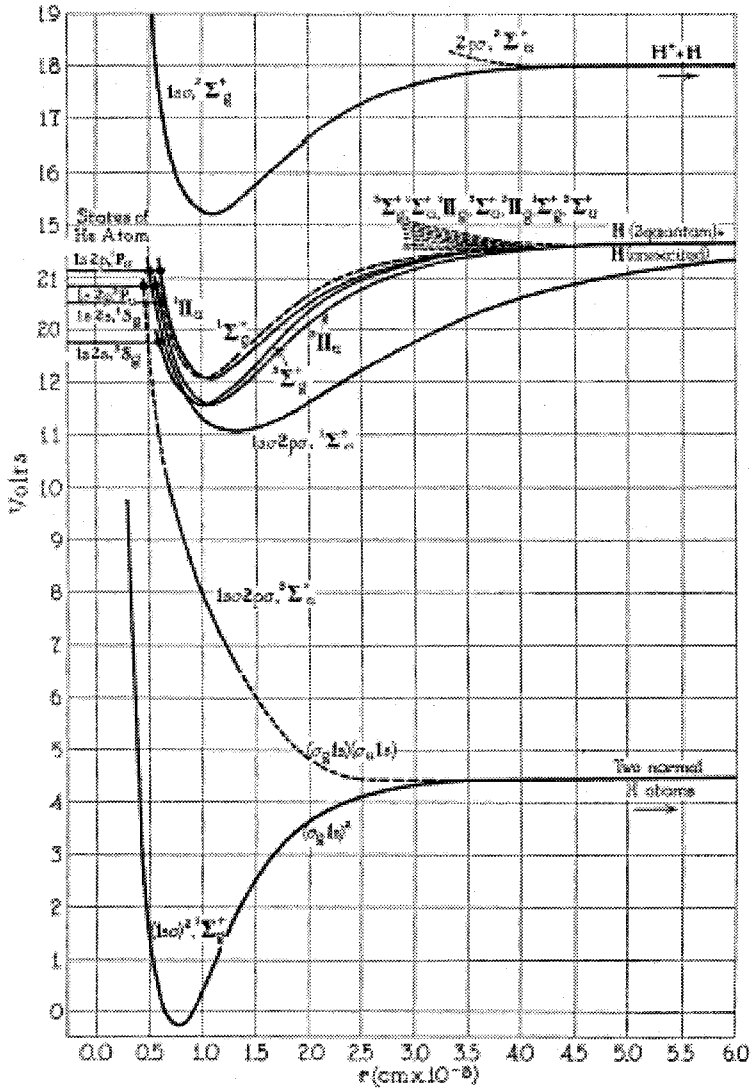

Figure 5-8. U(r) curves of electron states of H_2 which give a 1-qunatum atom plus a second 1-quantum or a 2-quantum atom on dissociation [72]. The curve for the normal state of H_2^+ is shown for comparison,

Chapter 6

Conclusion

I have studied confined biexciton properties in CuCl quantum dots by means of two-photon excitation spectroscopy and mid-infrared transient absorption spectroscopy.

The lowest biexciton state with the total angular momentum J = 0 in CuCl bulk crystal can not be created two-photon absorption by using a single beam with circularly polarization. Utilizing this polarization selection rule of the biexciton, I have succeeded in the first confirmation of direct creation of the lowest biexciton confined in semiconductor quantum dots by polarization dependence of the photoluminescence excitation spectra of confined biexciton on the excitation light. In addition, I have observed the two-photon absorption process of the excited biexciton state (J = 2) which plays the important roles in transition between biexciton and exciton confined in quantum dots.

These results provide us the important solution for the creation process of the confined biexcitons. When the excitation photon energy is lower than the one-photon absorption energy of confined excitons, the lowest biexciton of J = 0 is created directly. On the other hand, when the excitation photon energy falls inside the one-photon absorption band of the confined exciton, the exciton creation by the one-photon absorption and the biexciton creation into the excited state of J = 2 by the two-photon absorption occur simultaneously. In this case, the sizes of the dot, in which the biexcitons are created, are larger than that for the confined excitons.

Next, I tried to solve the dot-size dependence of the confined biexciton states. Since PL energy of the biexciton shows almost no dependence of the excitation energy in larger dots, it is difficult to estimate the dot size where the biexciton exists from the PL

energy. Therefore, I tried to clarify it by utilizing the transition dynamics of biexciton and exciton under the two-photon excitation of the confined biexciton. In this excitation condition, the exciton is created after the radiative-relaxation of the biexciton directly created. Therefore, one can estimated the dot sizes for the creation of the biexciton from the PL energy of the exciton. From analysis of the PL energy relation between the exciton and biexciton, I discussed the transition between the biexciton and exciton confined in the quantum dots. As a result, I concluded that the transition between confined biexciton and exciton might be different between absorption process and luminescence process. It is still an open question, so that more detailed measurement is necessary. However, I could show that the two-photon excitation spectroscopy is greatly useful for the study of the confined biexciton properties.

Further, I have measured the mid-infrared transient absorption spectroscopy for CuCl quantum dots with *ps* temporal resolution. As a result, I have observed two decay components in IRTA temporal profiles. The decay times of faster and slower components (~56 ps and ~490 ps) agree with the lifetimes of the biexcitons and exciton previously reported, respectively. The excitation intensity dependence of the IRTA intensities of the faster and slower components shows superlinearity and linearity, respectively. In addition, under the excitation condition of two-photon excitation of the biexciton, the fast component of the IRTA decreased with the circularly polarized excitation light compared to the linearly polarized one. This behavior obeys the polarization selection rule of the biexciton of the lowest state. From these results, I concluded that the fast and slow decay components of the IRTA are attributed to the confined biexciton and exciton, respectively. The IRTA due to the biexciton confined in semiconductor quantum dots is the first observation. IRTA spectrum of the biexciton has similar spectral shape to that of the confined exciton, which is mainly contributed by transition from Rydberg 1s state to 2p state of the exciton. In addition, the IRTA peak energy of the biexciton is almost same as that of the exciton. From these results, it is proposed that the observed excited biexciton state is composed of one lowest exciton (1s state) and one excited exciton (2p, 3p,… state). In the bulk crystal, such an excited biexciton is unstable and separated into two isolated excitons. However, in the confinement system like a quantum dot, the excited biexciton state would be stable because two excitons never separated. Thus my research opens a new concept of quantum confinement.

In this report, I showed the excited states of the confined biexciton in semiconductor quantum dots. However, many questions still remain. The IRTA energy of the biexciton can be different from that of the exciton but the difference was not clarified in my experiment. This reason is assumed to come from that dot radius studied in the experiment (~5.5 nm) is large, so that transition of 1s – 2p states of one exciton would not be strongly influenced from the existence of the other exciton. To clarify more detailed properties of the excited states of the confined biexciton, improvements of the experimental system is necessary to suppress noise of IRTA in order to observe the fine structures in IRTA spectra of both the biexciton and exciton. In addition, it is necessary to measure the size dependence of IRTA spectra of the biexciton and exciton. With decreasing the size of the dot, IRTA energy of the biexciton might be modulated from that of the exciton because correlation between two electrons and holes increases greatly and a concept of biexciton as a quasi-particle is broken. It is very interesting to study the change of excited biexciton state confined in smaller dots.

In near future, more detailed discussion will be realized for the biexciton properties confined in semiconductor quantum dots by means of two-photon excitation of the biexiciton and infrared transient absorption, as shown in this thesis.

Appendix A

Optical Properties of Biexciton

A.1 Electronic structure of biexciton

The electronic structure of the biexciton is discussed in the case of CuCl. It has a band structure with a top of the valence band at k = 0 (symmetry Γ_7) and the bottom of the conduction band at k = 0 (symmetry Γ_6). The conduction Bloch function Γ_6 is written as

$$c_{1/2} = \psi_c|\alpha\rangle \text{ and } c_{-1/2} = \psi_c|\beta\rangle \qquad \text{(A-1.1)}$$

where Ψ_c can be identified with 4s function of Cu. On the other hand, the valence Bloch functions are of the form

$$v_{-1/2} = \sqrt{\frac{2}{3}}\psi_{-1}|\alpha\rangle - \sqrt{\frac{1}{3}}\psi_0|\beta\rangle \text{ and } v_{1/2} = \sqrt{\frac{2}{3}}\psi_1|\beta\rangle + \sqrt{\frac{1}{3}}\psi_0|\alpha\rangle \quad \text{(A-1.2)}$$

where the orbital parts may be expressed as

$$\psi_{\pm 1} = \frac{1}{\sqrt{2}}(p_x \pm ip_y) \text{ and } \psi_0 = p_z \qquad \text{(A-1.3).}$$

Here, p_x, p_y, p_z are the normalized p-like functions.

The superposition of excitations of the valence electron into the conduction band gives two kinds of excitons which have Γ_2 (total angular momentum $J_{ex} = 0$) and Γ_5

(J_{ex} = 1) symmetry, respectively. The wave functions of Γ_2 and Γ_5 exciton states of the CuCl, in which the electron and hole are indicated by notations 1 and a, respectively, and the position vector of them are $\boldsymbol{r}_i$ (i =1, a), are expressed as

$$\begin{pmatrix} \left|\Gamma_2^{ex}\right\rangle \\ \left|\Gamma_{5m}^{ex}\right\rangle \end{pmatrix} = \frac{1}{\sqrt{V}} \exp[i\boldsymbol{K}\cdot(\alpha \boldsymbol{r}_1 + \beta \boldsymbol{r}_a)]\cdot\phi(\boldsymbol{r}_1 - \boldsymbol{r}_a)\cdot \begin{pmatrix} \left|P_0^0(1,a)\right\rangle\!\right\rangle \\ \left|P_1^m(1,a)\right\rangle\!\right\rangle \end{pmatrix} \quad (m = -1, 0, 1) \qquad \text{(A-1.4)}$$

where the parts of Bloch function are given by

$$\left|P_0^0(1,a)\right\rangle\!\right\rangle = \frac{1}{\sqrt{2}}\left[c_{1/2}(1)v_{-1/2}(a) - c_{-1/2}(1)v_{1/2}(a)\right]$$

$$\left|P_1^1(1,a)\right\rangle\!\right\rangle = c_{1/2}(1)v_{1/2}(a)$$

$$\left|P_1^0(1,a)\right\rangle\!\right\rangle = \frac{1}{\sqrt{2}}\left[c_{1/2}(1)v_{-1/2}(a) + c_{-1/2}(1)v_{1/2}(a)\right] \qquad \text{(A-1.5)}$$

$$\left|P_1^{-1}(1,a)\right\rangle\!\right\rangle = c_{-1/2}(1)v_{-1/2}(a),$$

α and β are given by

$$\alpha = \frac{m_h}{m_e + m_h} \quad \text{and} \quad \beta = 1 - \alpha .$$

The envelope function $\phi(\boldsymbol{r}_1 - \boldsymbol{r}_a)$ which describes the relative motion of the electron and hole is rewritten as

$$\phi(\boldsymbol{r}) = \frac{1}{\sqrt{\pi a_B^{\,3}}} \exp\left(-\frac{\boldsymbol{r}}{a_B}\right), \quad \boldsymbol{r} = \boldsymbol{r}_1 - \boldsymbol{r}_a \qquad \text{(A-1.6)}$$

by using the effective mass approximation.

The wave functions of biexcitons are also superposition of excitations of two valence electrons into the conduction band. The lowest state of the biexciton has singlet structure, which minimizes the intraband exchange interaction energy of two electrons and two holes. Consequently, it is Γ_1 state with total angular momentum J = 0, and the envelope function $\Phi^{+-}(\boldsymbol{r}, \boldsymbol{r}', \boldsymbol{R})$, where $\boldsymbol{r} = \boldsymbol{r}_1 - \boldsymbol{r}_a$, $\boldsymbol{r}' = \boldsymbol{r}_2 - \boldsymbol{r}_b$, $\boldsymbol{R} = \boldsymbol{r}_a - \boldsymbol{r}_b$, has even parity with respect to the permutation of two electrons and two holes. Here the second electron and hole are denoted by the notations 2 and b, respectively, and $\boldsymbol{r}_2$ and $\boldsymbol{r}_b$ express their position vectors. The first and second suffixes ± mean the parity of the envelope function with the respect to the permutation of electrons and holes,

respectively. The next higher state of the biexciton with symmetry Γ_4 is formed with sacrificing the exchange energy of two holes because the effective mass of the hole is heavier than that of the electron, and the envelope function is given as $\Phi^{+-}(\boldsymbol{r},\boldsymbol{r}',\boldsymbol{R})$. The wave functions of the biexciton are represented for two low-lying states as follows;

$$\left|\Gamma_1^{\mathrm{mol}}(\boldsymbol{K};1,\mathrm{a},2,\mathrm{b})\right\rangle = \frac{1}{\sqrt{V}}\left[\exp(\mathrm{i}\boldsymbol{K}\cdot\boldsymbol{R}_0)\right]\Phi^{++}(\boldsymbol{r},\boldsymbol{r}',\boldsymbol{R})\left|\Gamma_1(1,\mathrm{a},2,\mathrm{b})\right\rangle \qquad \text{(A-1.7)}$$

$$\left|\Gamma_4^{\mathrm{mol}}(\boldsymbol{K};1,\mathrm{a},2,\mathrm{b})\right\rangle = \frac{1}{\sqrt{V}}\left[\exp(\mathrm{i}\boldsymbol{K}\cdot\boldsymbol{R}_0)\right]\Phi^{+-}(\boldsymbol{r},\boldsymbol{r}',\boldsymbol{R})\left|\Gamma_4(1,\mathrm{a},2,\mathrm{b})\right\rangle$$

where

$$\left.\begin{matrix}\left|\Gamma_1(1,\mathrm{a},2,\mathrm{b})\right\rangle\\ \left|\Gamma_4(1,\mathrm{a},2,\mathrm{b})\right\rangle\end{matrix}\right\} \equiv \left\{\begin{matrix}\left|0,0\right\rangle\\ \left|1,0\right\rangle\end{matrix}\right\}$$

$$= \frac{1}{2}\left[c_{1/2}(1)c_{-1/2}(2) - c_{-1/2}(1)c_{1/2}(2)\right]\cdot\left[v_{1/2}(\mathrm{a})v_{-1/2}(\mathrm{b}) \mp v_{-1/2}(\mathrm{a})v_{1/2}(\mathrm{b})\right] \qquad \text{(A-1.8)}$$

and

$$R_0 = \frac{1}{2}\left[\alpha(\boldsymbol{r}_1+\boldsymbol{r}_2) + \beta(\boldsymbol{r}_\mathrm{a}+\boldsymbol{r}_\mathrm{b})\right] \qquad \text{(A-1.9).}$$

R_0 indicates the center-of-mass coordinate of the system. The envelope function $\Phi^{++}(\boldsymbol{r},\boldsymbol{r}',\boldsymbol{R})$ is given, by using the effective mass approximation, as

$$\Phi^{++}(\boldsymbol{r},\boldsymbol{r}',\boldsymbol{R}) = f(\boldsymbol{R})g(\xi_1,\xi_2,\eta_1,\eta_2;\boldsymbol{R}) \qquad \text{(A-1.10)}$$

where

$$\xi_i = (r_{i\mathrm{a}}+r_{i\mathrm{b}})/R \quad \text{and} \quad \eta_i = (r_{i\mathrm{a}}-r_{i\mathrm{b}})/R \qquad (i=1,2) \qquad \text{(A-1.11).}$$

The envelope function of the first rotational state $\Phi^{+-}(\boldsymbol{r},\boldsymbol{r}',\boldsymbol{R})$ may be given as

$$\Phi^{+-}(\boldsymbol{r},\boldsymbol{r}',\boldsymbol{R}) = f'(\boldsymbol{R})Y_{1\mathrm{m}}(\theta,\phi)g(\xi_1,\xi_2,\eta_1,\eta_2;\boldsymbol{R}) \qquad \text{(A-1.12)}$$

where $Y_{1\mathrm{m}}(\theta,\phi)$(m = -1, 0, 1) is a spherical harmonic of the first order and (θ, ϕ) describes the orientation of the vector $\boldsymbol{R}$.

The energy splitting between Γ_1 and Γ_4 states origins from the exchange energy of two electrons or two holes. The lowest states of the biexciton Γ_1 is formed by superposing the product of two electron state with $J_e = 0$ and two holes with $J_h = 0$ which minimize the intraband exchange energies, respectively.

In the limit of zero e–h exchange splitting, the lowest biexciton state (J = 0) consists of the linear combination of two J = 0 states which are made up of two $J_{ex} = 0$ excitons and two $J_{ex} = 1$ excitons, respectively, as follows;

$$|0,0\rangle = \frac{1}{2}\left[\left|\mathrm{J}=0;(\mathrm{J}_{ex}=0)^2\right\rangle + \sqrt{3}\left|\mathrm{J}=0;(\mathrm{J}_{ex}=1)^2\right\rangle\right]$$

$$= \frac{1}{2}\left[\left|P_1^1\right\rangle\left|P_1^{-1}\right\rangle + \left|P_1^{-1}\right\rangle\left|P_1^1\right\rangle - \left|P_1^0\right\rangle\left|P_1^0\right\rangle + \left|P_0^0\right\rangle\left|P_0^0\right\rangle\right]. \qquad \text{(A-1.13)}$$

The exciton state is hardly modified in the biexciton. Under this assumption, the e–h intraband exchange effect works only on the Γ_5 exciton component of a biexciton and it is evaluated as a perturbation in terms of the wave function, as follows:

$$\left\langle \Gamma_1^{\mathrm{mol}} \left| H_{\mathrm{e-h}}^{\mathrm{exch}} \right| \Gamma_1^{\mathrm{mol}} \right\rangle = 2 \times \frac{3}{4} \times \Delta E_{\mathrm{e-h}}^{\mathrm{exch}},$$

where $\Delta E_{\mathrm{e-h}}^{\mathrm{exch}}$ is the energy splitting of the Γ_5 and Γ_2 excitons. As a result, the energy of the lowest state of the biexciton is expressed by

$$E_{\mathrm{m}}(K) = 2E_{\mathrm{ex}}(\Gamma_2) - E_{\mathrm{b}} + \frac{3}{2}\Delta E_{\mathrm{e-h}}^{\mathrm{exch}} + \frac{\hbar^2 K^2}{2M_{\mathrm{mol}}}, \qquad \text{(A-1.14)}$$

where the biexciton binding energy E_{b} is measured with respect to the lowest two-Γ_2 excitons, which is not influenced by the e–h exchange effect, and the translational mass of the biexciton is

$$M_{\mathrm{mol}} = 2(m_{\mathrm{e}} + m_{\mathrm{h}}) \qquad \text{(A-1.15).}$$

A.2 Luminescence process

The luminescence due to the biexciton is originated from a radiative annihilation of one of the two excitons composing the biexcitons with leaving another exciton. Therefore, luminescence photon energy is expressed as

$$\hbar\omega = \left(2E_{\mathrm{ex}} - E_{\mathrm{b}} + \frac{\hbar^2 K^2}{2M_{\mathrm{mol}}}\right) - \left(E_{\mathrm{ex}} + \frac{\hbar^2 K^2}{2M_{\mathrm{ex}}}\right)$$

$$= E_{\mathrm{ex}} - E_{\mathrm{b}} - \frac{\hbar^2 K^2}{2M_{\mathrm{mol}}} \qquad \text{(A-2.1).}$$

Here, E_{ex} indicates the exciton energy of lowest 1s state and E_{b} indicates the biexciton binding energy.

The luminescence spectrum of the biexcitons with distribution $f_{\mathrm{mol}}(\boldsymbol{K})$ in CuCl can be evaluated in terms of the wave functions, by a simple perturbation method, as follows:

$$W_{\mathrm{l}}(\omega)=\frac{2\pi}{\hbar}\sum_{\boldsymbol{K},\mathrm{m}}\left|\left\langle \Gamma_{5\mathrm{m}}^{\mathrm{ex}}\left|H_{+}^{\prime}\right|\Gamma_{1}^{\mathrm{mol}}\right\rangle\right|^{2} f_{\mathrm{mol}}(\boldsymbol{K})\times\delta\left(\hbar\omega-E_{\mathrm{mol}}(\boldsymbol{K})+E_{\mathrm{ex}}(\boldsymbol{K})\right) \qquad \text{(A-2.2)}$$

where H'_{+} is the photon emission part of the electron-radiation interaction;

$$H'=\sum_{i}e\tilde{\boldsymbol{r}}_{i}\cdot\left\{E_{+}\exp\left(-\mathrm{i}\boldsymbol{p}\cdot\boldsymbol{r}_{i}\right)+E_{-}\exp\left(\mathrm{i}\boldsymbol{p}\cdot\boldsymbol{r}_{i}\right)\right\}$$

$$=\sqrt{\frac{8\pi\hbar\omega}{V}}\sum_{i}\left(e\boldsymbol{r}_{i}\cdot\boldsymbol{e}\right)\left\{a_{p}^{\dagger}\exp\left(\mathrm{i}\omega t-\mathrm{i}\boldsymbol{p}\cdot\boldsymbol{r}_{i}\right)+a_{p}\exp\left(-\mathrm{i}\omega t+\mathrm{i}\boldsymbol{p}\cdot\boldsymbol{r}_{i}\right)\right\} \qquad \text{(A-2.3)}$$

Here, $\boldsymbol{r}_i$ and $e\tilde{\boldsymbol{r}}_i$ are the position vector and the dipole-moment of the i-th electron, respectively, $\boldsymbol{e}$ is the unit polarization vector of the radiation field, a_p and $a_p^{\dagger}$ are the annihilation and creation operators of photon with the momentum $\boldsymbol{p}$. The following expression is obtained by multiplying $\left|\Gamma_{5\mathrm{m}}^{\mathrm{mol}}\right\rangle$ by $1/2\left\{v_{1/2}(3)v_{-1/2}(4)-v_{-1/2}(3)v_{1/2}(4)\right\}$ and inserting Eq. (A-1.4) and (A-1.7) into (A-2.2);

$$W_{\mathrm{l}}(\omega)=\frac{4\pi^{2}\omega_{0}}{3V}\left\{\left\langle\psi_{\mathrm{c}}\left|e\tilde{x}\right|p_{x}\right\rangle\phi(0)\int g(\boldsymbol{R})d\boldsymbol{R}\right\}^{2}\cdot\sum_{\boldsymbol{K}}f_{\mathrm{mol}}(\boldsymbol{K})\delta\left(\hbar\omega-E_{\mathrm{mol}}(\boldsymbol{K})+E_{\mathrm{ex}}(\boldsymbol{K})\right)$$

(A-2.4).

Here, we used the fact that

$$\left\langle\psi_{\mathrm{c}}\left|e\tilde{x}\right|p_{x}\right\rangle=\left\langle\psi_{\mathrm{c}}\left|e\tilde{y}\right|p_{y}\right\rangle=\left\langle\psi_{\mathrm{c}}\left|e\tilde{z}\right|p_{z}\right\rangle,$$

taking account of the isotropic symmetry of the crystal. The envelope function of the biexciton is approximated to be as

$\Phi^{++}(\boldsymbol{r},0,\boldsymbol{R})=\phi(\boldsymbol{r})\phi(0)g(\boldsymbol{R})$.

In addition, we neglected $(Ka_B\alpha/2)^2$ and $(Ka_{mol}/2)^2$ in comparison with one, where a_{mol} is the average separation of the two excitons of the biexciton and $g(\boldsymbol{R})$ was expressed as

$$g(\boldsymbol{R})=\frac{1}{\sqrt{\pi a_{\mathrm{mol}}^{3}}}\exp\left(-\frac{\boldsymbol{R}}{a_{\mathrm{mol}}}\right) \qquad \text{(A-2.5).}$$

When the Boltzmann distribution with the effective temperature T_{eff} is assumed for the kinetic energy of the biexcitons, the integration in (A-2.4) can be done as follows;

$$W_{\mathrm{l}}(\omega)=A\sqrt{E_{\mathrm{ex}}-E_{\mathrm{b}}-\hbar\omega}\cdot\exp\left[-\left(E_{\mathrm{ex}}-E_{\mathrm{b}}-\hbar\omega\right)/k_{\mathrm{B}}T_{\mathrm{eff}}\right] \qquad \text{(A-2.6)}$$

for $\hbar\omega\le E_{\mathrm{ex}}-E_{\mathrm{b}}$,

Here, with the biexciton density N_M,

$$A=\left(\frac{4\pi}{k_B T_{eff}}\right)^{3/2} N_M \frac{\omega_0}{3}\left\{\langle\psi_c|e\tilde{x}|p_x\rangle\phi(0)\int g(\boldsymbol{R})d\boldsymbol{R}\right\}^2.$$

As a result, luminescence spectrum rises by the biexciton binding energy below the exciton energy and the spectral shape shows an inversed Boltzmann distribution which has a tail to lower energy side.

The radiative annihilation of biexcitons, in which pure triplet Γ_2 free exciton remains, is forbidden in CuCl because of the group-theoretical property of Bloch function, i.e.,

$$\left\langle \Gamma_2^{ex}\left|H'\right|\Gamma_1^{mol}\right\rangle = 0.$$

This is also implied easily from the absence of product terms of the pure triplet Γ_2 exciton and optically active Γ_5 exciton in Eq.(1.21). The threefold degenerate state of Γ_5 exciton is split into the longitudinal exciton and the twofold transverse exciton due to the long-range dipole interaction.

A.3 Giant oscillator strength

An effect of giant oscillator strength works in one-photon absorption in presence of single excitons due to conversion of excitons into biexcitons, which is reverse process of luminescence of biexcitons. Let us consider that single Γ_5 excitons are accumulated in CuCl and distributed over the exciton dispersion curve with the Boltzmann distribution $f_{ex}(\boldsymbol{K})$. The transition probability of this conversion process is evaluated as the reverse process of luminescence by taking the hermite conjugate of the matrix element in Eq. (A-2.2) and replacing $f_{mol}(\boldsymbol{K})$ by exciton distribution function $f_{ex}(\boldsymbol{K})$;

$$W_c^{(1)}(\omega)=\frac{2\pi}{\hbar}\sum_{\substack{\boldsymbol{K}\\ m=-1,0,1}}\left|\left\langle\Gamma_1^{mol}(\boldsymbol{K}+\boldsymbol{p})\right|\times\sum_i e\tilde{\boldsymbol{r}}_i\boldsymbol{E}\left|\Gamma_{5m}^{ex}(\boldsymbol{K})\right\rangle\right|^2 f_{ex}(\boldsymbol{K})\delta\left(\hbar\omega+E_{ex}(\boldsymbol{K})-E_{mol}(\boldsymbol{K}+\boldsymbol{p})\right)$$

(A-3.1).

When we neglect the photon momentum $\boldsymbol{p}$ in comparison with $\boldsymbol{K}$ and assume the

simplified form for the biexciton envelope function $\phi(\boldsymbol{r})\phi(\boldsymbol{r}')g(\boldsymbol{R})$, Eq.(A-3.1) is rewritten as

$$W_{\mathrm{c}}^{(1)}(\omega)=\frac{\pi}{6\hbar}\left\{\langle\psi_{\mathrm{c}}|e\tilde{x}|p_x\rangle\phi(0)\int g(\boldsymbol{R})d\boldsymbol{R}\right\}^2 E^2\times\sum_{\boldsymbol{K}} f_{\mathrm{ex}}(\boldsymbol{K})\delta(\hbar\omega-E_{\mathrm{ex}}(\boldsymbol{K})-E_{\mathrm{mol}}(\boldsymbol{K}))$$

$$=A\sqrt{E_{\mathrm{ex}}-E_{\mathrm{b}}-\hbar\omega}\cdot\exp\left\{-\frac{2(E_{\mathrm{ex}}-E_{\mathrm{b}}-\hbar\omega)}{k_{\mathrm{B}}T}\right\}. \qquad \text{(A-3.2)}$$

We compare the total transition probability which is obtained by integrating (1.32) over ω, with that of the single exciton Γ_5,

$$W_{\mathrm{c}}^{(1)}/W_{\mathrm{ex}}^{(1)}=\left[\int g(\boldsymbol{R})d\boldsymbol{R}\right]^2\rho_{\mathrm{ex}} \quad (\rho_{\mathrm{ex}} \text{ is the exciton density}). \qquad \text{(A-3.3)}$$

When the relative motion of two holes g($\boldsymbol{R}$) is assumed by (A-2.5), Eq. (A-3.3) is

$$W_{\mathrm{c}}^{(1)}/W_{\mathrm{ex}}^{(1)}=64\pi a_{\mathrm{mol}}{}^3\rho_{\mathrm{ex}}. \qquad \text{(A-3.4)}$$

This strong enhancement of the transition from the exciton to the biexciton state is attributed to the effect of giant oscillator strength, which is coming from the factor $\int g(\boldsymbol{R})d\boldsymbol{R}$. This means that the biexciton could be created by exciting any valence electron in the large biexciton orbital around the existing the first exciton.

A.4 Giant two-photon absorption

The transition probability of the two-photon excitation from the ground state to the final state of the biexciton is expressed by

$$W^{(2)}(\Gamma_1;\omega)=\frac{2\pi}{\hbar}\left|\langle\Gamma_1^{\mathrm{mol}}(\boldsymbol{K})|H_-'\sum_i\frac{|i\rangle\langle i|}{E_{ig}-\hbar\omega}H_-'|\mathrm{g}\rangle\right|^2\times\delta(2\hbar\omega-E_{\mathrm{mol}}(\boldsymbol{K}))$$

$$=\frac{2\pi}{\hbar}\left[\frac{1}{6(E_{\mathrm{ex}}-\hbar\omega)}\left\{\langle\varphi_{\mathrm{c}}|e\tilde{z}|\varphi_0\rangle^2 E_{\parallel}E+\langle\varphi_{\mathrm{c}}|e\tilde{x}_+|\varphi_-\rangle\langle\varphi_{\mathrm{c}}|e\tilde{x}_-|\varphi_+\rangle\times\left(E_{\perp}^{+}E_{\perp}^{-}+E_{\perp}^{-}E_{\perp}^{+}\right)\right\}\right]^2$$

$$\times\left\{\phi(0)\int dr\int d\boldsymbol{R}\phi(r)\Phi^{++}(\boldsymbol{r},0,\boldsymbol{R})\right\}^2\delta(2\hbar\omega-E_{\mathrm{mol}}(\boldsymbol{K}))\qquad\text{(A-4.1)},$$

then, $W^{(2)}(\Gamma_1;\omega)$ is simplified as follows, by taking account of the cubic symmetry for CuCl,

$$W^{(2)}(\Gamma_1;\omega)=\frac{2\pi}{\hbar}\left(\frac{\langle\psi_c|e\tilde{x}|p_x\rangle^2}{6(E_{\mathrm{ex}}-\hbar\omega)}\phi^2(0)\int d\boldsymbol{R}g(\boldsymbol{R})E^2\right)^2\times\delta\left(2\hbar\omega-2E_{\mathrm{ex}}+E_{\mathrm{b}}-\frac{\hbar^2(2p)^2}{2M_{\mathrm{mol}}}\right)$$

(A-4.2).

The transition probability of one-photon absorption due to a single exciton is

$$W^{(1)}(\Gamma_5^{\mathrm{ex}};\omega)=\frac{2\pi}{\hbar}\left(\frac{\langle\psi_c|e\tilde{x}|p_x\rangle}{\sqrt{3}}\phi(0)\right)^2E^2\times\delta\left(\hbar\omega-E_{\mathrm{ex}}-\frac{\hbar^2p^2}{2M_{\mathrm{ex}}}\right)\qquad\text{(A-4.3)}.$$

In comparison with the case of an ordinary two-photon absorption due to band-to-band transitions, we have furthermore, two strong enhancement factors in the case of the biexcitons. The first enhancement factor is $[\phi(0)\int g(\boldsymbol{R})d\boldsymbol{R}]^2$ which comes from the two-electron excitation and the second one comes from the resonant effect.

The first enhancement is explained as follows: in the process of the transition from exciton to biexciton, we can choose the any valence electron in the range within the large molecule radius a_{mol} around the first exciton in order to make an biexciton coherently. This is contrast to the ordinal case where the electron excited to the intermediate state should interact again with the second photon.

As a result, we have the factor

$$\left[\phi(0)\int g(\boldsymbol{R})d\boldsymbol{R}\right]^2\cong 64\left(\frac{a_{\mathrm{mol}}}{a_{\mathrm{B}}}\right)^3\cong 10^3.$$

The second enhancement factor of the resonance effect is estimated to be of an order of 10^4 at $E_{\mathrm{ex}}-E_{\mathrm{b}}/2$ if we assume a few electron volts for the energy denominator in the band-to-band transition.

These two effects are combined to give the extremely strong two-photon absorption due to the biexciton. As a result, in two-photon spectroscopy, the biexciton will be confirmed as the sharp absorption peak at $E_{\mathrm{ex}}-E_{\mathrm{b}}/2$. which are embedded in the rather weak background of the one-photon absorption tail of an exciton and the ordinary two-photon absorption due to band-to-band transition.

A.5 Selection rules of biexciton

Next, we discuss selection rules and polarization dependence for the direct creation of the biexciton by GTA. The transition probability for absorption of two photons of the frequencies $\omega_1$and ω_2 and polarization e_1 and e_2 can be expressed in the from

$$W(\omega_1,\omega_2)\propto\sum_{f^\mu}G_\mu(\boldsymbol{e}_1,\boldsymbol{e}_2)\delta\left(E_{f^\mu}-E_g-\hbar\omega_1-\hbar\omega_2\right)\times\left|\sum_{\phi^\lambda}\Lambda^{\pm}_{\phi^\lambda}\left\langle f^\mu\left\|P^\lambda\right\|\phi^\lambda\right\rangle\left\langle\phi^\lambda\left\|P^\lambda\right\|g\right\rangle\right|^2,$$

(A-5.1)

where the geometric factors, expressed in terms of Clebsch-Gordan coefficients, are

$$G_\mu(\boldsymbol{e}_1,\boldsymbol{e}_2)=\sum_{\phi^\lambda}\left|\sum_{l,l'}e^\lambda_{2l}e^\lambda_{1l'}\left(\mu m|\lambda l,\lambda l'\right)\right|^2 \qquad \text{(A-5.2)},$$

and the dynamical factors are

$$\Lambda^{\pm}_i\equiv\frac{1}{E_i-E_g-\hbar\omega_1}\pm\frac{1}{E_i-E_g-\hbar\omega_2} \qquad \text{(A-5.3)},$$

the sign + (–) being appropriate for the final states which is contained in the symmetric (antisymmetric) product of the momentum representation. In the above expression,$|g\rangle$is the crystal ground state of energy E_g, belonging to the identity representation. $\left\langle\phi^\lambda\left\|P^\lambda\right\|g\right\rangle$ is the reduced matrix element of the momentum operator $\boldsymbol{P}$ (belonging to the λ irreducible representation) between the ground state and an intermediate state $\left|\phi^\lambda\right\rangle$ of the energy E_{ϕ^λ} and $\left\langle f^\mu\left\|P^\lambda\right\|\phi^\lambda\right\rangle$ is the reduced matrix element of the momentum operator $\boldsymbol{P}$ between the intermediate state and the final state of the energy E_{f^μ}.

We have three types of the selection rules from the expression (A-5.1–3) for the two-photon absorption.

1) Dipole selection rule

Two-photon transitions are possible only to final states belonging to the direct product of the irreducible representations of the two photons. For CuCl, we have

$$\Gamma_5\times\Gamma_5=\Gamma_1+\Gamma_3+\Gamma_4+\Gamma_5 \qquad \text{(A-5.4)}.$$

2) Geometrical selection rule

Two-photon transitions to a final state are possible only when the corresponding geometrical factor is not zero. Selection rules allows for particular directions of the polarization vectors with respect to one another or with respect to the crystallographic axes. The geometrical factors for the CuCl have been calculated from (1.39) and are shown in Table 1-1.

3) Dynamical selection rule

Two-photon transitions to a final state belonging to the antisymmetric product of the irreducible representations of the two photons are forbidden when $\omega_1 = \omega_2$, as it can be seen from (1.40). The dynamical selection rules are resulted from the properties of Clebsch-Gordan coefficients: $(\mu m|\lambda l', \lambda l) = \pm(\mu m|\lambda l, \lambda l')$ for the exchange of $\boldsymbol{e}_1$ with $\boldsymbol{e}_2$ and ω_1 with ω_2 in the second order transition probability.

For CuCl, the symmetric and antisymmetric products are respectively

$$[\Gamma_5 \times \Gamma_5] = \Gamma_1 + \Gamma_3 + \Gamma_5 \qquad \text{(A-5.5)}$$

and

$$\{\Gamma_5 \times \Gamma_5\} = \Gamma_4 . \qquad \text{(A-5.6)}$$

The strength of the transitions to the Γ_1, Γ_3, Γ_5 final states involves the factor $\Lambda^{+}_{\phi\lambda}$, while that to the Γ_4 final state involves the factor $\Lambda_{\phi\lambda}$. Therefore the former states are strongly allowed, and latter is weakly allowed and forbidden for $\omega_1 = \omega_2$.

Figure 1-3 shows a schematic diagram of biexciton states in CuCl with indication of strongly allowed and weakly allowed transitions due to the dynamical factors. In the case of direct creation of biexcitons by two photons of a unique laser beam ($\boldsymbol{e}_1 = \boldsymbol{e}_2$, $\omega_1 = \omega_2$), the transition from ground state (Γ_1) to biexciton state with Γ_4 is forbidden both by dynamical rule and geometrical selection rule, which gives $G_{\Gamma_4} = 0$ for $\boldsymbol{e}_1 = \boldsymbol{e}_2$, as can be seen from Table A-1. Consequently, only Γ_1 biexciton state can be created by giant two-photon absorption by a unique laser beam with linearly polarization. It is possible to create the Γ_4 biexciton state with use of two tunable laser beams with difference frequencies, and the transition probability increases in proportional to $|\boldsymbol{e}_1 \times \boldsymbol{e}_2|^2$. Since the transition probability to Γ_1 biexciton state is proportional to $|\boldsymbol{e}_1 \cdot \boldsymbol{e}_2|^2$, this transition becomes forbidden for perpendicularly polarized beams or a unique laser beam with circularly polarization.

Table A-1. Geometric factor for T_d point group

$$G_{\Gamma_1}(\boldsymbol{e}_1,\boldsymbol{e}_2)=\frac{1}{3}\left|\boldsymbol{e}_1\cdot\boldsymbol{e}_2\right|^2$$

$$G_{\Gamma_4}(\boldsymbol{e}_1,\boldsymbol{e}_2)=\frac{1}{2}\left|\boldsymbol{e}_1\times\boldsymbol{e}_2\right|^2$$

$$G_{\Gamma_3}(\boldsymbol{e}_1,\boldsymbol{e}_2)=\frac{2}{3}\left(e_{1x}{}^2e_{2x}{}^2+e_{1y}{}^2e_{2y}{}^2+e_{1z}{}^2e_{2z}{}^2\right)-\frac{2}{3}\left(e_{1x}e_{1y}e_{2x}e_{2y}+e_{1y}e_{1z}e_{2y}e_{2z}+e_{1z}e_{1x}e_{2z}e_{2x}\right)$$

$$G_{\Gamma_3}(\boldsymbol{e}_1,\boldsymbol{e}_2)=\frac{1}{2}\left[\left(e_{1x}e_{2y}+e_{1y}e_{2x}\right)^2+\left(e_{1y}e_{2z}+e_{1z}e_{2y}\right)^2+\left(e_{1z}e_{2x}+e_{1x}e_{2z}\right)^2\right]$$

Appendix B

Estimation of Dot Radius for Creation of Excited Biexcitons

When the excitation energy falls inside the one-photon absorption band of the confined excitons, the excited biexciton is created into the excited state by two-photon absorption. Here, the estimation of the dot sizes for the biexciton creation is discussed.

According to the transition energy from the exciton (J_{ex} = 1) to excited biexciton (J = 2) previously reported [31, 37], the exciton energy dependence of the transition energy is expressed as follows:

$$E_{XX2} - E_{bulk} = \alpha(E_{ex} - E_{bulk}) \qquad \text{(B-1)}$$

where E_{XX2}, E_{ex} and E_{bulk} indicate the transition energy from the exiciton to the excited biexciton, the exciton energy in a spherical dot and in the bulk crystal, respectively, α is reported to be 2 experimentally [31] and 2.4 theoretically [37]. The confined exciton energy is

$$E_{ex} = \frac{\hbar^2\pi^2}{2M_{ex}}\left(\frac{1}{a-0.5a_B}\right)^2 + E_{bulk} \qquad \text{(B-2).}$$

Therefore, E_{XX2} is given by

$$E_{XX2} = \alpha \cdot \frac{\hbar^2\pi^2}{2M_{ex}}\left(\frac{1}{a-0.5a_B}\right)^2 + E_{bulk} \qquad \text{(B-3).}$$

The two-photon absorption energy for the excited biexciton state is given by

$$\hbar\omega = \frac{E_{XX2} + E_{ex}}{2}$$
$$= \frac{\alpha+1}{2} \cdot \frac{\hbar^2\pi^2}{2M_{ex}} \left(\frac{1}{a - 0.5a_B} \right)^2 + E_{bulk} \qquad \text{(B-4)}$$

When the excitation energy is equal to the confined exciton energy, the dot size relation between the biexciton creation (a_{mol}) and the exciton creation (a_{ex}) is given by

$$\frac{\hbar^2\pi^2}{2M_{ex}} \left(\frac{1}{a_{ex} - 0.5a_B} \right)^2 + E_{bulk} = \frac{\alpha+1}{2} \cdot \frac{\hbar^2\pi^2}{2M_{ex}} \left(\frac{1}{a_{mol} - 0.5a_B} \right)^2 + E_{bulk}$$

$$\left(\frac{a_{mol} - 0.5a_B}{a_{ex} - 0.5a_B} \right)^2 = \frac{\alpha+1}{2} \qquad \text{(B-5).}$$

When one uses the experimental value of $\alpha = 2$ and neglects the dead layer effect, the size relation is simplified as

$$a_{mol} / a_{ex} = \sqrt{\frac{3}{2}} \approx 1.22 \qquad \text{(B-6).}$$

Acknowledgements

I have carried out this study at Osaka University.

I am most grateful sincerely to my supervisor, Prof. Itoh for his continuing support, advices and discussions. I wish to acknowledge valuable discussions with Prof. Cho and Prof. Kobayashi. I am indebted to Prof. Edamatsu of Tohoku University for his support, advices and discussions. I wish to thank Dr. Ashida for his advices and support. Special thanks are due to Mr. Oohata of Tohoku University for his support and discussions. I thank students of Itoh laboratory, especially Mr. Kagotani for his help in my experiments. Finally, I wish to express my gratitude to Mrs. Fukuda for her support.

References

[1] R. Dingle, A.C. Gossard, W. Wiegmann, "Direct observation of supperlattice formation in a semiconductor heterostructure", Phys. Rev. Lett. **34**, 1327 (1975).

[2] S. V. Gaponenko, *Optical Properties of Semiconductor Nanocrystals* (Cambridge University Press, Combredge, 1998).

[3] A. Y. Cho, "Film deposition by molecular-beam techniques", J. Vac. Sci. Technol. **8**, 531 (1971).

[4] M. J. Ludowise, "Metalorganic chemical vapor deposition of III-V semiconductors", J. Appl. Phys. **58**, R31 (1985).

[5] P. K. Kondratko, S. Chuang, G. Walter, T. Chung, N. Horonyak. Jr., "Observations of near-zero linewidth enhancement factor in a quantum-well couples quantum-dot-laser", Appl. Phys. Lett. **83**, 4818 (2003).

[6] M. Troccoli, F. Capasso, "Mid-infrared electroluminescence in quantum cascade structures with InP/InGaAs active regions", J. Appl. Phys. **94**, 7101 (2003).

[7] A. V. Malko, A. A. Mikhailovsky, M. A. Pertrusta, J. A. Hollingsworth, H. Htoon. M. G. Bawendi, and V. I. Klimov, "From amplified spontaneous emission to microring lasing using nanocrystal quantum dot solids", Appl. Phys. Lett. **81**, 1303 (2002).

[8] Z. Shen, E. T. Kim and A. Madhukar, "Infrared photo diode of InAs quantum dots", Appl. Phys. Lett. **80**, 2490 (2002).

[9] S. Sauvage, P. Boucaud, T. Brunhes, A. LemaitreJ. M. Gerard, "Photoluminescence in infrared region of InAs quantum dots ", Phys. Rev. B **60**, 15589 (1999).

[10] A. I. Ekimov and A. A. Onushchenko, "Quantum size effect in the optical spectra of semiconductor microcrystals", Sov. Phys. Semicond, **16**, 775 (1982).

[11] T. Itoh, Y. Iwabuchi and T. Kirihara, "Study on the size and shape of CuCl microcrystals embedded in alkali-chrolide matrices and their correlation with exciton confinement", phys. stat. sol. (b) **145**, 567 (1988).

[12] T. Itoh, Y. Iwabuchi and T. Kirihara, "Size-quantutized excitons in microcrystals of cuporous halides embedded in alkali-halaide matrices", phys. stat. sol. (b) **146**, 531 (1988).

[13] B. O. Dabbousi, J. Rodriguez-Viejo, F. V. Mikulec, J. R. Heine, H. Mattoussi, R. Ober, K F. Jenson, and M. G. Bawendi, "(CdSe)ZnS core – Shell quantum dots: Synthesis and characterization of a size series of highly luminescent nanocrystallites", J. Phys. Chem. B **101**, 9463 (1997).

[14] Al. L. Efros and A. L. Efros, "Interband absorption of light in a semiconductor sphere", Sov. Phys. Semicond. **16**, 1209 (1981).

[15] Y. Kayanuma. "Wannier exciton in microcrystal". Solid State Commun. **59**, 405(1986).

[16] Y. Kayanuma. "Quantum size effect". Phys. Rev. B **38**, 9797 (1988).

[17] H. Ishihara, K. Cho, "Nonlinear optical response due to resonant enhancement of the internal field with particular spatial distribution", Phys. Rev. B **53**, 15823 (1996).

[18] H. Haug and S. Koch "On the theory of laser action in dense exciton system", phys. stat. sol. (b) **82**, 531 (1997).

[19] M. Cardona, "Optical properties pf the silver and cuprous halides", Phys. Rev. **129**, 69, 1963 (1963).

[20] K. Saito, M. Hasuno, T. Hatano, N. Nagasawa, "Band gap energy and binding energys of Z_3- excitons in CuCl", Solid State Commmun. **94**, 33 (1995).

[21] Nakamura, H. Yamada and T. Tokizaki, "Size-dependent radiative decay of excitons in CuCl semiconductor quantum spheres embedded in glasses", Phys Rev. B **40**, 8585 (1989).

[22] T. Kataoka, T. Tokizaki and A. Nakamura, "Mesoscopic enhancement of optical nonlinearity in CuCl quantum dots: Giant-oscillator-strength effect on the confined excitons", Phys Rev. B **48**, 2815 (1993).

[23] B. Kippelen, R. Levy, P. Gilloit ad L. Bellegui, "Picosecond excite and probe nonlinear absorption measurements in CuCl quantum dots", Appl. Phys. Lett. 59, 3378 (1991).

[24] Y. Masumoto, M. Yamazaki, H. Sugawara, "Optical nonlinerities of excitons in CuCl microcrystals". Appl. Phys. Lett. **53**, 1527 (1988).

[25] T. Itoh, M. Hurumiya, T. Ikezawa, "Size-dependent radiative decay time of confined excitons in CuCl microcrystals", Solid State Commun. **73**, 271 (1990).

[26] K. Naoe, Lev G. Zimin and Y. Masumoto, "Persistent spectral hole burning in semiconductor nanocrystals", Phys. Rev. B **50**, 18200 (1994).

[27] E. Hanamura. "Giantnic nonlinear optical poralizability of semiconductor microcrisllites". Solid State Commun. **62**, 465 (1987).

[28] E. Hanamura. "Very large optical nonlinearity of semiconductor microsrystalites". Phys. Rev. B **37**, 1273 (1988).

[29] E. Hanamura, "Rapid radiative decay and enhanced optical nonlinearlity of excitons in a quantum well", Phys. Rev. B **38**, 1228 (1988).

[30] Y. Masumoto, S. Okamoto, S. Katayanagi, "Biexciton binding energy in CuCl quantum dots", Phys. Rev B **50**, 18658 (1994).

[31] M. Ikezawa and Y. Masumoto, "Observation of excited biexciton states in CuCl quantum dots: control of the quantum dot energy by a photon", Jpn. J. Appl. Phys. **36**, 4191 (1997).

[32] T. Itoh, "Biexciton luminescence and superraddiance", Nonlinear Optics **1**, 61 (1991).

[33] E. Edamatsu, S. Iwai, T. Itoh, S. Yano and T. Goto, "Subpicosecond spectroscopy of the optical nonlinearities of CuCl quantum dots", Phys. Rev. B **51,** 11205 (1995).

[34] S. Yano, T. Goto, T. Itoh and A. Kasuya, "Dynamics of excitons and biexcitons in CuCl nanocrystals embedded in NaCl at 2 K", Phys. Rev. B **55**, 1667 (1997).

[35] S. Yano, A. Yamamoto and T. Goto, "Relaxation dynamics of carriers at 77 and 2 K", Phys. Rev. B **57**, 7203 (1998).

[36] S. V. Nair and T. Takagahara, "Weakly correlated exciton pair states in large quantum dots", Phys. Rev B **53**, R10516 (1996).

[37] S. V. Nair and T. Takagahara, "Theory of exciton pair states and their nonlinear optical properties in semiconductor quantum dots", Phys. Rev B **55**, 5153 (1997).

[38] Y. Masumoto and T. Kawamura, "Biexciton lasing of CuCl quantum dots", Appl. Phys. Lett. **62**, 225 (1993).

[39] G. M. Gale and A. Mysyrowicz, "Direct Creation of Excitonic Molecules in CuCl by Giant Two-Photon Absorption", Phys. Rev. Lett. **32**, 727 (1974).

[40] H. Souma, T, Goto, T. Ohta, "Formation and radiative recombination of free excitonic molecule in CuCl by ruby laser excitation", J. Phys. Soc. Jpn. **29**, 697 (1970).

[41] S. Shionoya, H. Saito, E. Hanamura and O. Akimoto, "Anisotropic excitonic molecules in CdS and CdSe", Solid State Commun. 12, 223 (1973).

[42] Y. Unuta Y. Masumoto, S. Shionoya, "Picosecond spectroscopy of excitonic

molecules in CuBr", J. Phys. Soc. Jpn. **29**, 1200 (1982).

[43] J. M. Hvam, G. Blattner, M. Reuscher, C. Klingshirn, "The biexciton levels and nonlinear optical transitions in ZnO", phys. stat. sol. (b) **118**, 197 (1983).

[44] O. Akimoto, E. Hanamura, "Excitonic molecule. I.", J. Phys. Soc. Jpn. **33**, 1537 (1972).

[45] W. F. Brinkmen, T. M. Rice, B. Bell, "The excitonic molecule", Phys. Rev. B **8**, 1570 (1973).

[46] W. T. Huang, "Binding energy of excitonic molecules in isotropic semiconductors", phys. stat. sol. (b) **60**, 309 (1973).

[47] E. Hanamura, "Excitonic molecule. IV", J. Phys. Soc. Jpn. **39**, 1516 (1975).

[48] E. Doni, R. Girlanda and G. Pastori Parravicini, "Selection rule direct creation of biexcitons by giant two-photon absorption", Solid State Commun. **17**, 189 (1975).

[49] H. Akiyama, T, Kuga, M. Matsuoka, M. Kuwata-Gonokami, "Radiative decay and phonon scattering of biexcitons in CuCl", Phys. Rev. B **42**, 5621 (1990).

[50] V. D. Phach, A. Bivas, B. Honerlage, J. B. Grun, "Biexciton resonant two-photon absorption in CuCl", phys. stat. sol. (b) **84**, 731 (1977).

[51] N. Nagasawa, T. Mita and M. Ueta, "Resonant Two-Photon Excitation of Excitonic Molecule in CuCl with Using Circularly Polarized Light", J. Phys. Soc. Jpn. 45, 713 (1978).

[52] T. Itoh, S. Watanabe, M. Ueta, "Phonon Interaction of Excitonic Molecule in CuCl", J. Phys. Soc. Jpn. **48**, 542 (1980).

[53] K. Yamanaka, E. Edamatsu and T. Itoh, "Excited-state absorption of excitons confined in CuCl quantum dots", J. Luminescence **87-89**, 312 (2000).

[54] T. Uozumi, Y. Kayanuma, K. Yamanaka, K. Edamatsu and T. Itoh, "Excited-state absorption of excitons confined in spherical quantum dots", Phys Rev. B **59**, 9826 (1999).

[55] T. Uozumi and Y. Kayanuma, "Excited states of an electron-hole pair in spherical quantum dots and their optical properties", Phys Rev. B **65**, 165318 (2002).

[56] R. W. G. Wyckoff. *Crystal Structure*, 1 Interscience Pblischers, New York, second edition, 1963.

[57] B. Honerlage, C. Klingshirn, J. B. Grun, "Exciton spatial dispersion determined through the two-photon raman scattering in semiconductors", phys. stat. sol. (b) **78**, 599 (1976).

[58] T. Nanba, K. Hachisu, M. Ikezawa, "Optical constant of cuprous halide crystal in the far-infrared region at 2K", J. Phys. Soc. Jpn. **20**, 1724 (1965).

[59] S. Lewonczyk, J. Ringeissen, S. Nikitine, "Spectre excitonique de CuBr. comparaison avec CuCl", J. Physique **32**, 941 (1971).

[60] T. Mita, K. Sotome, M. Ueta, "Stepwise two-photon excitation into excitonic molecule state via exciton state of large wave vectors in CuCl", J. Phys. Soc. Jpn. **42**, 496 (1980).

[61] T. Mita, K. Sotome, M. Ueta, "Exciton spatial dispersion determined through the two-photon raman scattering via excitonic molecule state at large wave vectors in CuCl", Solid State Commun. **33**, 1135 (1980).

[62] C. I. Yu, T. Goto, M. Ueta, "Emission of cuprous halide crystals at high density excitation", J. Phys. Soc. Jpn. **34**, 693 (1973).

[63] V. D. Phach and R. Levy, "Biexciton two-photon absorption in CuBr", Solid State Commun. **29**, 247 (1979).

[64] Y. Nozue, T, Itoh, M. Ueta, "Resonant raman scattering under two-photon excitation of excitonic molecules in CdS", J. Phys. Soc. Jpn. **44**, 1305 (1977).

[65] K. Brunner, G. Abstreiter, G. Bohm, G. Trankle and G Weimann, "Sharp-line photoluminescence and two-photon absorption of zero-dimensional biexcitons in a GaAs/AlGaAs structure", Phys. Rev. Lett. **73**, 1138 (1994).

[66] H. Ajiki, K. Cho, "Longitudinal and transverse components of excitons in a spherical quantum dot", Phys. Rev. B **62**, 7402 (2000).

[67] S. Sauvage, P. Boucaud and F. H. Julian, "Infrared spectroscopy of intraband transitions in self-organized InAs/GaAs quantum dots", J. Appl. Phys. **82**, 3396 (1997).

[68] P. Guyot-Sionnest and M. A. Hines, "Transition of $1s_e$-$1p_e$ states confined electron in CdSe nanocrystal colloids", Appl. Phys. Lett. **72**, 686 (1998).

[69] P. Guyot-Sionnest, M. Shim, C. Matranga and M. Hines, "Intraband relaxation in CdSe quantum dots", Phys Rev. B **60**, R2181 (1999).

[70] P. Boucaud, V. L. Thanh, S. Sauvage, D. Debarre, and D. Bouchier, "Intraband absorption in Ge/Si self-assembled quantum dots", Appl. Phys. Lett. **74,** 401 (1999).

[71] G. Herzberg, "The dissociation energy of the hydrogen molecule", J. Mol. Spectrosc. **33**, 147 (1970).

[72] R. Mulliken and W. C. Ermler, "Interpretation of band spectra", Rev. Mod. Phys. **4**, 1 (1932).

List of publications

1. K. Miyajima, K. Edamatsu, T. Itoh.
"Infrared Transient Absorption of Excitons and Biexcitons Confined in CuCl Quantum Dots"
physica status solidi (c) **0,** 1275~1278 (2003).

2. K. Miyajima, K. Edamatsu and T. Itoh
"Infrared Transient Absorption and Excited-States of Excitons and Biexcitons Confined in CuCl Quantum Dots"
Journal of Luminescence, in press.

Related papers

1. H. J. Ko, Y. F. Chen, T. Yao, K. Miyajima, A. Yamamoto, T. Goto.
"Biexciton emission from high-quality ZnO films grown on epitaxial GaN by plasma-assisted molecular-beam epitaxy"
Applied Physics Letters **77**, 537~539 (2000).

2. K. Miyajima, A. Yamamoto, T. Goto, H. J. Ko, T. Yao.
"PHOTOLUMINESCENCE OF BIEXCITON IN ZnO EPITAXIAL THIN FILMS"
Proceedings of 2000 International Conference on Excitonic Processes in Condensed Matter, edited by K. Cho and A. Matsui (World Scientific, 2001) 43~46.
International Journal of Modern Physics B, 15, 3611~3614.

3. A. Yamamoto, K. Miyajima, T .Goto, H. J. Ko, T. Yao.
"Biexciton luminescence in high-quality ZnO epitaxial thin films"
Journal of Applied Physics **90**, 4973~4976 (2001).

4. A. Yamamoto, K. Miyajima, T. Goto, H. J. Ko, T. Yao
"Dynamics of newly observed biexcitons in ZnO epitaxial thin films"
Journal of Luminescence. **94-95**, 373~377 (2001).

5. A. Yamamoto, K. Miyajima, T. Goto, H. J. Ko, T. Yao
"Bound Biexciton Photoluminescence in ZnO Epitaxial Thin Films"
physica status solidi (b) **229**, 871~875 (2002).

Presentation at international conferences

1. K. Miyajima, Y. Kagotani, K. Edamatsu, T. Itoh.
   "Infrared Transient Absorption of Excitons and Biexcitons Confined in CuCl Quantum Dots"
   2nd International Conference on Semiconductor Quantum Dots (QD2002), September 2002, Tokyo, Japan.

2. K. Miyajima, Y. Kagotani, K. Edamatsu, T. Itoh.
   "Excited-State Absorption of Excitons and Biexcitons Confined in CuCl Quantum Dots"
   Europe Quantum Electronics Conference (EQEC2003), June 2003, Munchen, Germany.

3. K. Miyajima, Y. Kagotani, K. Edamatsu, T. Itoh.
   "Study of Biexciton Excited States Confined in CuCl Quantum Dots by Infrared Transient Absorption"
   CREST & QNN'03 Joint International Workshop, July 2003, Hyogo, Japan.

4. K. Miyajima, Y. Kagotani, K. Edamatsu, T. Itoh.
   "Infrared Transient Absorption and Excited-States of Excitons and Biexcitons Confined in CuCl Quantum Dots"
   International Conference on Dynamical Processes in Excited States of Solids (DPC'03), September 2003, Christchurch, New Zealand.